NASA TN D-294

TECHNICAL NOTE

D-294

TURBULENCE STUDIES OF A RECTANGULAR SLOTTED NOISE-SUPPRESSOR NOZZLE

By James C. Laurence

Lewis Research Center
Cleveland, Ohio

NATIONAL AERONAUTICS AND SPACE ADMINISTRATION

WASHINGTON

September 1960

NATIONAL AERONAUTICS AND SPACE ADMINISTRATION

TECHNICAL NOTE D-294

TURBULENCE STUDIES OF A RECTANGULAR SLOTTED NOISE-SUPPRESSOR NOZZLE

By James C. Laurence

SUMMARY

The problem of noise suppression of turbojet engines has shown a need for turbulence data within the flow field of various types of nozzles used in ad hoc investigations of the sound power. The result of turbulence studies in a nozzle configuration of four parallel rectangular slots is presented in this report with special attention to the effect of the spacing of the nozzles on the intensity of turbulence, scale of turbulence, spectrum of turbulence, and the mean stream velocity.

Taylor's hypothesis, which describes the convection of the turbulence eddies, was tested and found correct within experimental error and certain experimental and theoretical limitations. The convection of the pressure patterns was also investigated, and the value of the convection velocity was found to be about 0.43 times the central core velocity of the jets.

The effect of the spacing-to-width ratio of the nozzles upon the turbulence intensity, the scale of turbulence, and the spectral distribution of the noise was found in general to produce a maximum change for spacing-to-width ratios of 1.5 to 2.0. These changes may be the cause of the reduction in sound power reported for similar full-scale nozzles and test conditions under actual (static) engine operation. A noise reduction parameter is defined from Lighthill's theory which gives qualitative agreement with experiments which show the noise reduction is greatest for spacing-to-width ratios of 1.5 to 2.0.

INTRODUCTION

The flow of air through nozzles of various sizes and shapes has been of interest for many years. The jets of air issuing from circular nozzles and rectangular slots have been under rather intensive investigation to determine the mean and fluctuating flow properties of the stream. Of

interest also has been the effect of adjacent jets upon each other as exemplified by the change in the mean flow and turbulent parameters as the positions, the number, and the shapes of the adjacent jets were changed. The results of these studies have been reported in the literature (refs. 1 to 4). Recently, however, there has been a shift in interest from purely aerodynamic investigations to those primarily interested in noise reduction or suppression (refs. 5 and 6). Greatrex has found that the arrangement of essentially rectangular slots on the periphery of a circle gave good noise reduction over certain bands of frequencies (ref. 5). Coles and Callaghan report for a linear array of rectangular slots a relation between the width of the slot and the spacing between the slots which resulted in a maximum reduction of the noise generated (ref. 6). Coles (ref. 7) was able to predict from turbulence data of a circular nozzle and a single long slot nozzle that the noise output of the slot is one-half that of the circular nozzle of equal area. This prediction was verified by actual measurements.

With Lighthill's analysis (ref. 8) as a guide, several authors (refs. 9, 10, and 11) have been able to predict, by dimensional analysis methods, the noise produced by a circular jet of air from the mean flow and from the turbulent velocity fluctuations characteristic of the flow from the nozzle. In each of these analyses the turbulent structure of the jet - the intensity and scale of the turbulence - is required as a basis of the method proposed. These methods have attempted to relate fundamental flow parameters to the noise output. If they are successful, the design of effective noise suppressors can be accomplished without extensive ad hoc investigations, which involve expensive models and extensive testing, often on a full-scale basis.

These attempts to calculate the noise field have been characterized by the authors' use of turbulence information which can be acquired by hot-wire anemometry and pressure transducer measurements within or adjacent to the jet of air. The hot-wire method has been developed to a high degree of efficiency and accuracy for obtaining flow data. In order to supply the type of turbulence data needed, the experimental program reported herein was undertaken as a part of the aerodynamic noise research program at the Lewis Research Center.

EXPERIMENTAL PROGRAM

Facilities and Measuring Instrumentation

The air handling facilities and measuring instrumentation were those described in reference 12. The nozzle configuration (fig. 1) was bolted to a large plenum-bellmouth combination to which air was supplied at 40 pounds per square inch. The rate of flow was controlled by a remotely operated valve system ahead of the plenum.

The total pressure and total temperature of the air supply were measured in the plenum downstream of a filter designed to remove dirt particles from the airstream. The air temperature was essentially room temperature, and the flow was adjusted to give a Mach number of 0.3 and a Reynolds number of 2.06×10^6 per foot.

For total-pressure surveys of the flow field, the pressure indications of a total head tube were changed to electrical signals by an appropriate transducer, and these signals were recorded on a strip chart X-Y recorder as a function of position within the air jets.

The hot-wire anemometers were the constant-temperature type described in reference 13. Because of the constant-temperature feature, the data taking could be automatized to the extent that the electrical signals from which the mean-square velocity fluctuations and the average velocity within the flow field of the nozzles could be calculated were recorded on an X-Y recorder as a continuous function of probe position within the field. These charts, the recordings from the hot-wire anemometers and the recordings of the total pressure, were used to obtain profiles or contours of constant turbulence intensity and of constant mean velocity throughout the jets.

The fluctuating pressures near the boundary of the flow field were measured with condenser-type microphones with appropriate power supplies. The microphones (see fig. 2) were located out of the airflow but as near the boundaries as practical.

The fluctuating voltages - hot-wire and microphone - were recorded, as a function of time for specific points within the flow field, on dual-channel magnetic-tape recorders and, as a function of frequency, on an audiofrequency spectrum analyzer with filters one-tenth decade in band pass.

The frequency response of the instruments used for recording these fluctuating signals was in all cases from 25 to 20,000 cycles per second within ± 2 decibels. This response, essentially the tape recorder's response, was adequate for the studies planned in this experiment.

Nozzles

The nozzles used in this program were the same as those of reference 4 except that they were arranged with the long dimension of the rectangle vertical instead of horizontal (see sketch (a)). The

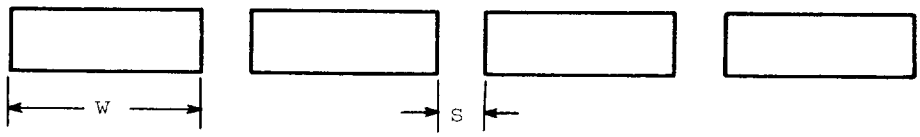

Arrangement of nozzles, ref. 4

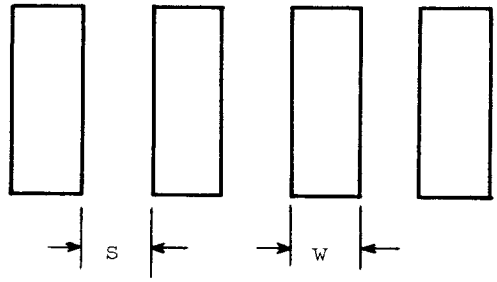

Arrangement of nozzles, this report

(a)

dimensions of the individual nozzles were made so that the total area available for air discharge was equivalent to that of a 4-inch-diameter circular nozzle. This arrangement would result in the same noise output for the slots as for the circular nozzle except for interference effects. The interference effects are, of course, the objects of the experiment.

It was realized that the entrance conditions would affect the flow through the nozzles both as to amount of air discharged through each nozzle and as to the similarity of the flow through the individual nozzles. Thus, an attempt was made to ensure smooth, well-distributed flow in each jet. The extent to which this was attained will be pointed out in the appropriate section of this report.

Since one of the objects of this experiment was to determine the effect of the spacing-to-width ratio of the nozzles on the turbulence and mean flow parameters, five different spacings of the nozzles were used. The separation of the nozzles varied from a distance large enough that the jets were operating essentially independent of each other to a small spacing at which considerable interference with adjacent jets took place.

While the entire flow field was investigated, enough similarity about the centerline was found that maps were prepared for only a limited portion of the field. Because the flow field is symmetrical about the centerline, the maps were limited to the field of the two nozzles on one side of the centerline.

Data Processing Instrumentation

The processing of the data stored on magnetic tapes was done by a special system of instrumentation designed and built at the Lewis Research Center. This system of instrumentation is described in detail in reference 14. The component parts of the system include a profile plotter, noise spectrum digitizer, an autocorrelator, and a probability-density analyzer. These instruments make possible the rapid processing of the data to a form which is suitable for use.

The profile plotter examines the input signal, selects the level of the signal, and by appropriate circuitry plots the point as a function of position within the field. It combines in one instrument the processes necessary to plot a given parameter, say, turbulence intensity as a function of position, and a cross plot to obtain contours or profiles of constant turbulence intensity as a function of position.

The noise spectrum digitizer takes the output voltages of the filters of the audiospectrum analyzer mentioned previously, averages this voltage, and digitizes it. The information is then stored on punched paper tape which can be used to program an electronic computer.

The probability-density analyzer has a gate circuit which determines the fractional part of the time that the fluctuating signal has an amplitude within a variable height e, but constant width Δe, gate (see sketch (b)).

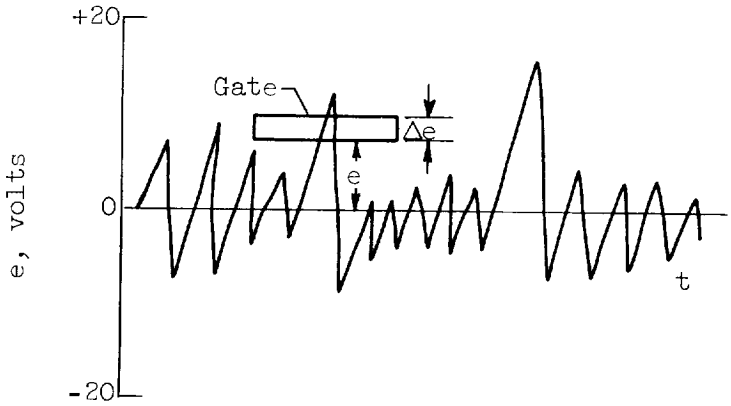

(b)

The result is described by the probability-density function:

$$p(e) = \lim_{\substack{\Delta e \to 0 \\ t \to \infty}} \frac{\text{Number of values in } \Delta e \text{ at } e}{\text{Total number of values } N} \cdot \frac{1}{\Delta e} \qquad (1)$$

or

$$p(e) = \lim_{\substack{\Delta e \to 0 \\ t \to \infty}} \frac{\text{Time the voltage is in range } \Delta e \text{ at } e}{\text{Total time}} \cdot \frac{1}{\Delta e} \qquad (2)$$

This voltage $p(e)$ is averaged and presented to one axis of a flat-bed X-Y recorder, while the gate is driven at a constant rate which is presented to the other axis of the recorder. The result is a plot of the probability-density function.

The autocorrelator uses signals which are recorded identically on both channels of a magnetic-tape recorder. If signals from two different transducers, separated in space, are recorded on the two channels, a space-time correlation analysis can be made. In the autocorrelation method $u(t)$ and $u(t \pm \tau)$ are two identical signals except for a time delay or lead. Then,

$$R_\tau = \frac{\overline{u(t)u(t \pm \tau)}}{\sqrt{\overline{u(t)^2}}\sqrt{\overline{u(t \pm \tau)^2}}} \qquad (3)$$

where the bar indicates an average over a time which is large compared with the period of any component wave. This expression (eq. (3)) is an approximation of the autocorrelation coefficient:

$$R_\tau = \frac{\lim_{T \to \infty} \int_{-T}^{T} u(t)u(t \pm \tau)dt}{\sqrt{\lim_{T \to \infty} \frac{1}{T} \int_{-T}^{T} u^2(t)dt \lim_{T \to \infty} \frac{1}{T} \int_{-T}^{T} u^2(t \pm \tau)dt}} \qquad (4)$$

When $u_1(t)$ and $u_2(t \pm \tau)$ are the longitudinal velocity fluctuations at two points in space, then for any specified time delay τ,

$$R_{12}(\tau) = \frac{\overline{u_1(t)u_2(t \pm \tau)}}{\sqrt{u_1(t)^2}\sqrt{u_2(t \pm \tau)^2}} \qquad (5)$$

is the cross or space correlation coefficient. If the space correlation can be obtained as a function of the time delay τ, the space-time correlation results.

In the instrument used in this report, the time delay is accomplished by a special playback head configuration in which one head can be moved, in the direction of the tape motion, with respect to the other head. The output of an electronic multiplier properly calibrated and adjusted is presented to the y-axis of an X-Y recorder as the correlation coefficient. The head position, expressed as a direct-current voltage, is calibrated, adjusted, and presented to the x-axis of the recorder as the time delay. The result is a space-time correlogram.

EXPERIMENTAL PROCEDURES

There were two distinct procedures used in these experiments: the continuous survey and the point-to-point survey.

Continuous Survey

In this part of the experiment the probe (a hot-wire or total-pressure probe) was mounted in a remotely controlled actuator which gave a continuous indication of the position of the probe within the flow field. The voltages which were related to the desired flow parameter were recorded on strip charts as a function of position within the field. With proper calibration these charts are used to obtain a map of the flow field.

Point-to-Point Survey

At preselected points in the field, the fluctuating voltages from the probes (hot-wire or microphone) were recorded on magnetic tape. The recordings were of one hot-wire probe (identical on both channels) if the autocorrelation was desired.

If the space-time correlation was to be measured, the procedure was somewhat different. Two condenser microphones were placed side by side along the boundary of the outside jet, and the signals from these two were recorded on the two channels of the tape recorder. One of the microphones was held stationary, and the other was moved to a new location upstream and/or downstream of this fixed microphone. A similar experiment was performed using two hot-wire probes mounted in the airstream of the outside jet. From these recordings pressure cross correlations and velocity cross correlations as well as space-time correlations of the pressures and velocities were obtained.

RESULTS AND DISCUSSION

The results of the experimental measurements are presented in a series of graphs and charts. The mean flow results are given in figures 3 and 4. Figure 3 shows a survey of the flow from the four nozzles when the spacing-to-width ratio is 0.94. The velocity profiles are shown for distances from the nozzle exit of $x/D = 0.5$, 1.0, 1.5, 2.0, and 3.0 and show the ratio of the local mean velocity to core velocity. In this report D is defined as $\sqrt{4A/\pi}$, the diameter of the equivalent-area circular nozzle. This value is an appropriate one to use since it makes the average core length about equal to the core length of a circular nozzle (4D). For this particular spacing-to-width ratio (see fig. 4(e)) the flow through the four nozzles is rather uniform, and the maximum value of the velocity ratio U_l/U_c decreases slightly along any z/D = constant line until the end of the core at $x/D = 4.0$. At distances farther downstream the decrease is larger, and eventually the four jets disappear as separate entities and coalesce into a single jet.

Figure 4 presents contour maps of the flow field for all five spacing-to-width ratios used in this research. They are cross plots of figures similar to figure 3 and show the constant-velocity profiles. The effect of the interference of the jets is especially evident in figures 4(d) and (e) when the separation of the nozzles is the least value used in this experiment. Also noticeable is the deformation of the flow field (fig. 4(a)) because of the (1) unequal distribution of the airflow to the nozzles by the entrance section and (2) a Bernoulli effect of adjacent regions of high-speed flow and essentially zero flow as shown in figure 4(a) and following. This unequal distribution of airflow may be an inherent effect of the nozzle configuration at all subsonic Mach numbers. Since the static pressure between the nozzles is probably lower than atmospheric because of the Bernoulli effect, more air flows from the central nozzles than from the outside ones.

The deformation of the flow, as shown by a change in the length of the central core of the individual jets, can be seen by comparing the parts of figure 4 but is noted more markedly in figure 5. In this figure the ratio of the turbulence intensity to the core velocity u'/U_c is shown as a function of lateral distance across the flow field for x/D values of 0.5, 1.0, 1.5, 2.0, 3.0, and 4.0 for the spacing-to-width ratio of 0.94. Near the nozzle exit ($x/D = 0.5$) the turbulence intensity is very low (approx. 0.010 to 0.015), but, as x/D increases, the interference begins to take effect and the intensity of turbulence increases. This increase is especially noticeable in the flow region between the nozzles. This effect is best seen on figure 5 at the arrows.

There is also a marked change in the maximum turbulence intensity found in the high shear region downstream of the lips of the inner nozzles. As the distance from the nozzle exit increases, this maximum value decreases to a value about the same as that at the outermost edge of the flow (see points marked by arrows on fig. 5). A comparison of the results of this nozzle configuration and a circular nozzle (ref. 12) shows that the maximum intensity is less for the rectangular slots but that the entire volume of the turbulent mixing region is increased. This result would account for the reduction in sound power, which is proportional to $(u')^8$ but no more than linearly with the volume of the turbulent mixing region.

Other obvious differences in the turbulence profiles as compared to the mean flow profiles (figs. 3 and 4) are shown in figure 6. Two peaks are evident at the boundaries between the high-speed and low-speed flows, and, in general, there is less uniformity or regularity of the profiles. In each jet there is, of course, the low-turbulence-intensity central core which is characterized by the 0.005 to 0.03 contours. If a comparison is made with the core lengths obtained from figure 4, it is seen that the 0.01 or 0.02 (or less) turbulence contours are characteristic of the central core of each jet. After the breakup of the core, the turbulence intensity increases rapidly as shown by the curves of figure 6 with the maximum values occurring at or near the projection of the lip of the nozzle downstream. The distortion in the profile of the first nozzle is attributed to the entrance conditions in the nozzle.

To investigate the effect of the spacing-to-width ratio on the flow within the jet, figures 7 and 8 were prepared. Figure 7 is a cross plot of the velocity ratio U_l/U_c as a function of the spacing-to-width ratio s/w. The curves were plotted at two locations in the flow where the interference effects would be expected to be large. These are at $z/D = -0.25$ and $x/D = 2.0, 4.0, 6.0, 8.0, 10.0$, and 12.0 and at z/D values corresponding to projections of the vertical lips of the inside nozzle and at $x/D = 2.0, 4.0, 6.0, 8.0, 10.0$, and 12.0. These points are well within the flow field and show the effects of the interfering flows upon each other. While the effects are of the order of 20 percent or so, the curves show very definite peaks for spacing-to-width ratios of approximately 1.5 and a minimum at $s/w \approx 2$, except for the outside slot at $x/D = 2.0$ and 4.0 (see figs. 7(a) and (b)). This anomaly, if it exists, may perhaps be caused by the deformation of the flow in the outside nozzle by the entrance section of the nozzles.

Figure 8 is similar to 7 except that in this figure the turbulence intensity is plotted as a function of the spacing-to-width ratio s/w. Here it is necessary to discuss the figure in terms of two ranges of x/D: one less than the core length and the other greater than the core length. In figure 8(a) for $x/D = 2.0$ and 4.0, the curves have peaks

at a spacing-to-width ratio of approximately 1.5 to 2.0. For the x/D values of 6.0 and 8.0, however, where the mixing is the greatest, the effect of an increase in the spacing-to-width ratio is to increase the intensity of turbulence by about 50 percent over the range of spacings investigated. At larger distances downstream (x/D = 10.0 and 12.0) the curves show a minimum of turbulence intensity at a spacing-to-width ratio of about 1.5.

Reference 6 shows that the reduction in sound power, in slot nozzles similar to these, is proportional to the spacing-to-width ratio. It is seen, therefore, that the turbulence intensity in the mixing zone is a function of the spacing-to-width ratio as assumed in reference 6 but that the jets expand to a smaller half-angle than 9.4°, which was used in reference 6. Undoubtedly, the expansion of the jets is a function of Mach number, and in these tests the Mach number is much less (0.3) than in the tests of reference 6. It may be said that the turbulence intensity is altered by the spacing-to-width ratio. Since for nozzles of the same characteristic length (diameter) the sound power is proportional to $(u')^8$, this may perhaps be part of the explanation of the effectiveness of the interfering-type nozzles as noise suppressors.

The series of figures starting with figure 9 are the results of the analyses which were made to determine the statistical characteristics of the turbulent flow. The recorded hot-wire signals (recorded as described in the section entitled Facilities and Measuring Instrumentation) were processed on an audiospectrometer to obtain the power-spectral-density curves $F(f) = \frac{1}{B}\frac{\overline{e_B^2}}{\overline{e^2}}$, a typical example of which is shown in figure 9. The method of obtaining the power-spectral-density from the spectrum analysis (described in the section entitled Data Processing Instrumentation) is given in reference 12. In these figures (9(a) and (b)) the spectral-density curves are given for x/D values of 2.0 and 4.0 at y/D = 0 and z/D = -0.25. The interesting feature of these figures is the effect of the spacing-to-width ratio on the spectral density. It can be seen that for any frequency band (1/10 decade) the effect of the change in spacing-to-width ratio is to increase the spectral density to a maximum after which the effect is reversed. Figure 9(c) gives similar information for positions midway between the first two nozzles.

Figure 10 was plotted to show this effect more clearly. In this figure the spectral density in specific bands of frequencies is plotted against the spacing-to-width ratio. In general, the curves peak at values of $s/w \sim 1.5$, and in only one of the examples shown is the character of the curve exceptionally different from all the others. This is the curve for the frequency band at 3000 cycles per second and for an x/D = 2.0.

Still another presentation of this spectral information is made in figure 11. In this figure a nondimensional spectral density has been chosen as well as a nondimensional frequency. The nondimensionalizing parameters in both cases are the diameter of the nozzle and the local mean velocity. Hence, if we multiply the spectral density by the local velocity and divide by the diameter, we have

$$\text{Nondimensional spectral density} = \frac{F(f)U_l}{D}$$

For the frequency, multiply by the diameter and divide by the local velocity to obtain the Strouhal number

$$N_{st} = \frac{fD}{U_l}$$

In this figure the peak values of the spectral-density function were read from the spectrum curves along with the corresponding values of the frequency. The resulting curves, which show a tremendous scatter, seem to indicate a trend towards a relation such as the following: assuming a linear relation on a log-log plot with a slope of -1 gives:

$$\ln \frac{F(f_m)}{D} U_l = \ln a - \ln N_{st}$$

or

$$\frac{F(f_m)}{D} U_l N_{st} = a \tag{6}$$

This gives a relation between the spectral-density peak and the frequency as follows:

$$F(f_m) = \frac{a}{f_m}$$

$$\frac{E_{f_m}}{E_{tot}} = \frac{b}{f_m} \tag{7}$$

Even though the scatter is large, the trend towards the -1 slope is real.

As further evidence of the statistical characteristics of the turbulence signals, a probability-density analysis was made as described in the section entitled Data Processing Instrumentation. The hot-wire

signals were processed using the probability-density analyzer described in detail in reference 15. The result of this analysis is presented in figure 12, which is an original curve as it comes from the plotter.

These curves were analyzed as follows: The moments of the probability-density curve are defined by

$$\mu_k = k^{th} \text{ moment about } \bar{e} = \frac{\sum_i p(e_i)(e_i - \bar{e})^k}{\sum_i p(e_i)} \tag{8}$$

or

$$\mu_k = \frac{\int_{-\infty}^{\infty} p(e)(e - \bar{e})^k \, de}{\int_{-\infty}^{\infty} p(e) de} \tag{9}$$

By definition $\mu_0 = 1$, $\mu_1 = 0$, and $\sqrt{\mu_2} = \sigma$, where σ is the standard deviation. Also by definition the skewness and flatness factors are:

$$S = \sqrt{\beta_1} = \mu_3/\sigma^3 = \sqrt{\mu_3^2/\mu_2^3} \tag{10}$$

$$F = \beta_2 = \mu_4/\mu_2^2 \tag{11}$$

The results of the probability-density analysis may be summarized as follows: The skewness is nearly zero at all places in the flow field. In fact, the values of S depart from zero by no more than 0.5. The flatness factors have values very nearly equal to 3. Values of the flatness factor less than 3 tend to show periodicities in the signal, while those greater than 3 are characterized by a signal which shows intermittency or bursts in the turbulent structure of the airflow. Figure 13 was plotted to show the intermittency of the turbulent signals. The intermittency factor, which is defined as $3/\beta_2$, is seen by this figure to be very closely the same throughout the jet and numerically equal to unity. This value is characteristic of signals (velocity fluctuations) with little or no intermittency.

The autocorrelation analysis of random or statistical-type signals has received extensive study (refs. 12, 14, and 15). The recorded

hot-wire signals were processed by means of the computer described in reference 14, and autocorrelograms were obtained throughout the flow field at the specified or preselected points. These autocorrelograms are the basis for the eddy-size measurements in this research. A typical correlogram shows the characteristics described in the appendix of reference 12. Figure 14 is the primary or original record as it comes from the plotter. The result is a curve of the autocorrelation coefficient as a function of time delay as indicated in equation (3). Reference 12 shows that autocorrelations similar to figure 14 are Fourier transforms of spectral-density distributions containing a characteristic or peak frequency. Much evidence exists (refs. 4, 12, and 15) which confirms this result.

The summary curves of figure 15 were prepared to show the results of this autocorrelation analysis. The delay time τ_0 when the autocorrelation coefficient is zero has been plotted as a function of downstream distance from the nozzle exit x/D for different lateral positions z/D in the jet. The successive parts of figure 15 show two positions in the region where the outside jet mixes with the room air: one is taken along the centerline of the outside jet and two others on lines between the outside and inside jet. The results can be described as follows: As the nozzle spacing is decreased from its largest dimension to the smallest, the time delay for zero autocorrelation decreases its value until about $s/w = 1.97$, after which further decreases in the spacing-to-width ratio have very little effect on the value of τ_0. Figure 16 illustrates this result. The time delay for zero correlation is plotted as a function of spacing-to-width ratio. It is seen that the minimum value of τ_0 occurs at $s/w \approx 1.0$ to 1.5.

As expected, the figures (15 and 16) show very little effect of the spacing-to-width ratio on the value of τ_0 in the outer mixing zone of the outside nozzle. This nozzle effectively operates, on the one side, independently of the configuration of the rectangular slots. On the other side at positions in the jet, however, the effect of the spacing change is more apparent. For instance, figure 15(c) shows the variation of τ_0 down the centerline of the first jet. No data points are shown for $x/D < 3.0$ because these points fall in the central core of the air jet. But from $x/D = 3.0$ on downstream to $x/D = 6.0$, the effect of the spacing-to-width ratio is greatest for the value of $s/w = 2.44$ and then decreases. From $x/D = 6.0$ to $x/D = 12.0$ (the largest distance investigated in this experiment) the effect of the change in s/w is a regular decrease in the value of τ_0 as the spacing decreases.

All the parts of figure 15 show a decrease in τ_0 which reaches a minimum at about $x/D = 8.0$ and a slight increase thereafter over the range of x/D values used in this experiment.

If, as in other turbulence experiments, the Taylor hypothesis (ref. 16) holds, the autocorrelograms can be related to the cross correlations in space and from them to the eddy size. Taylor's hypothesis states that the space and time domains are related to each other by the local mean velocity. Thus, the turbulence patterns are relatively unchanged in the time required for the turbulent eddy to move a given distance in the stream. This condition must be limited by the requirement that the turbulent velocity fluctuations be small compared to the local mean velocity. From the accompanying sketch, it can be seen that the trans-

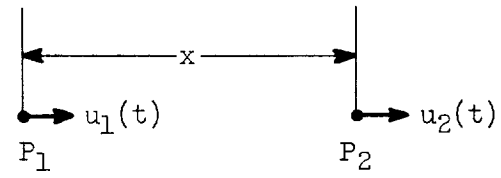

Space domain

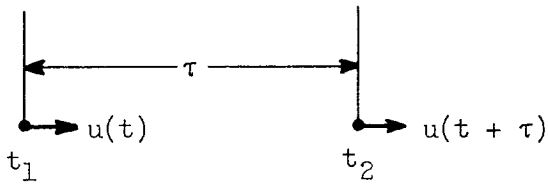

Time domain

(c)

formation from the time domain to the space domain is by the relation between probe separation in the airstream and the time for the eddy to move a distance X in the airstream. In order to test the Taylor hypothesis, a space-time correlation experiment was undertaken for the turbulent velocity fluctuations. Two hot-wire anemometers, as described in the section entitled EXPERIMENTAL PROCEDURES, were used to measure the cross correlation of the turbulent velocities at $x/D = 2.0$ and 4.0, $z/D = 0.25$, and $y/D = 0$.

An exactly similar experiment was conducted using two microphones located along the boundary of the first jet. The cross correlation of the fluctuating pressures was measured at $x/D = 2.0$ and 4.0, $y/D = 0$, corresponding to the points used for the hot-wire measurements but with the microphones outside the airstream. From these pressure correlations a convection velocity of the pressure patterns in the flow adjacent to the measuring points was obtained.

The results of the cross-correlation measurement are shown in figure 17 for the pressures and figure 18 for the turbulent velocities. The pressure correlations were measured for all five s/w values used in these experiments, but the velocity correlations were measured only in the outside jet for $s/w = 3.00$.

The cross correlations (figs. 17 and 18) are asymmetrical because of the influence of the local mean velocity on the convection velocity of the pressure patterns and the turbulent eddies. The asymmetry is more marked, however, in the case of figure 18(a) than for 18(b) since at $x/D = 2.0$ the velocity gradient in the x/D direction is more severe than at $x/D = 4.0$.

To show the effect of the convection velocity even better, the space-time correlations were obtained (fig. 19). Figure 19 is an example of the space-time correlograms obtained from the signals of the two hot-wire anemometers which were mounted in the outside jet. Similar figures were obtained for the pressure fluctuations measured by the microphones. The curves for the different hot-wire probe separations are superimposed in figure 19 to show the space-time relation. In addition, the envelope of the curves has been drawn in as a dotted line. This envelope represents the correlation in the convected frame of reference (see, e.g., ref. 17). These envelope correlograms can be used to obtain the eddy size in the convected frame of reference. This eddy size or scale should not, however, be confused with the Lagrangian scale of turbulence (see refs. 17 and 18).

Two different methods of presentation were used for this space-time correlation analysis. In figure 20 isocorrelation figures are presented for each of the five s/w ratios used at x/D values of 2.0 and 4.0. To prepare these cross plots, values of the microphone separation and the delay time were read for constant values of the cross-correlation coefficient $R_{12}(\tau)$. This procedure resulted in a family of concentric ellipses for each x/D and s/w used. The value of U_k, which has been used to obtain the abscissas of these curves, was obtained by reading the probe separation and the time delay for the successive maximum values of R_{12} from the space-time correlograms. A plot of these separations and time delays results in a straight line, the slope of which has the dimensions of a velocity. This velocity is called the convection velocity. Figure 21 shows a family of convection velocity diagrams for the pressure fluctuations (figs. 21(a) to (e)) and for the turbulent velocity fluctuations (fig. 21(f)). If the correct or approximate value of U_k has been found, the slope of the major axis of the family of ellipses should be 1. Since the average of many U_k's was used, this criterion was fulfilled rather well in most cases.

Table I is a summary of all the space-time correlation measurements. It shows that the convection velocity of the turbulence eddies varied over a considerable range (19 percent) depending on the value of the local mean velocity used. The average values correspond to values of U_l approximately midway between the location of the fixed wire and the extreme position of the movable one. At the points chosen in the jet, the velocity gradients are severe as can be seen by referring to figure 4. Probe misalinement, therefore, can contribute large variations in U_l by unavoidable shifts from one streamline to another in the jet.

There are other sources of possible error in the measurements of the convection velocity of the turbulent eddies. At the points chosen in the jet the measured intensities of turbulence are large compared to the local mean velocity. Thus, the measurements themselves are suspect since the linearization process used to evaluate the hot-wire information breaks down. In addition, the assumption of small intensity of turbulence is inherent in the Taylor hypothesis. These limitations on the experimental measurements may be used to explain the results obtained for the convection velocity given in table I(b).

The convection velocity of the sound patterns is expressed in percent of core velocity since the measurements were made along the boundary of the jet but outside the flow. There is considerable scatter in the data and no clearly defined effect of spacing-to-width ratio or a systematic effect of distance from the nozzle exit. The average value of the convection velocity of the sound patterns is thus 0.43 of the central core velocity.

The autocorrelograms were used to obtain the distribution of eddy size throughout the flow field. The method used is that of references 4 and 13. At specific points in the flow and with the use of Taylor's hypothesis, the autocorrelograms can be converted to cross correlograms, and these can be integrated to give the eddy size. Thus, by using equations (3) and (12),

$$L = \int_0^x R \, dx \tag{13}$$

$$L = \int_0^{U_l \tau} R_\tau U_l \, d\tau$$

$$= U_l \int_0^{U_l \tau} R_\tau \, d\tau \tag{14}$$

In the autocorrelograms of this work, both positive and negative values of R_τ are obtained. Many methods have been used to overcome this difficulty but the most obvious one is

$$L' = U_l \int_0^{U_l \tau} |R_\tau| \, d\tau \tag{15}$$

This is the method used in this report. A summary of the eddy size measurements has been prepared as figures 22 and 23. In figure 22, the variation of eddy size with distance from the nozzle exit is shown. Figure 22(a) shows the variation in eddy size with distance from the nozzle exit at different (z/D) locations in the jets for $s/w = 0.94$. It can be seen from this figure that in the flow of the outside nozzle the variation is quite uniform and similar to that which has been reported for other single jets (refs. 4 and 13). The eddy size increases linearly with distance from the nozzle exit and approaches a maximum at 3 to 4 diameters downstream. After this distance the size remains more or less constant until distances in excess of 10 to 12 diameters when the decay process begins. During decay a slight increase in size may take place.

Figures 22(b) and (c), however, show the variation in eddy size as it varies with nozzle spacing-to-width ratio and distance from the nozzle exit. These plots were prepared for two constant z/D distances from the centerline; that is, $z/D = 0.25$ and 0.50. The figures show the growth in size of the eddies from the nozzle exit to 3 or 4 diameters downstream and essentially no change thereafter for as far downstream as the surveys were made. The effect of nozzle spacing is evident from these figures, but this effect will be discussed when figure 23 is considered.

In figures 22(c) and (d), however, where the adjacent jets of air are mixing with the indrawn air from the room and finally interfering with each other, the picture is quite different. There is a large increase in eddy size when the interference takes place (1 to 3 diam downstream of the nozzle exit). After this the flow reverts to more or less normality with the variation being the same as for the noninterfering jets. This normality indicates that a complete mixing has taken place, and the whole configuration then acts as a single jet. This increase in eddy size during the interfering and mixing of the jets may be the effect which is characterized by a decrease in sound power output of the nozzle as reported in reference 5.

To show further evidence of this mixing, figure 23 (a cross plot of fig. 22) was prepared to illustrate the relation of eddy size to spacing-to-width ratio s/w. Figure 23(a), which shows the variation of eddy size with x/D as did figure 22, shows the effect of s/w. As has been

illustrated in several other of the jet parameters investigated, the effect under study seems to be most prominent for a value of s/w of approximately 1.5 to 2.0. For the eddy size, at least, the results are not as conclusive as for, say, turbulence intensity. But, nevertheless, for x/D values of 2.0 and 4.0 (see figs. 23(a)), the same conclusion is reached. The maximum effect on the eddy size occurs at a spacing-to-width ratio of about 1.5 to 2.0. Further downstream the effect is sometimes lost in the scatter of the data but is well defined at x/D values of 6.0, 8.0, and 10.0 for the region of the flow midway between the outer and inner nozzles (see figs. 23(b)).

In order to test the results of the changes in intensity and scale of turbulence with the spacing-to-width ratio, a noise reduction parameter P is defined as

$$P = \left(\frac{L'}{D}\right)^2 \left(\frac{u'}{U_c}\right)^8 \tag{16}$$

This parameter results from Lighthill's equation (ref. 8):

$$W \propto f^4 \rho_0 \left(\sqrt{\overline{u^2}}\right)^4 (L')^6 a_0^{-5} \tag{17}$$

But, if

$$\sqrt{\overline{u^2}} \propto U_c$$

then

$$P = \frac{W}{U_c^8 D^2} \propto \left(\frac{\sqrt{\overline{u^2}}}{U_c}\right)^8 \left(\frac{L'}{D}\right)^2 \tag{18}$$

The results of this calculation are shown in figure 24 for $x/D = 8.0$, 10.0, and 12.0. The result is seen to be a qualitative agreement between the noise reduction parameter, as defined by equation (18), as a function of spacing-to-width ratio and the experimental results of reference 6, and unpublished data obtained at the Lewis Research Center.

SUMMARY OF RESULTS

The following conclusions can be drawn from the experimental results presented in this report:

1. In a configuration of rectangular slots several of the turbulence parameters, measured in the interfering regions of the jets, are influenced or changed by the spacing-to-width ratio of the nozzles. For the turbulence intensity, the turbulent eddy size, and spectral-density function, the maximum changes occur at a spacing-to-width ratio value of about 1.0 to 2.0.

2. Taylor's hypothesis for the relation of space to time in the flow field of the jets is verified with certain limitations. This means that the turbulent eddies are convected along the stream with the local mean velocity.

3. The convection of the pressure fluctuation patterns is found to be at approximately 0.43 of the velocity of the central core of the jets.

4. The velocity fluctuations in the flow field of the jets are shown to be random in character and, in general, follow a Gaussian distribution with very little intermittency except along the boundaries of the jets and the ambient air.

5. A noise reduction parameter involving the turbulence intensity and scale is defined. The variation of this parameter with the spacing-to-width ratio is in qualitative agreement with measured noise reductions in similar nozzle configurations. The maximum noise reduction occurs at a spacing-to-width ratio of approximately 1.5 to 2.0.

Lewis Research Center
National Aeronautics and Space Administration
Cleveland, Ohio, April 20, 1960

APPENDIX - SYMBOLS

A	area of slot
a	constant
a_0	sound velocity at ambient conditions
B	band pass of filters of spectrum analyzer
b	constant
D	diameter
E_{f_m}	energy at f_m
E_{tot}	total energy
e	fluctuating voltage from hot-wire bridge
$\overline{e}$	average voltage from hot-wire bridge
e_B	fluctuating voltage filtered by a filter of band pass B
e_i	fluctuating voltage from hot-wire bridge in the i^{th} instant
F	flatness factor
$F(f)$	power-spectral-density
f	frequency
f_m	frequency of spectral-density peak
i	instant $i = 1, 2, 3, \ldots$
k	a number
L	scale of turbulence, $\int R\, dx$
L'	scale of turbulence, $\int \lvert R \rvert\, dx$
N	total number of intervals
N_{st}	Strouhal number

P	$(u'/U_c)^8(L'/D)^2$
$p(e)$	probability density
$p(e_i)$	probability density at any instant $i = 0, 1, 2, \ldots$
R	correlation coefficient
R_τ	autocorrelation coefficient
R_{12}	longitudinal space correlation
S	skewness
s	spacing of nozzles
T	period
t	time
U_c	core velocity
U_k	convection velocity
U_l	local mean velocity
u	longitudinal component of turbulent velocity fluctuation
u'	$\sqrt{\overline{u^2}}/U_l$
u_1, u_2	longitudinal component of turbulent velocity fluctuation at points 1 and 2
W	sound power
w	width of nozzle
x,y,z	space coordinates with x in flow direction
β_1	μ_3^2/μ_2^3
β_2	μ_4/μ_2^2
μ_k	k^{th} moment of probability-density curve, $k = 0, 1, 2, \ldots$

ρ_0 density of air at ambient conditions

σ standard deviation

τ delay time

τ' delay time (arbitrary reference)

τ_0 delay time when $R_\tau = 0$

REFERENCES

1. Corrsin, Stanley: Investigation of the Behavior of Parallel Two-Dimensional Air Jets. NACA WR W-90, 1944. (Supersedes NACA ACR 4H24.)

2. Okaya, T., and Hasegawa, M.: On the Velocity Distribution of Flow Behind Parallel Rods. Japanese Jour. Phys., vol. 14, no. 1, Jan. 1941, pp. 1-10.

3. Miller, David Radford: Static Pressure Gradients in Turbulent Jet Mixing. Ph.D. Thesis, Purdue Univ., June 1957.

4. Laurence, James C., and Benninghoff, Jean M.: Turbulence Measurements in Multiple Interfering Air Jets. NACA TN 4029, 1957.

5. Greatrex, F. B.: Jet Noise. Preprint No. 559, Inst. Aero. Sci., 1955.

6. Coles, Willard D., and Callaghan, Edmund E.: Full-Scale Investigation of Several Jet-Engine Noise-Reduction Nozzles. NACA TN 3974, 1957.

7. Coles, Willard D.: Jet-Engine Exhaust Noise from Slot Nozzles. NASA TN D-60, 1959.

8. Lighthill, M. J.: On Sound Generated Aerodynamically. I - General Theory. Proc. Roy. Soc. (London) ser. A, vol. 211, no. 1107, Mar. 20, 1952, pp. 564-587. (See also pt. II - Turbulence as a Source of Sound, ser. A, vol. 222, no. 1148, Feb. 23, 1954, pp. 1-32.)

9. Sanders, Newell D., and Laurence, James C.: Fundamental Investigation of Noise Generation by Turbulent Jets. Trans. SAE, vol. 65, 1957.

10. Corcos, G. M.: Some Measurements Bearing on the Principle of Operation of Jet Silencing Devices. Rep. SM-23114, Douglas Aircraft Co., Inc., Mar. 1958.

11. Williams, J. E. Ffowcs: Measuring Turbulence with a View to Estimating the Noise Field. Rep. 20,381, British ARC, Sept. 11, 1958.

12. Laurence, James C.: Intensity, Scale, and Spectra of Turbulence in Mixing Region of a Free Subsonic Jet. NACA Rep. 1292, 1956. (Supersedes NACA TN's 3561 and 3576.)

13. Laurence, James C., and Landes, L. Gene: Auxiliary Equipment and Techniques for Adapting the Constant-Temperature Hot-Wire Anemometer to Specific Problems in Air-Flow Measurements. NACA TN 2843, 1952.

14. Carlson, Edward R., et al.: Special Electronic Equipment for the Analysis of Statistical Data. Proc. IRE, vol. 47, no. 5, pt. 1, May 1959, pp. 956-962.

15. Favre, A., Gaviglio, J., and Dumas, R.: Some Measurements of Time and Space Correlations in a Wind Tunnel. NACA TM 1370, 1955.

16. Taylor, G. I.: Statistical Theory of Turbulence. Proc. Roy. Soc. (London), ser. A, vol. 151, no. A873, pts. 1-IV, Sept. 2, 1935, pp. 421-478; pt. V, ser. A., vol. 156, no. 888, Aug. 17, 1936, pp. 307-317.

17. Baldwin, Lionel V.: Turbulent Diffusion in the Core of Fully Developed Pipe Flow. Ph.D. Thesis, Case Inst. Tech., 1959.

18. Mickelsen, William R.: An Experimental Comparison of the Lagrangian and Eulerian Correlation Coefficients in Homogeneous Isotropic Turbulence. NACA TN 3570, 1955.

TABLE I. - SPACE-TIME CORRELATIONS

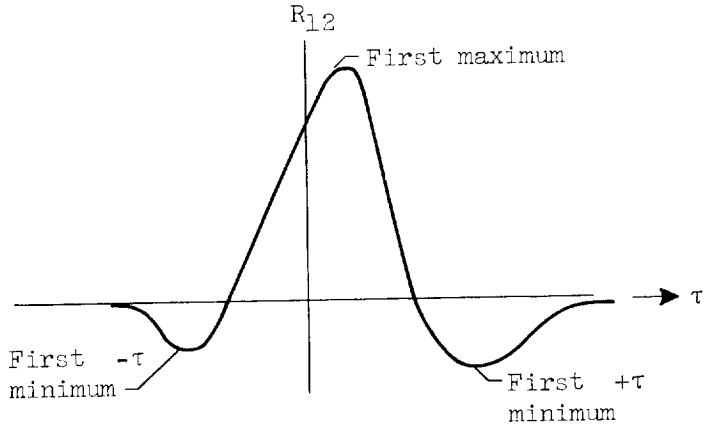

Typical space-time correlogram

(a) Pressure fluctuations

s/w	Location of fixed microphone, x/D	x-direction of motion of movable microphone	U_k/U_c		
			First maximum	First $+\tau$ minimum	First $-\tau$ minimum
0.94	2.0	Increasing	0.553	0.490	0.519
	4.0	Increasing	.385	.517	-----
	2.0	Decreasing	.387	.492	.468
1.44	2.0	Increasing	0.278	0.424	0.541
	4.0	Increasing	.383	.448	-----
	2.0	Decreasing	.368	.434	.358
1.97	2.0	Increasing	0.468	0.473	0.544
	4.0	Increasing	.370	.458	-----
	2.0	Decreasing	.373	.486	.553
2.44	2.0	Increasing	0.358	0.441	0.544
	4.0	Increasing	.336	.256	.392
	2.0	Decreasing	.393	.486	.453
3.00	4.0	Increasing	0.383	0.344	0.344

(b) Velocity fluctuations

s/w	Location of fixed wire, x/D	x-direction of motion of movable wire	U_k/U_l		
			U_l at fixed wire	U_l at movable wire	Average
3.00	2.0	Increasing	0.974	0.894	0.934
	4.0	Increasing	.822	.998	.910
	2.0	Decreasing	.813	.861	.837
	4.0	Decreasing	.822	.934	.878

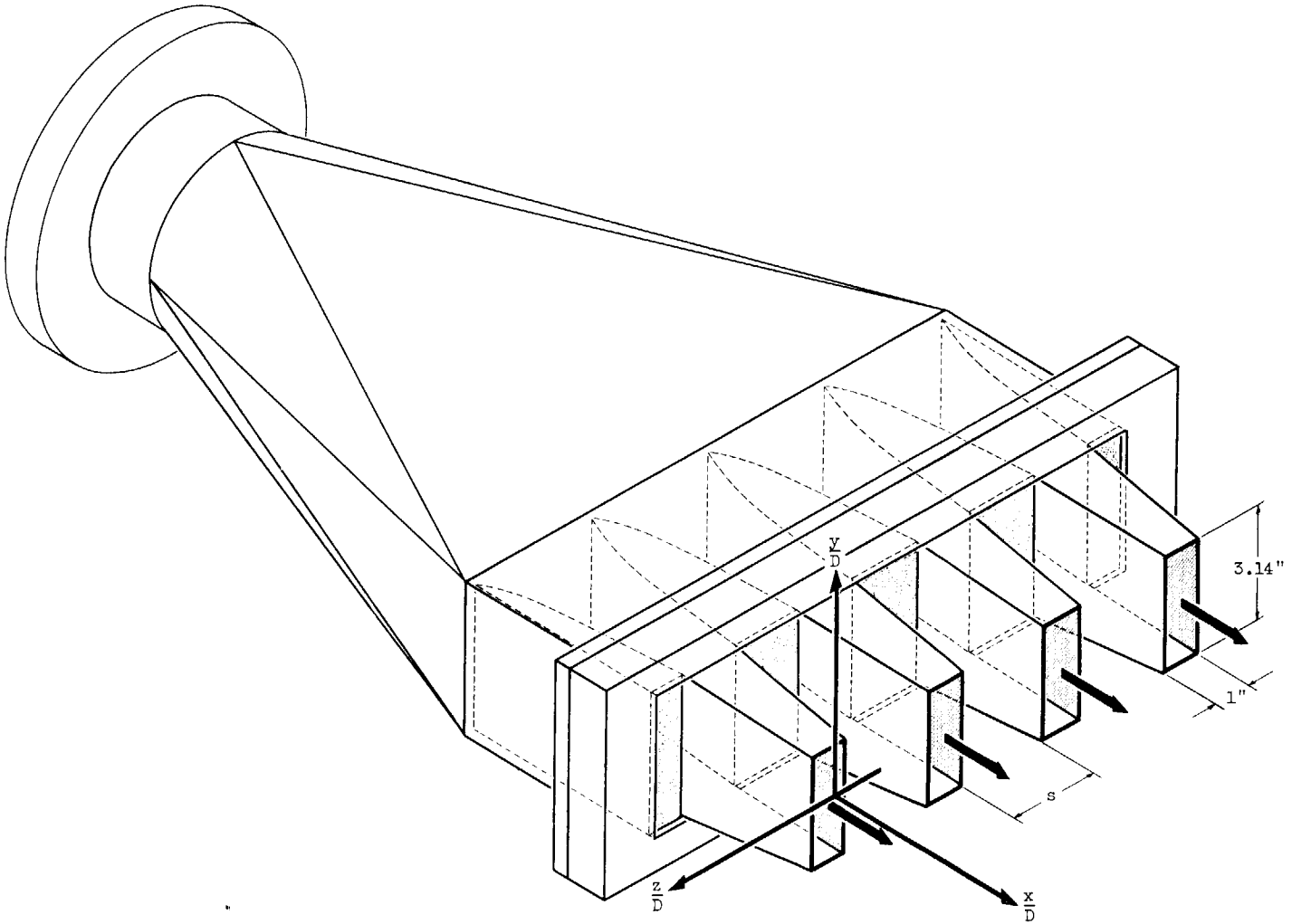

(a) Sketch.

CD-6931

Figure 1. - Rectangular slotted nozzle.

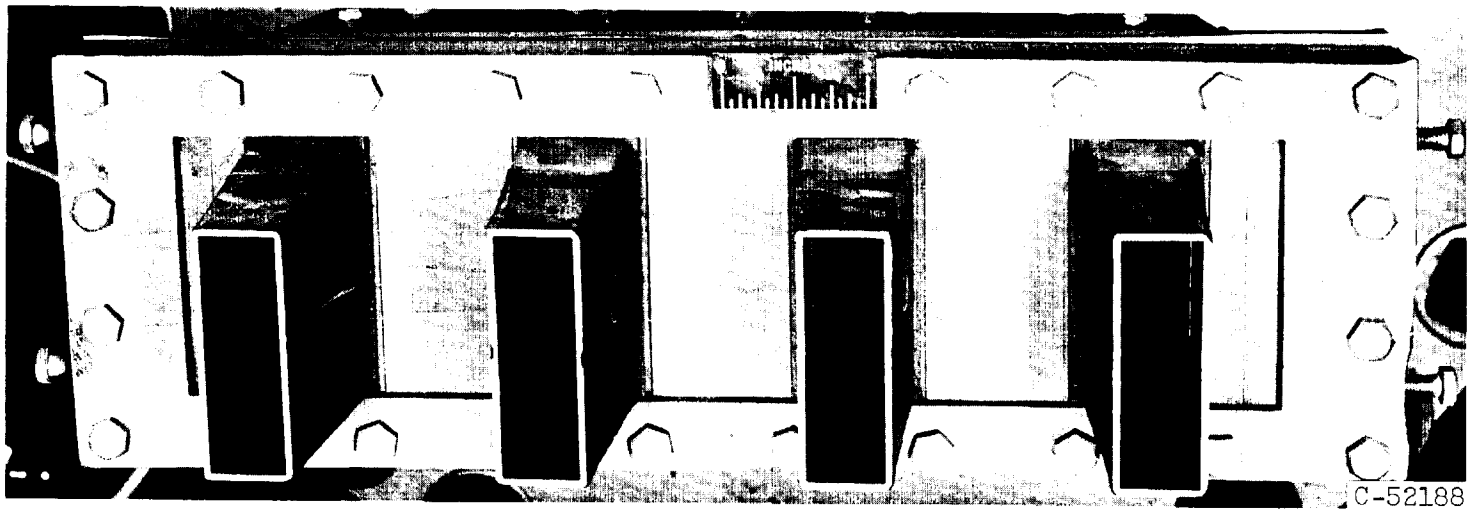

(b) Photograph.

Figure 1. - Concluded. Rectangular slotted nozzle.

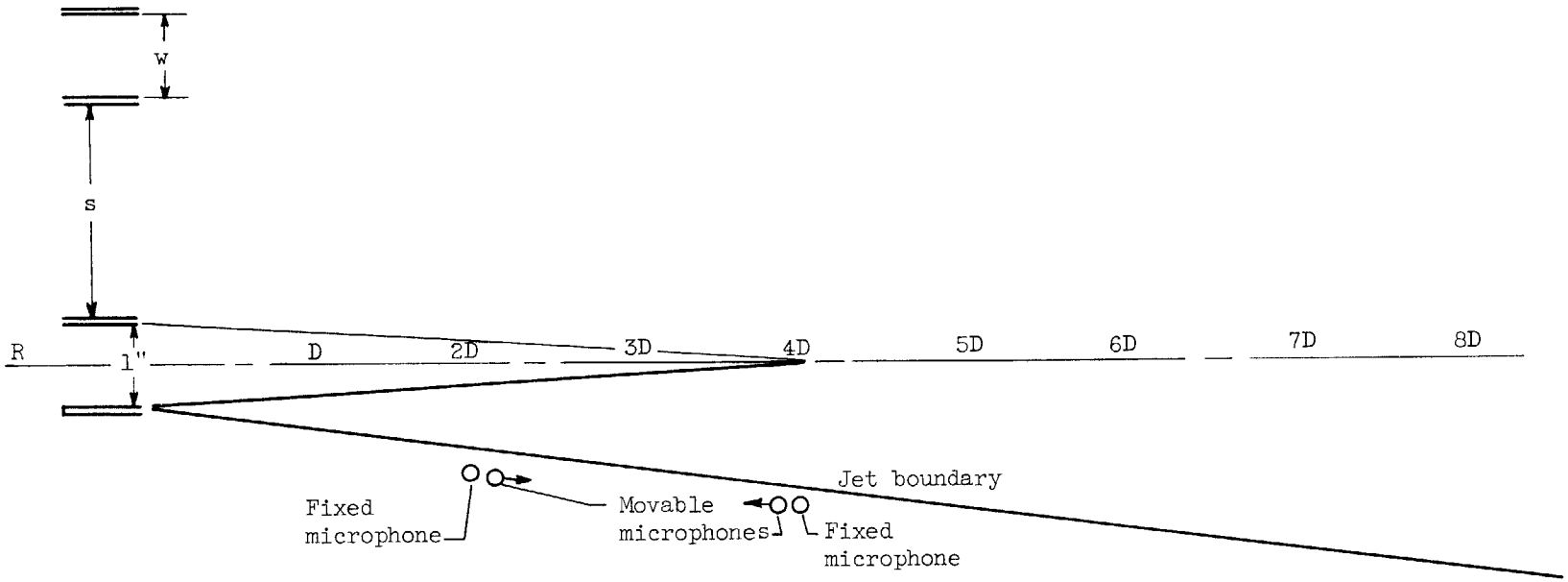

Figure 2. - Microphone measurement stations for pressure cross correlations.

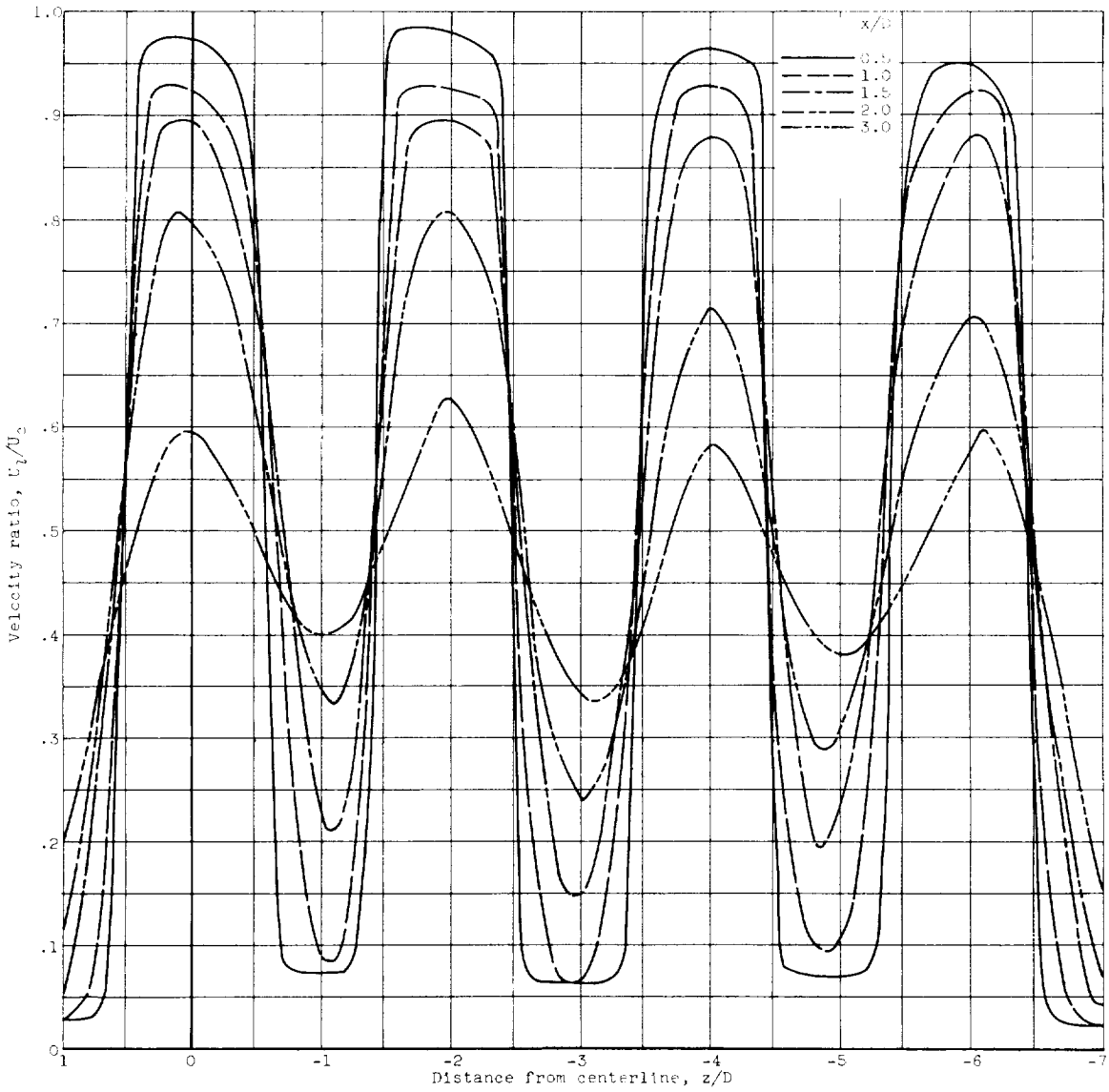

Figure 3. - Flow field of rectangular slotted nozzle. y/D = 0; s/w = 0.94.

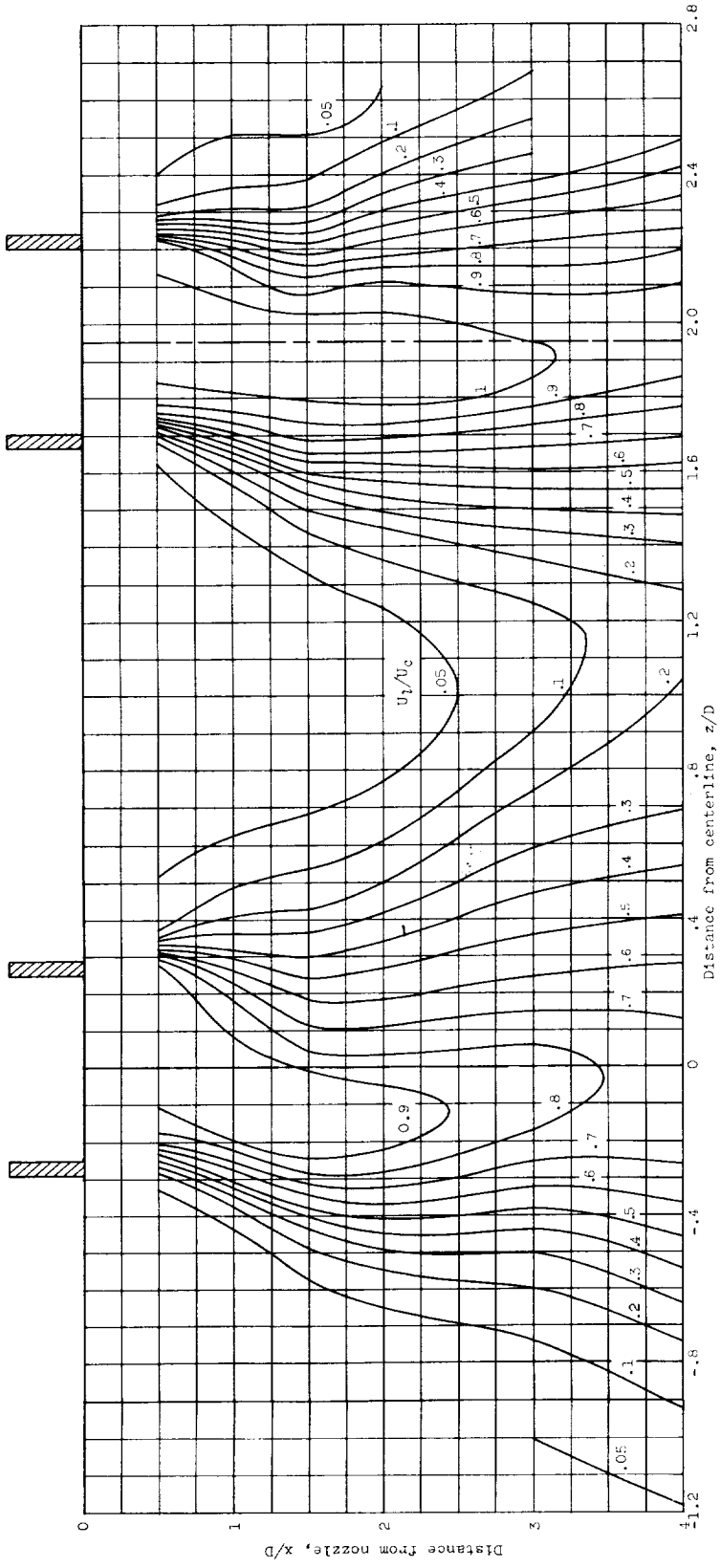

(a) s/w = 3.0.

Figure 4. - Mean velocity contours.

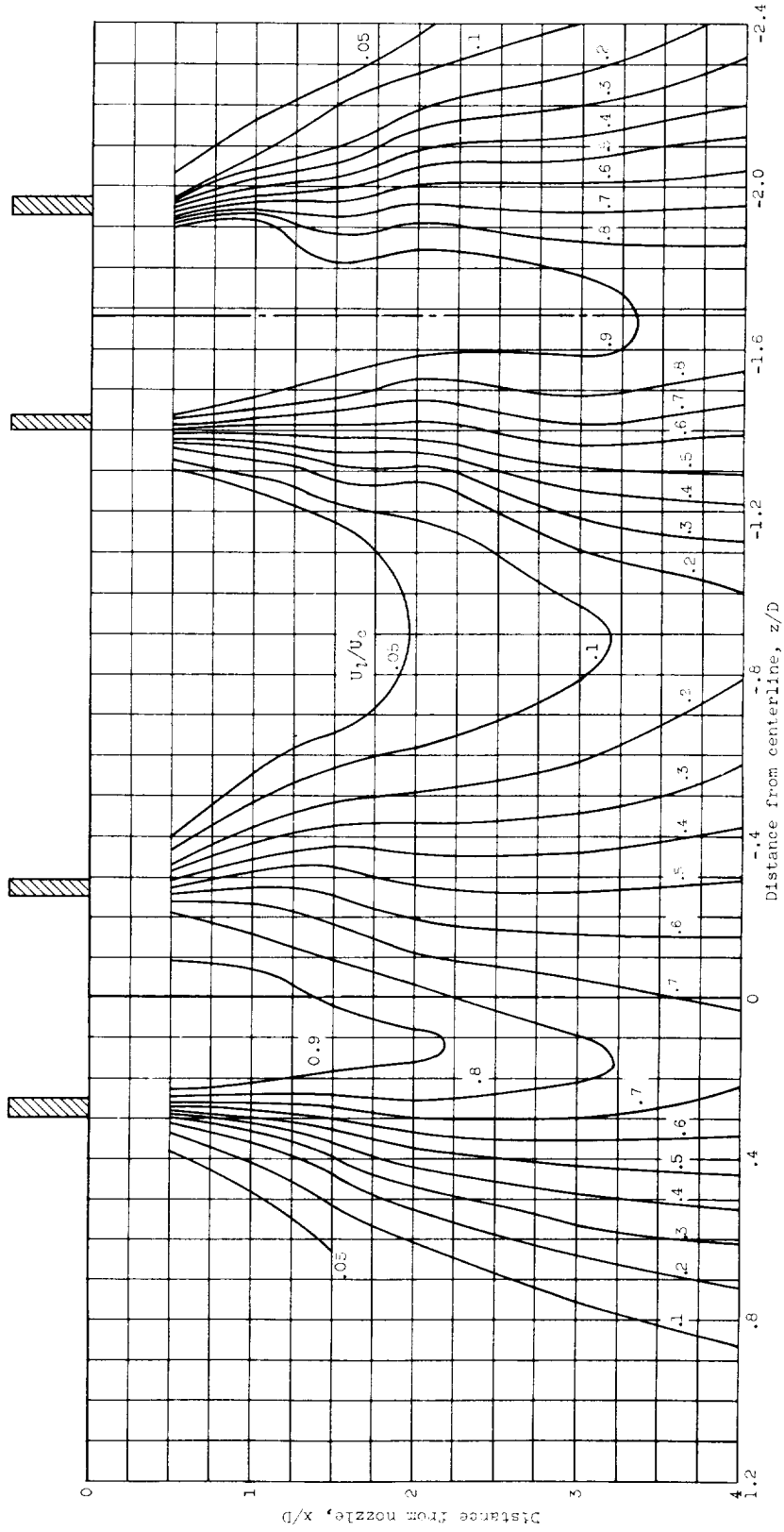

(b) s/w = 2.44.

Figure 4. - Continued. Mean velocity contours.

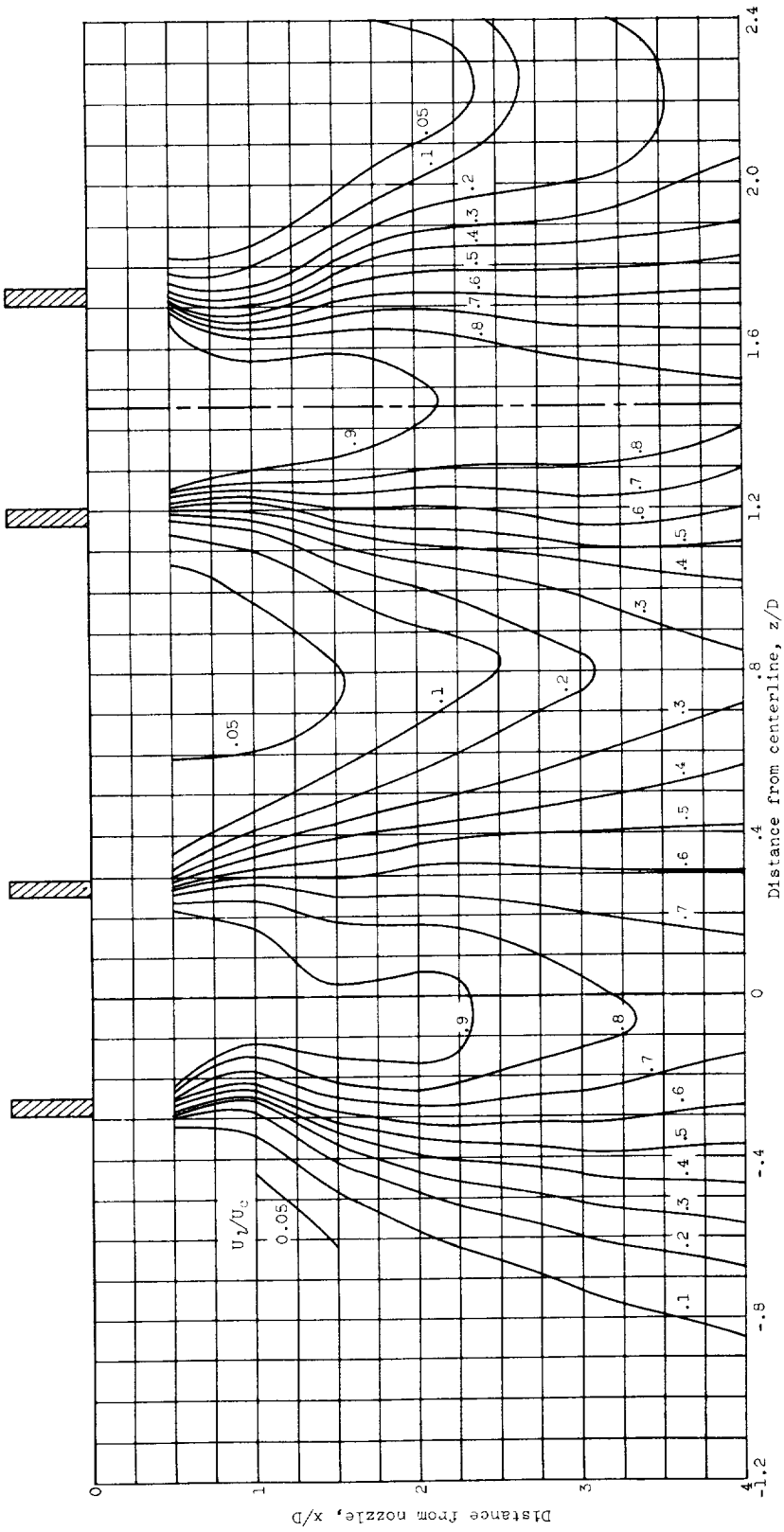

(c) s/w = 1.97.

Figure 4. - Continued. Mean velocity contours.

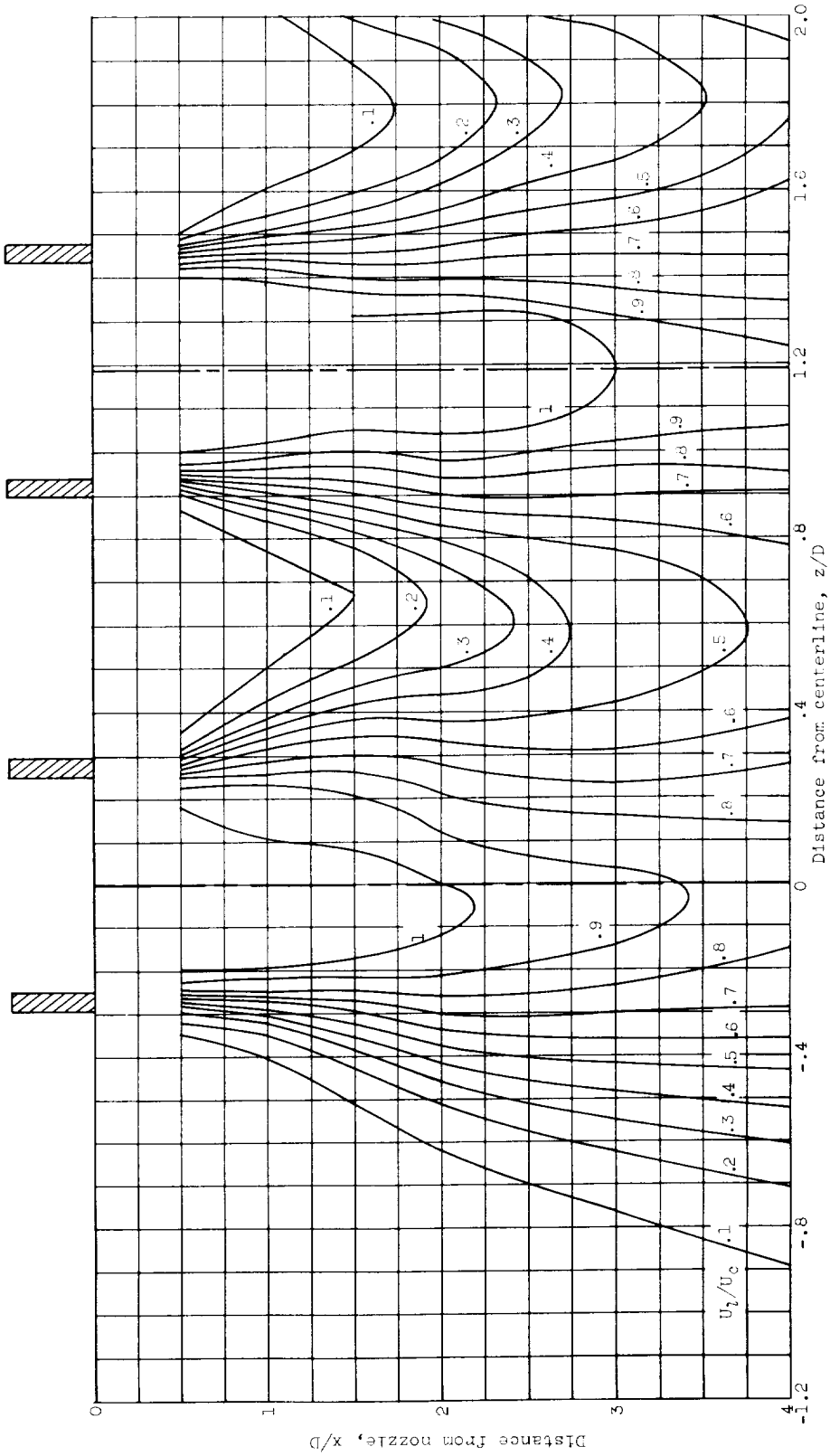

(d) s/w = 1.44.

Figure 4. - Continued. Mean velocity profiles.

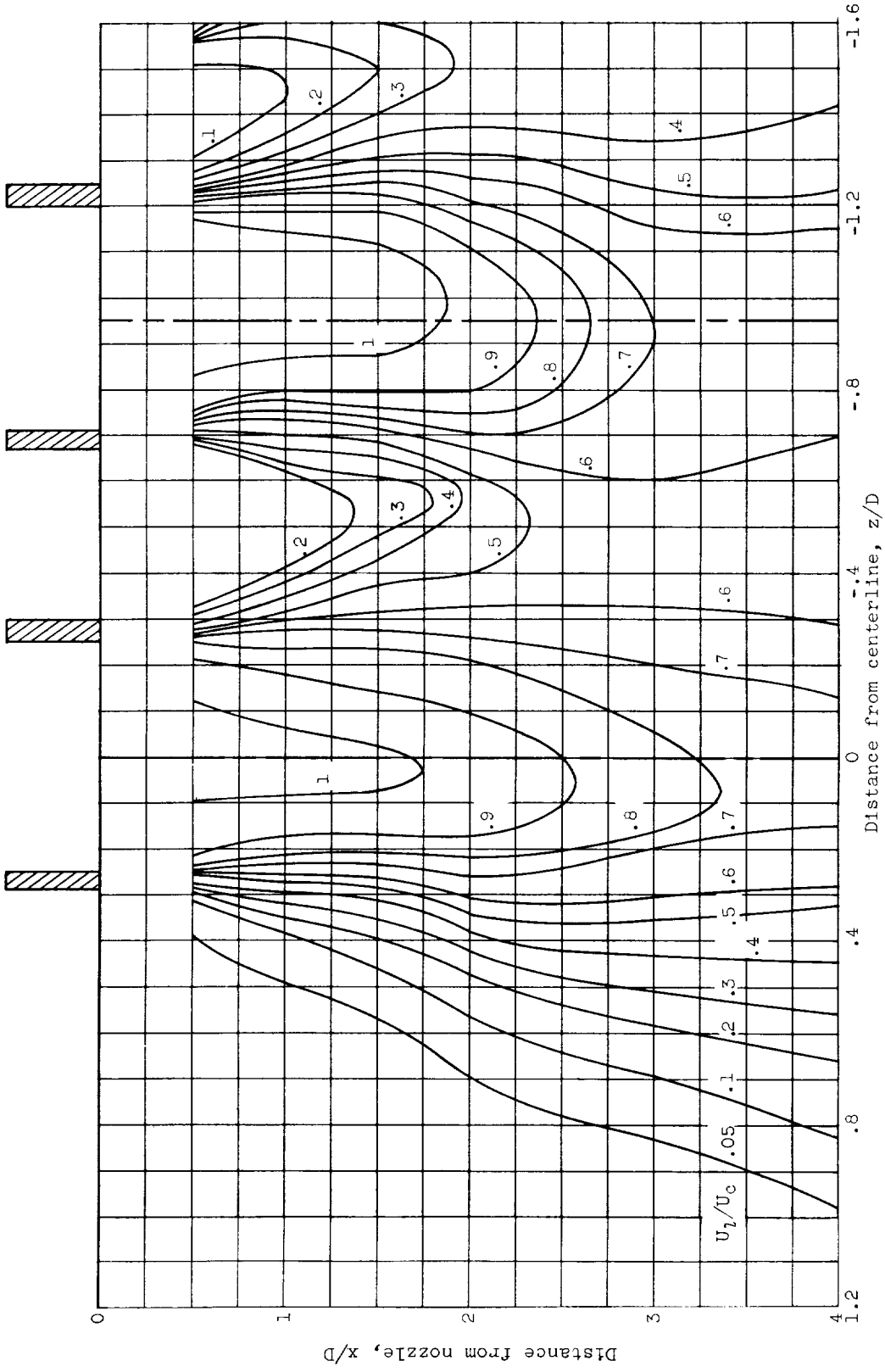

(e) s/w = 0.94.

Figure 4. - Concluded. Mean velocity contours.

E-384

CC-5 back

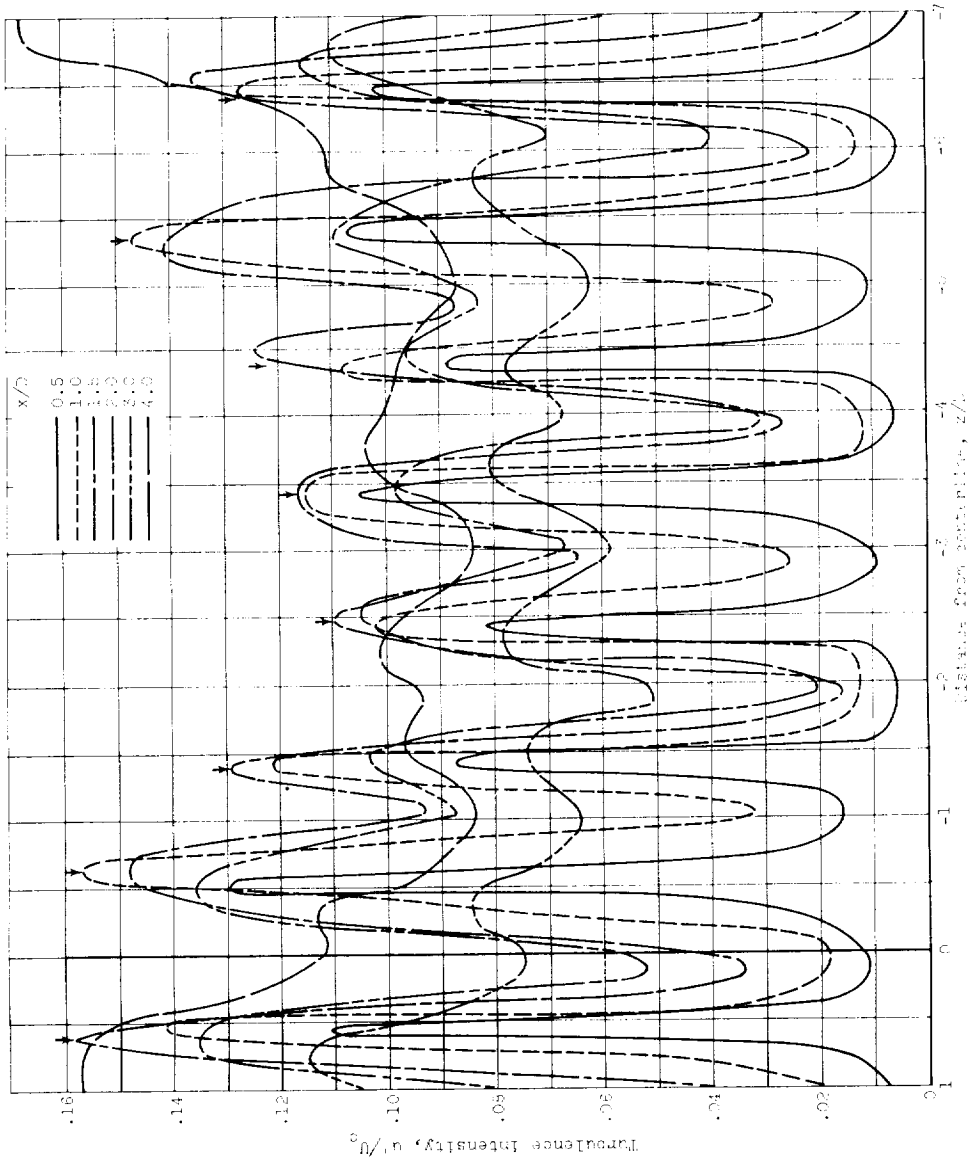

Figure 8. - Turbulence intensity on cross, x/h = 3.0; x/D = 4.0.

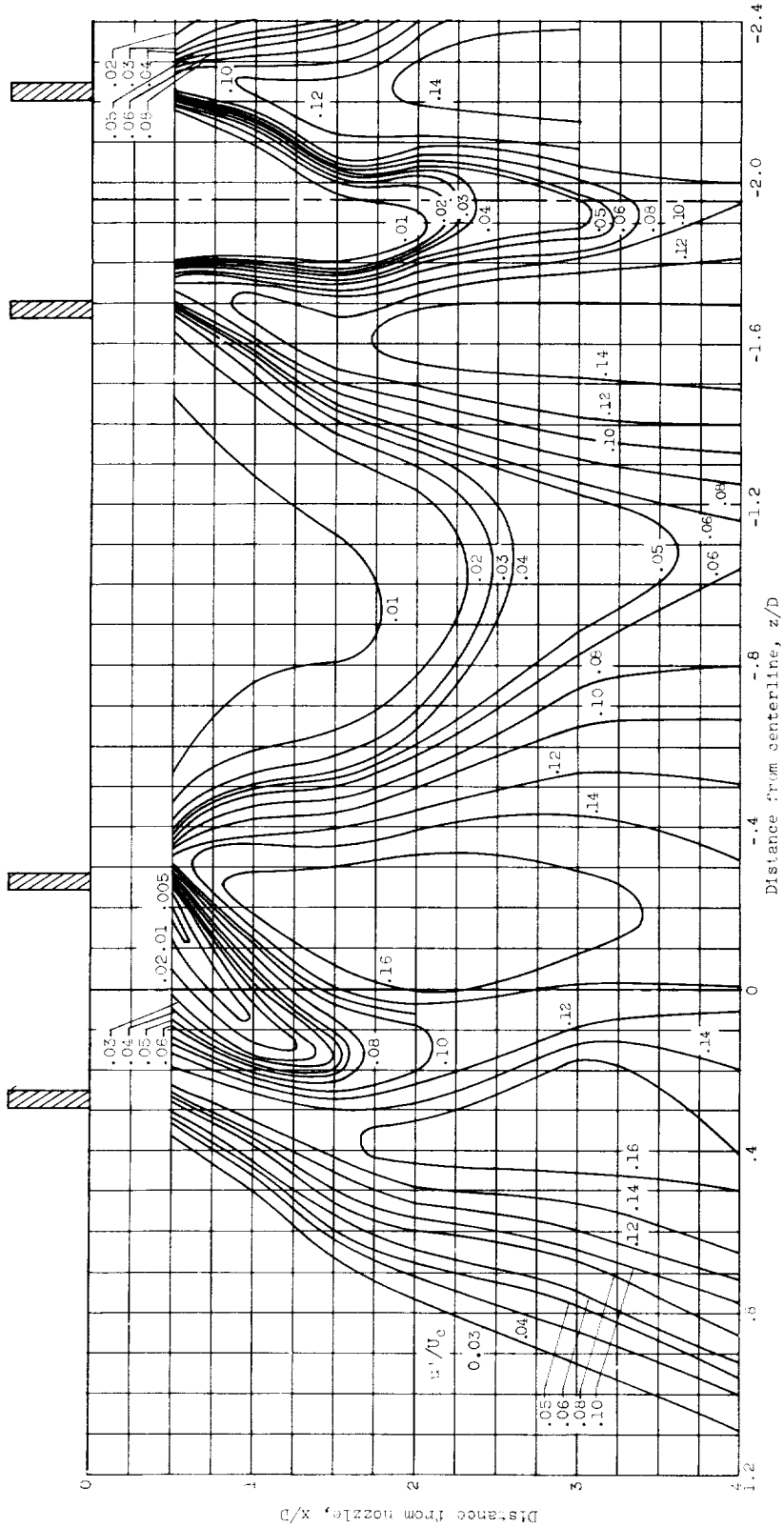

(a) s/x = 3.00.

Figure 6. - Turbulence intensity contours.

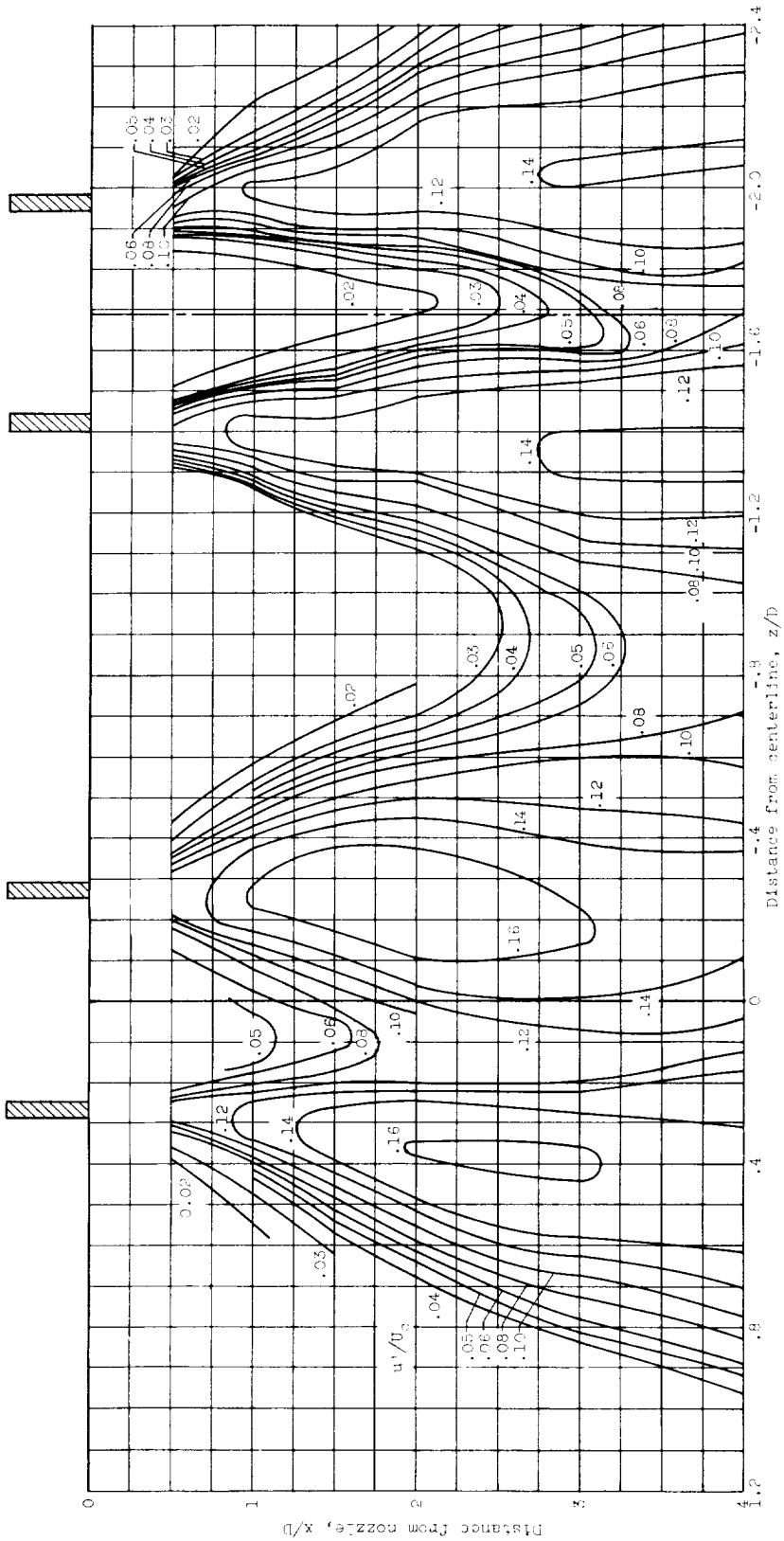

(b) s/w = 2.44.

Figure 6. - Continued. Turbulence intensity contours.

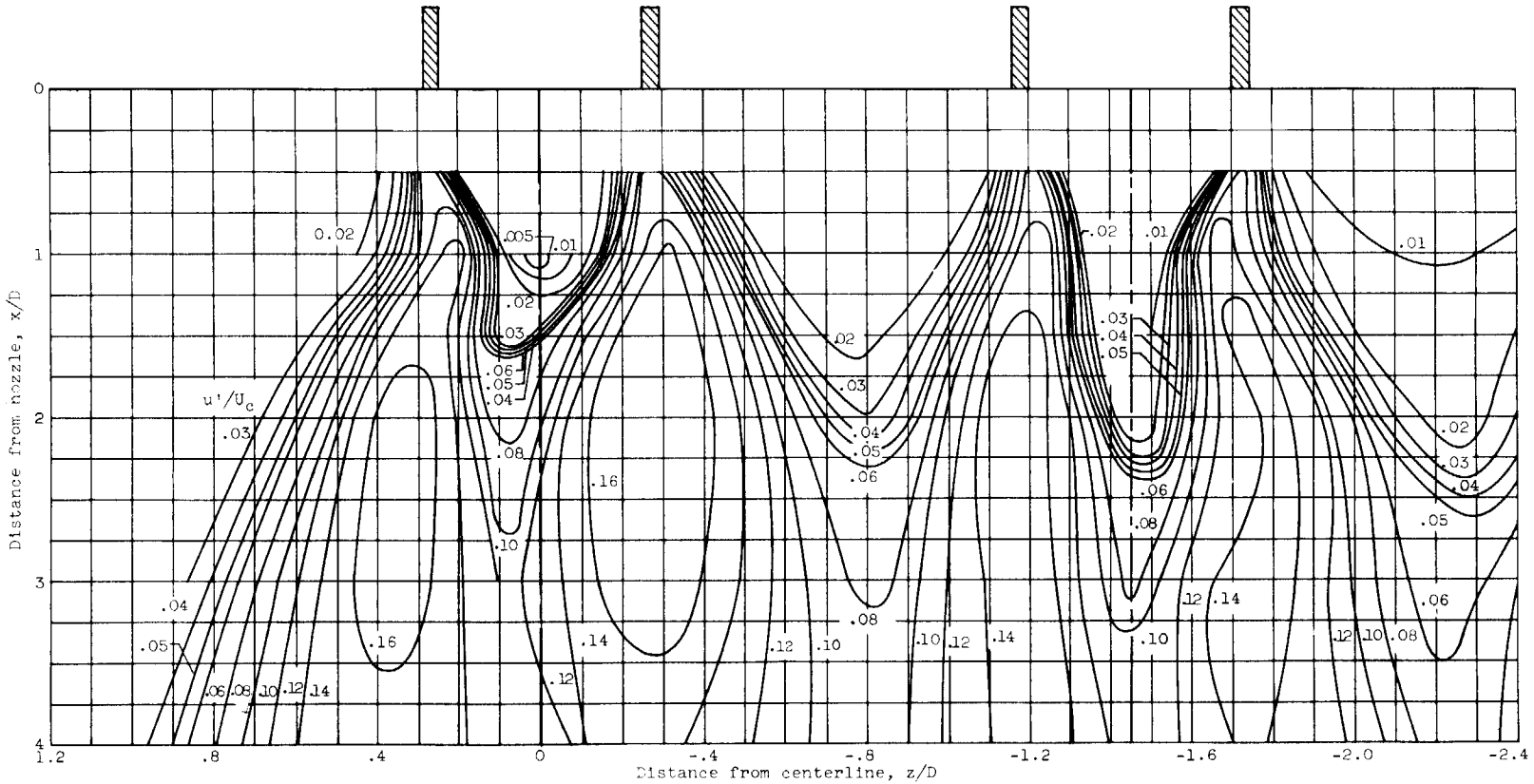

(c) s/w = 1.97.

Figure 6. - Continued. Turbulence intensity contours.

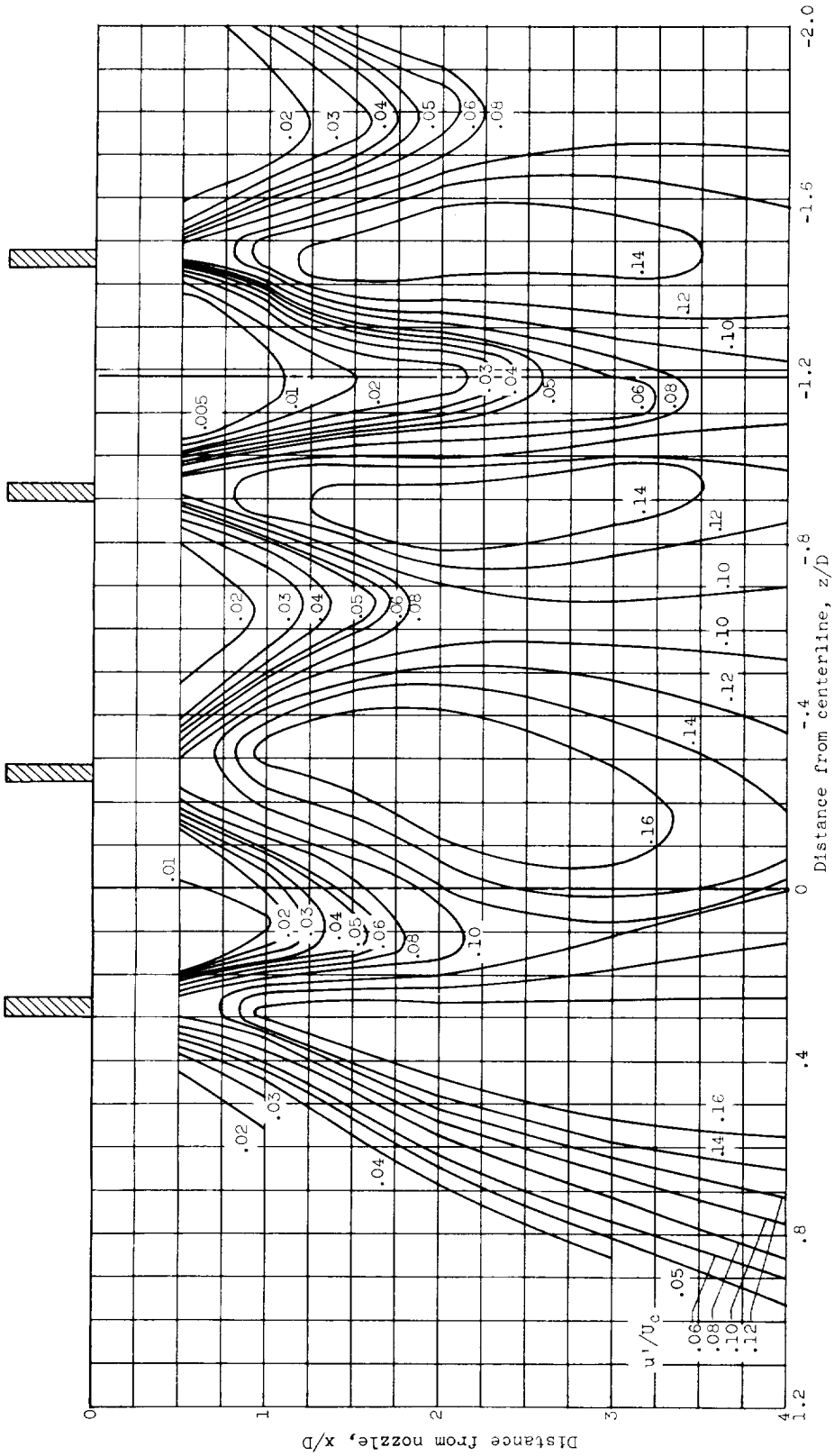

(d) s/w = 1.44.

Figure 6. - Continued. Turbulence intensity contours.

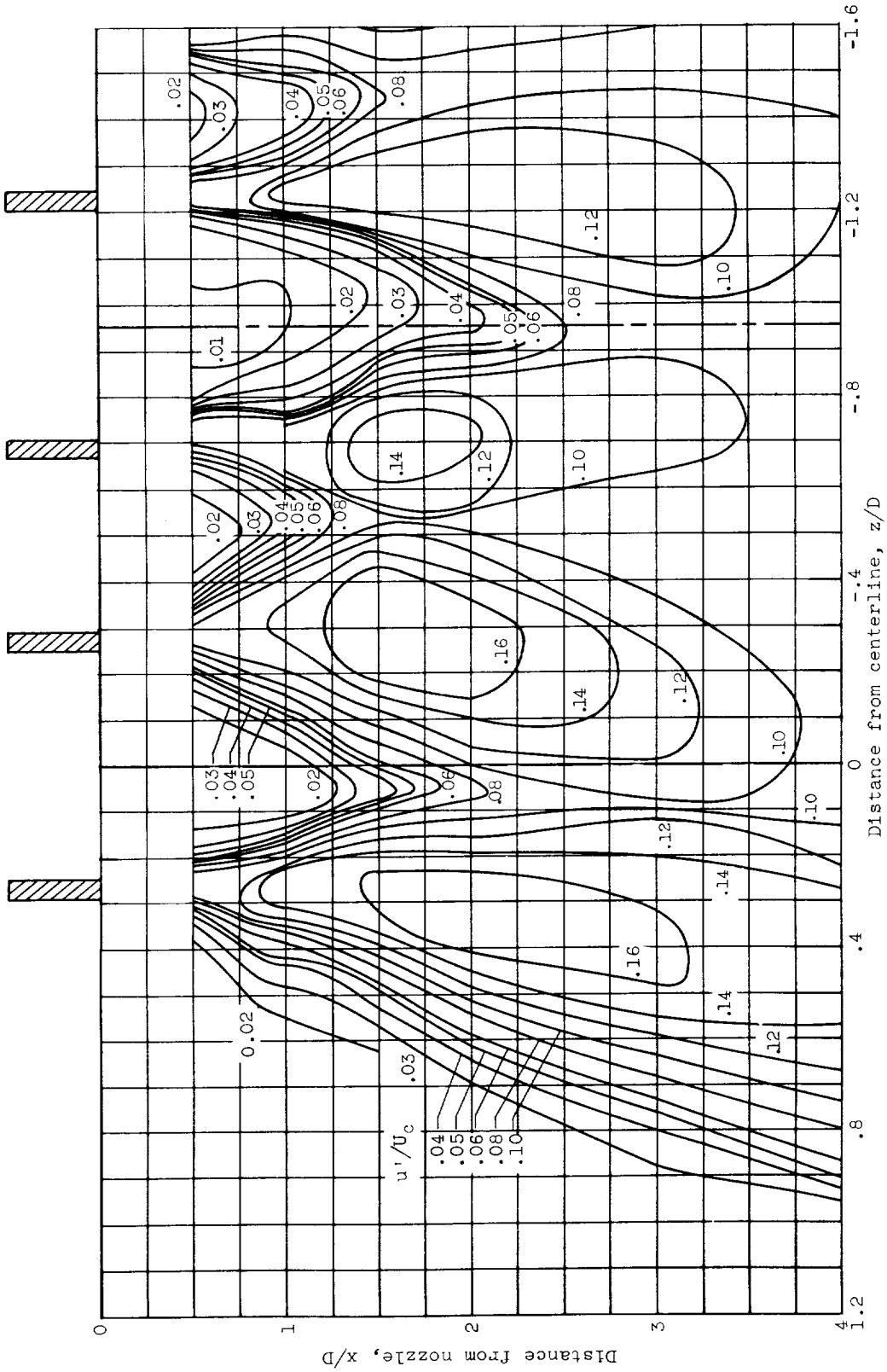

(e) s/w = 0.94.

Figure 6. - Concluded. Turbulence intensity contours.

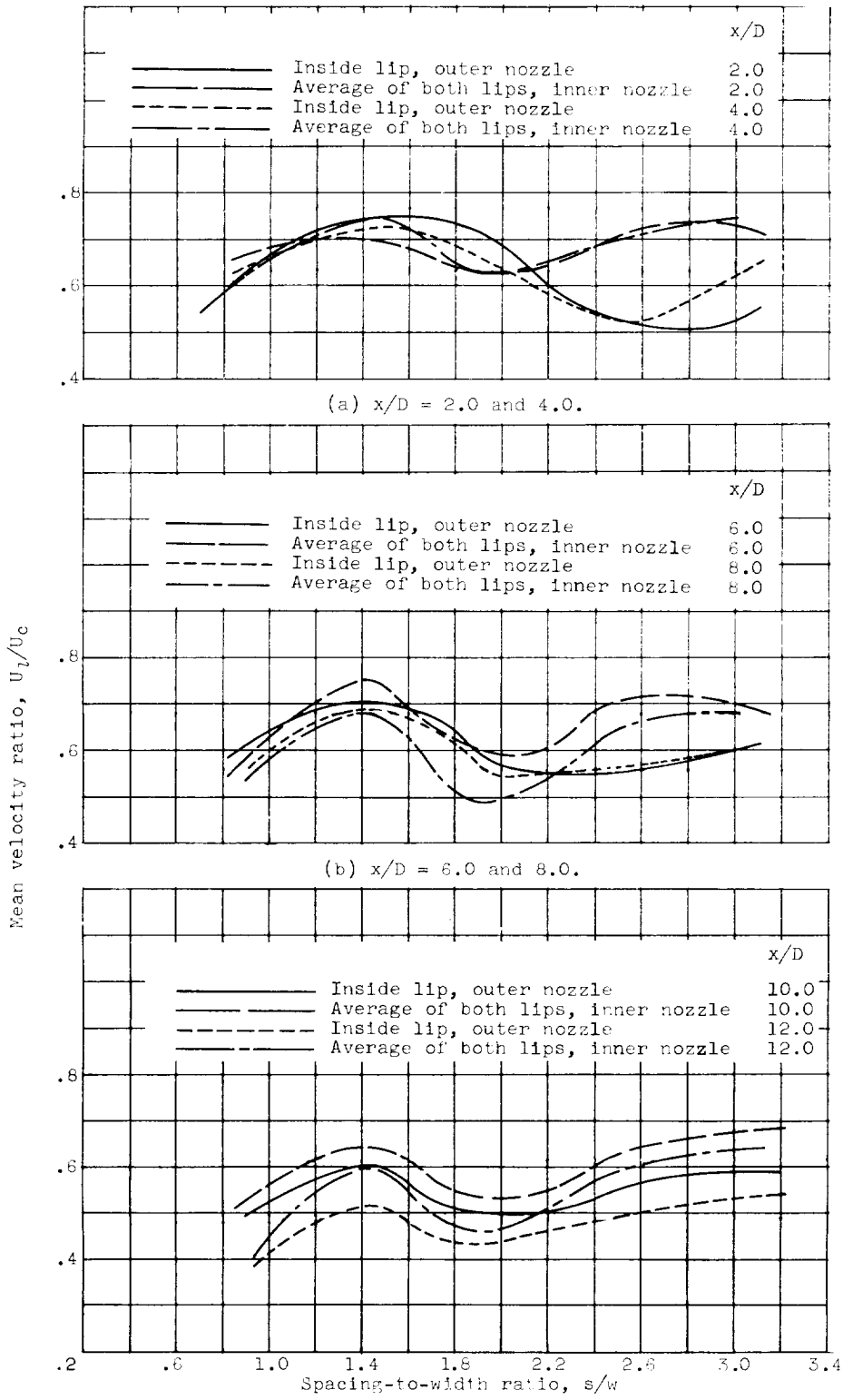

Figure 7. - Mean velocity ratio as function of spacing-to-width ratio.

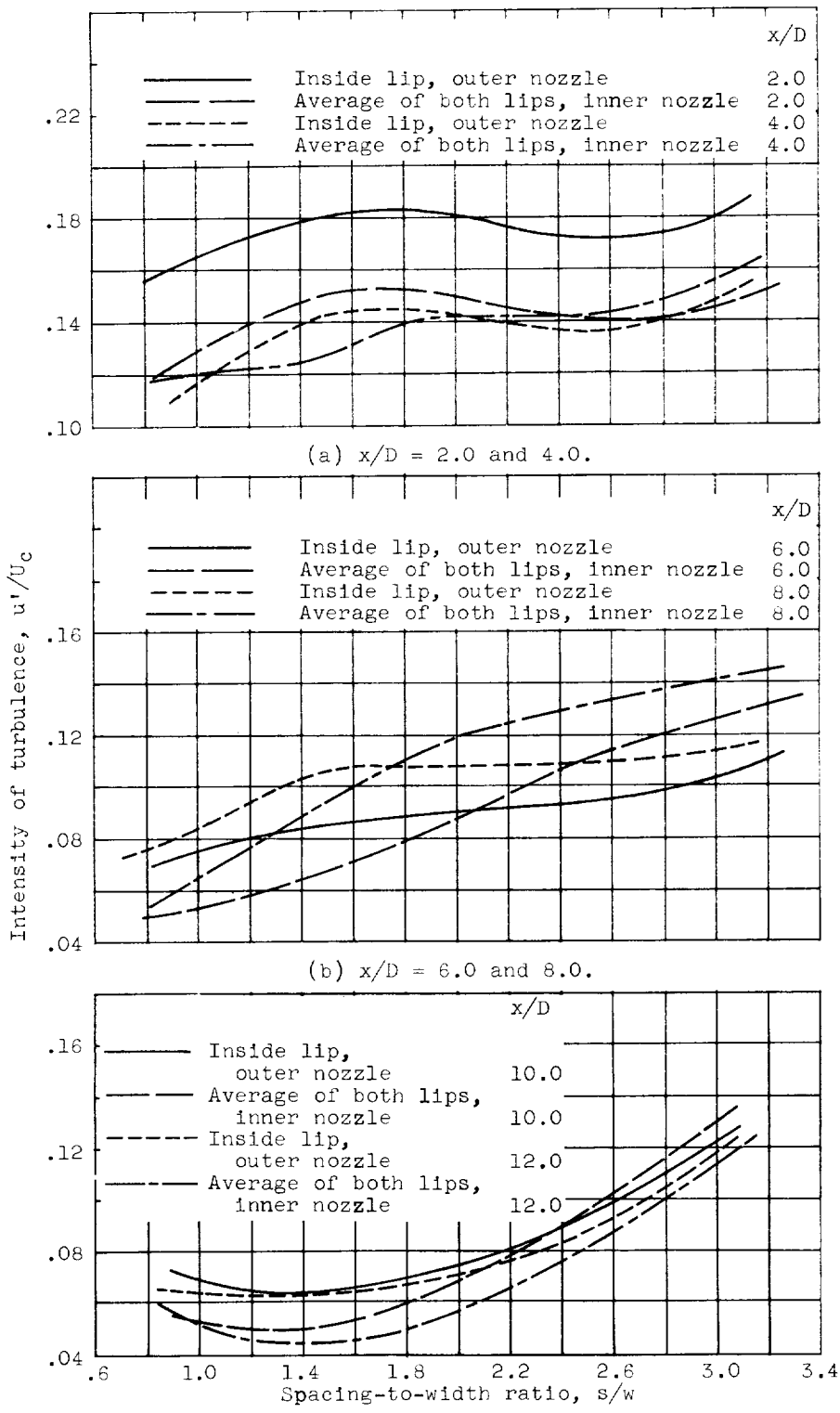

Figure 8. - Intensity of turbulence as function of spacing-to-width ratio.

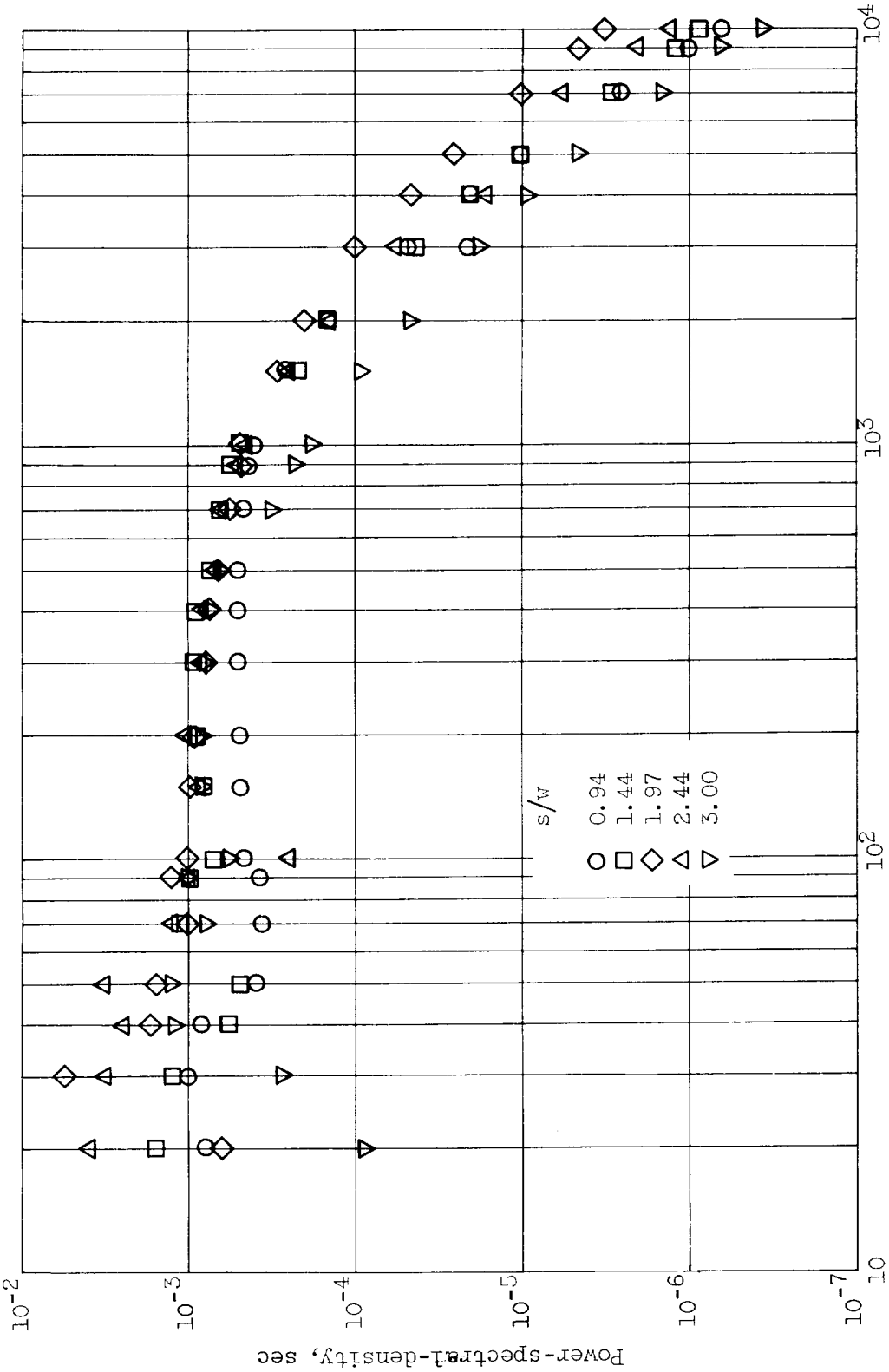

(a) x/D = 2.0; z/D = -0.25.

Figure 9. - Spectral-density curves.

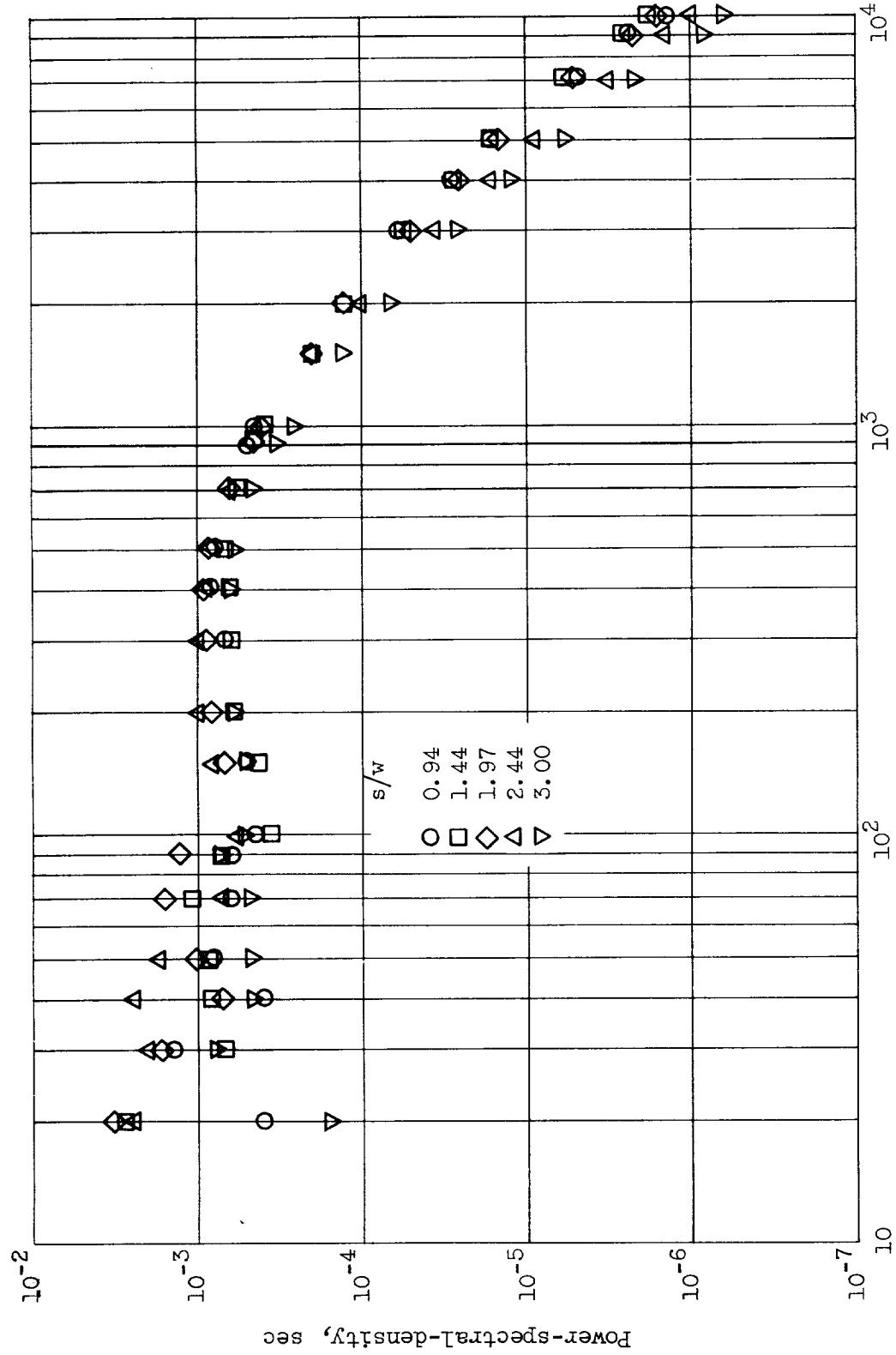

(b) x/D = 4.0; z/D = -0.25.

Figure 9. - Continued. Spectral-density curves.

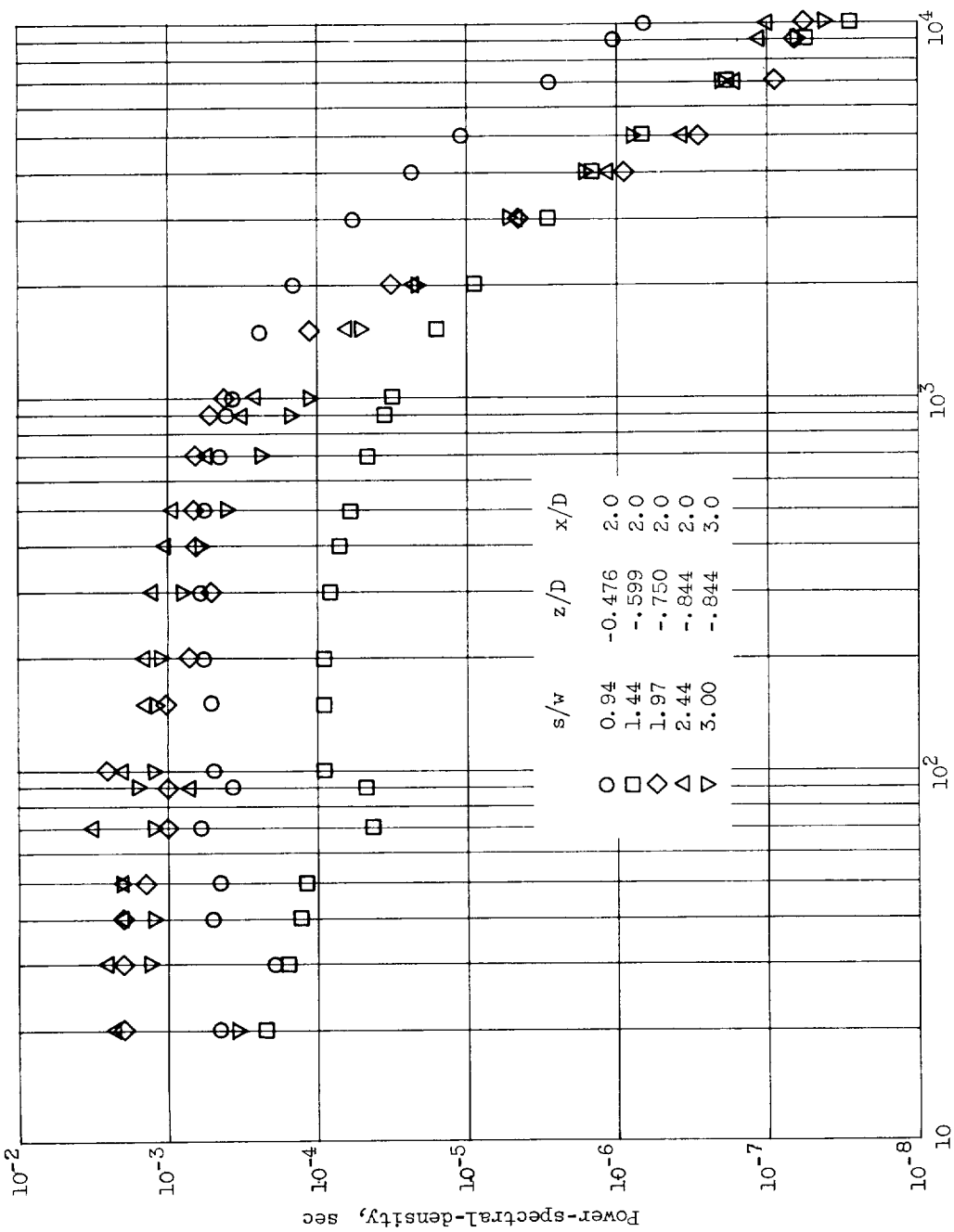

(c) Survey line halfway between outside nozzles. y/D = 0.

Figure 9. - Concluded. Spectral-density curves.

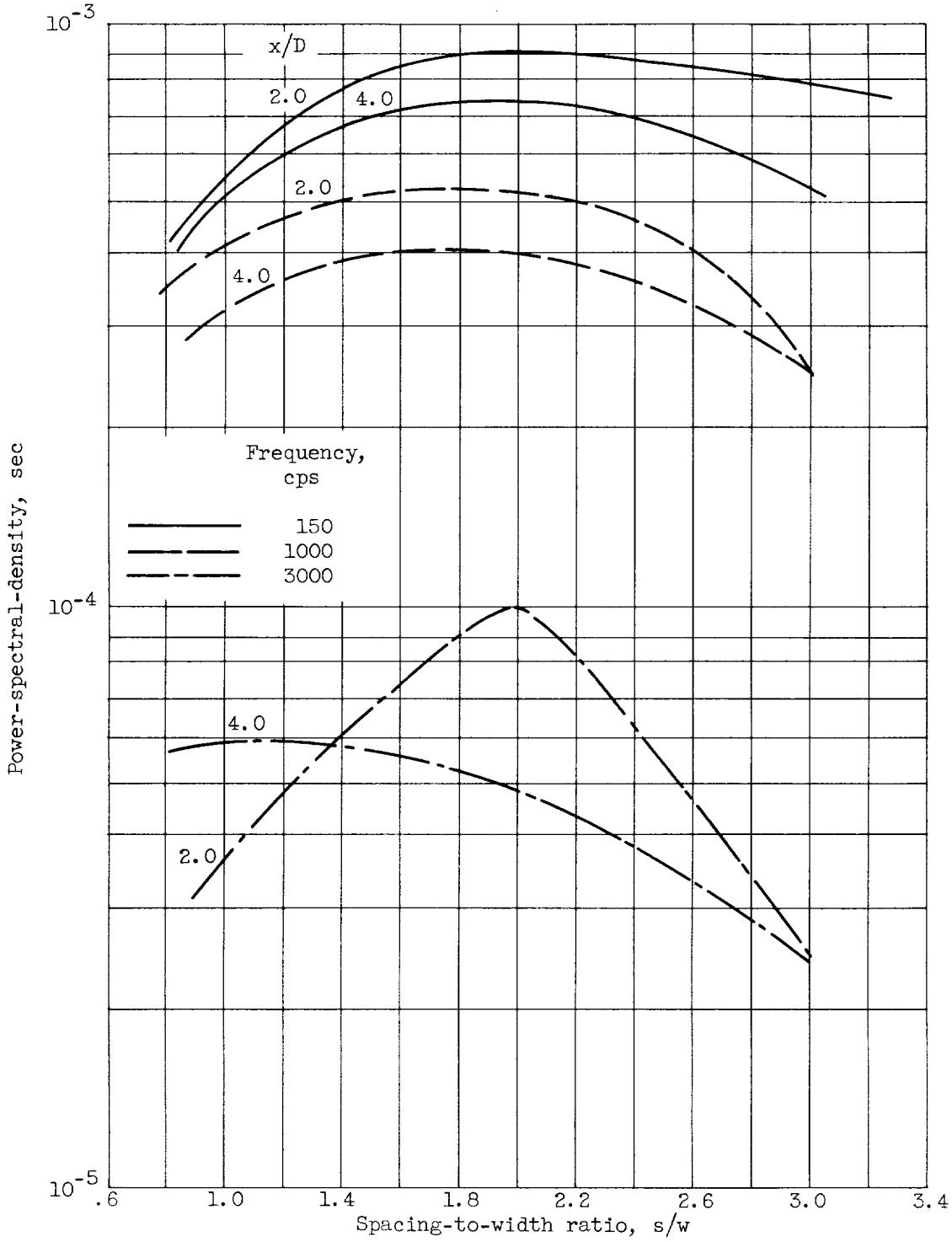

(a) x/D = 2.0 and 4.0.

Figure 10. - Power-spectral-density for specific bands of frequencies as function of spacing-to-width ratio. z/D = -0.25.

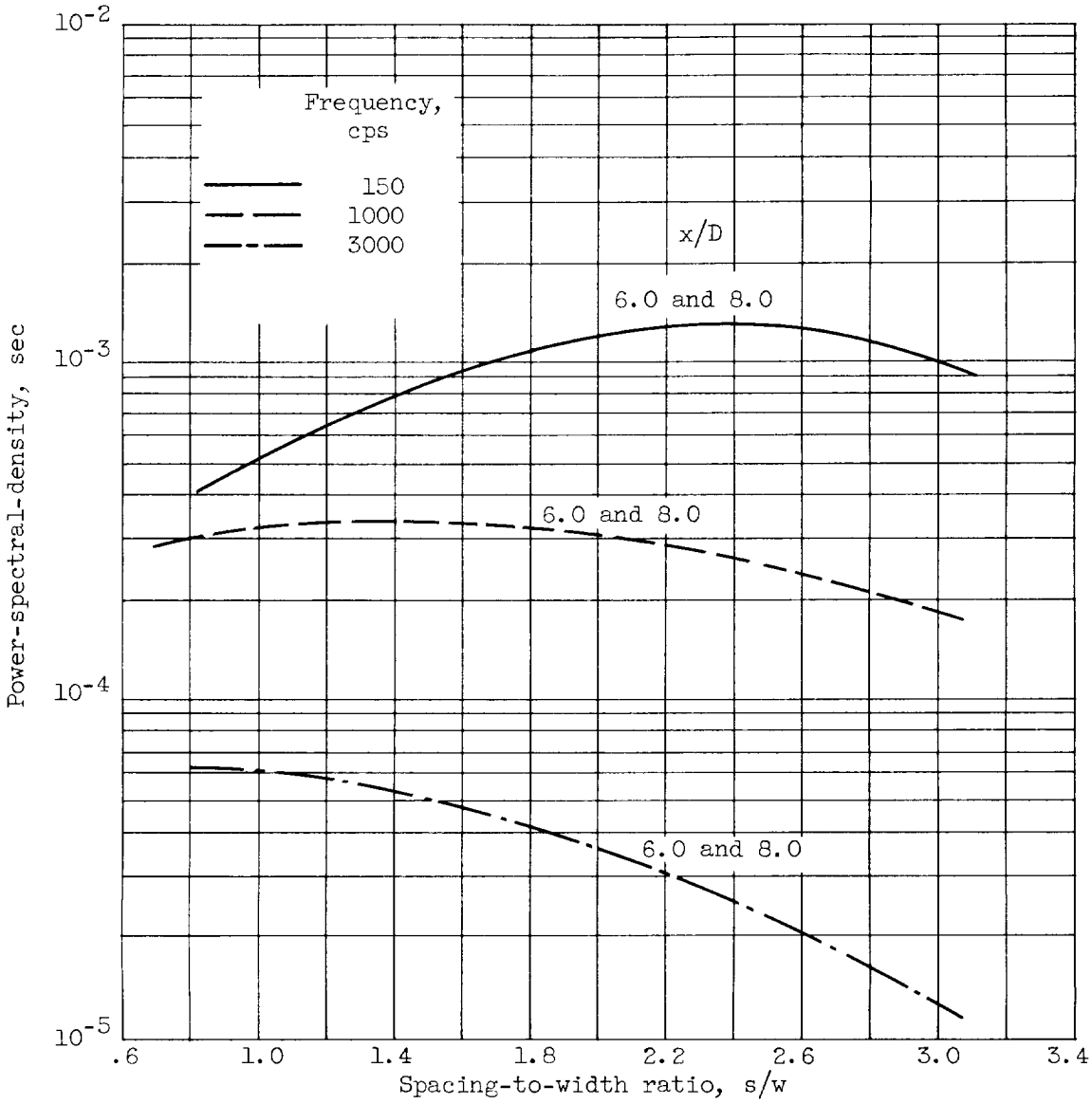

(b) x/D = 6.0 and 8.0.

Figure 10. - Continued. Power-spectral-density for specific bands of frequencies as function of spacing-to-width ratio. z/D = -0.25.

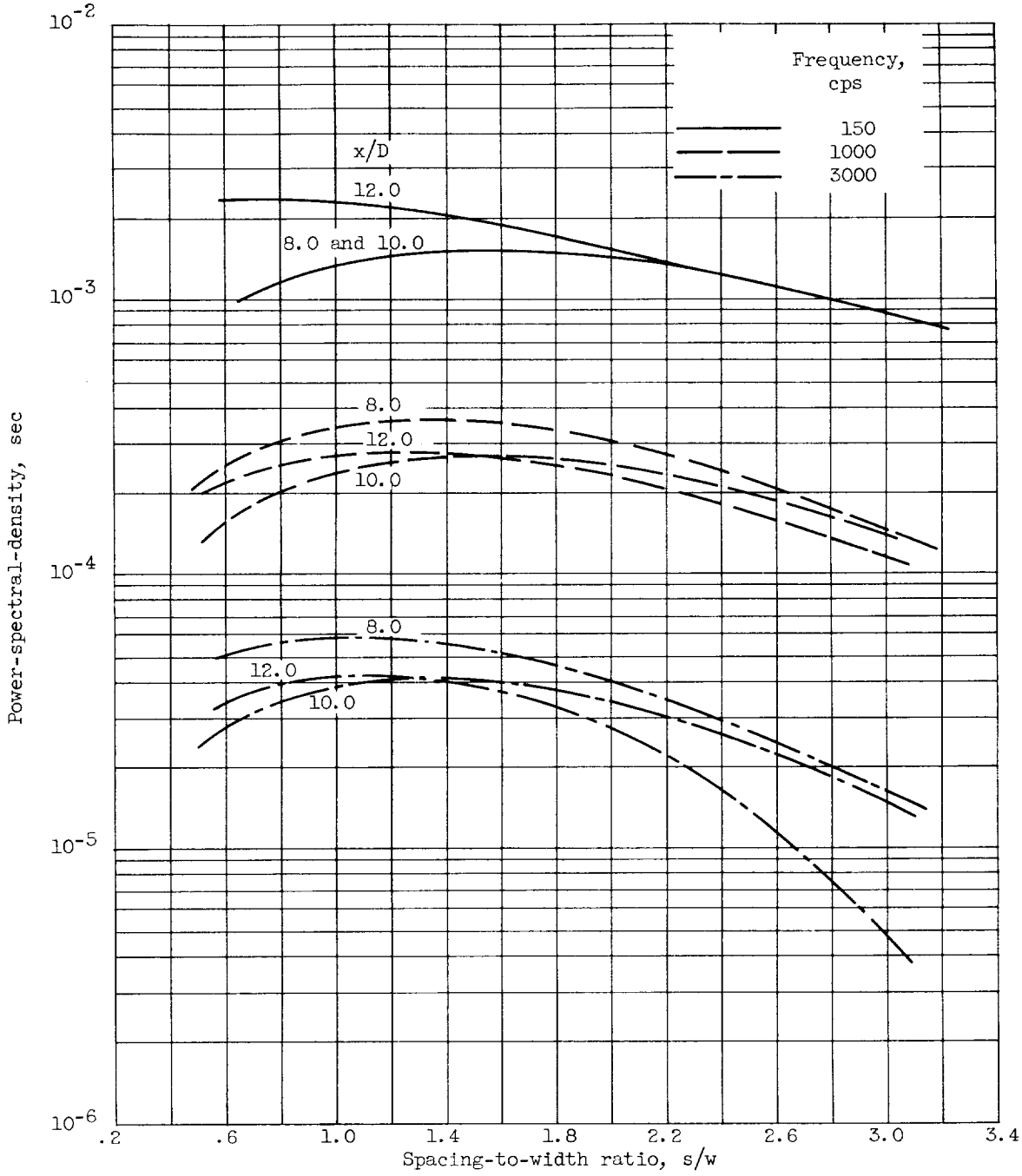

(c) x/D = 8.0, 10.0, and 12.0.

Figure 10. - Concluded. Power-spectral-density for specific bands of frequencies as function of spacing-to-width ratio. z/D = -0.25.

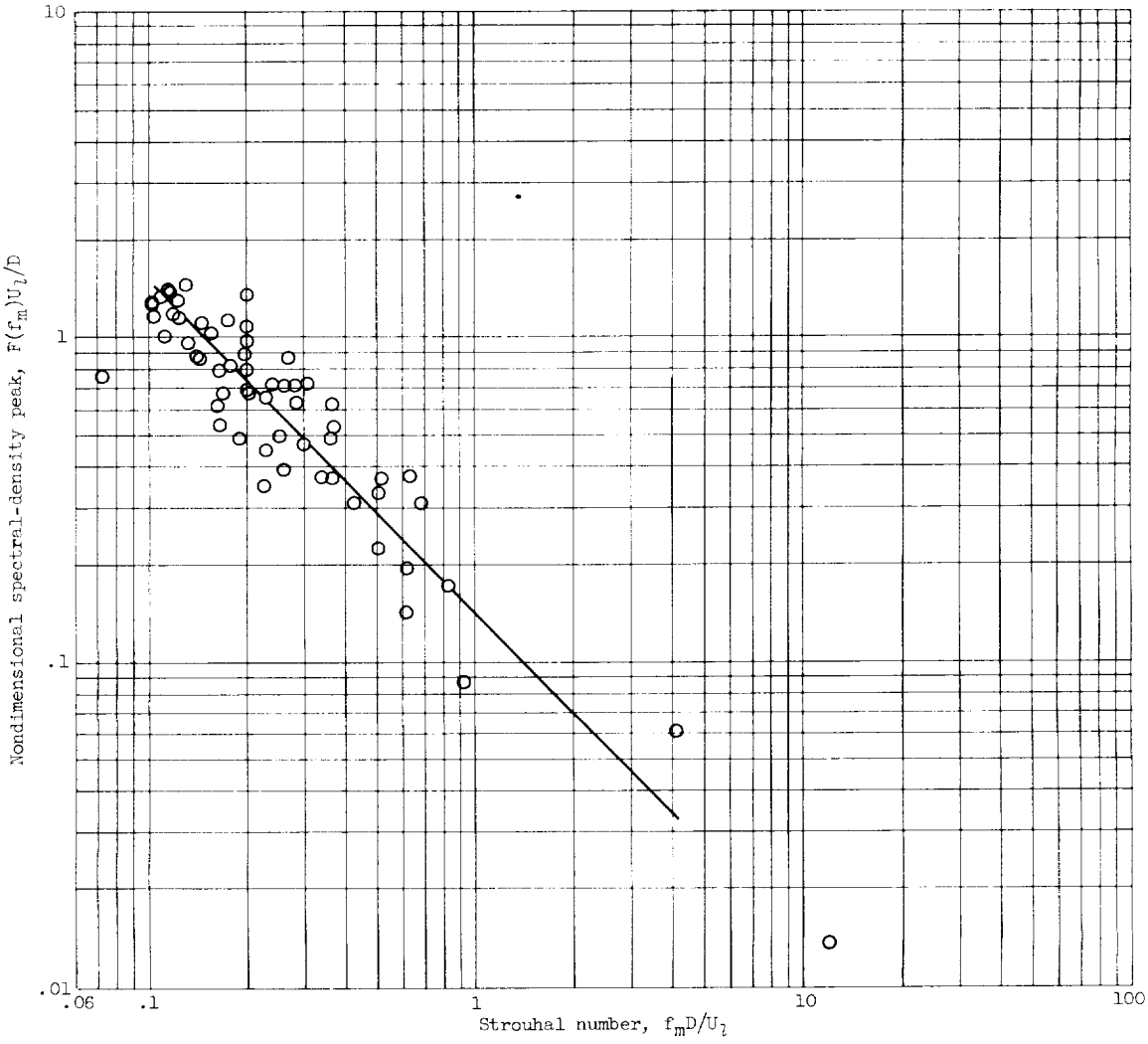

(a) s/w = 3.00.

Figure 11. - Relation of peak turbulent energy per cycle to frequency. All x/D, z/D, but y/D = 0.

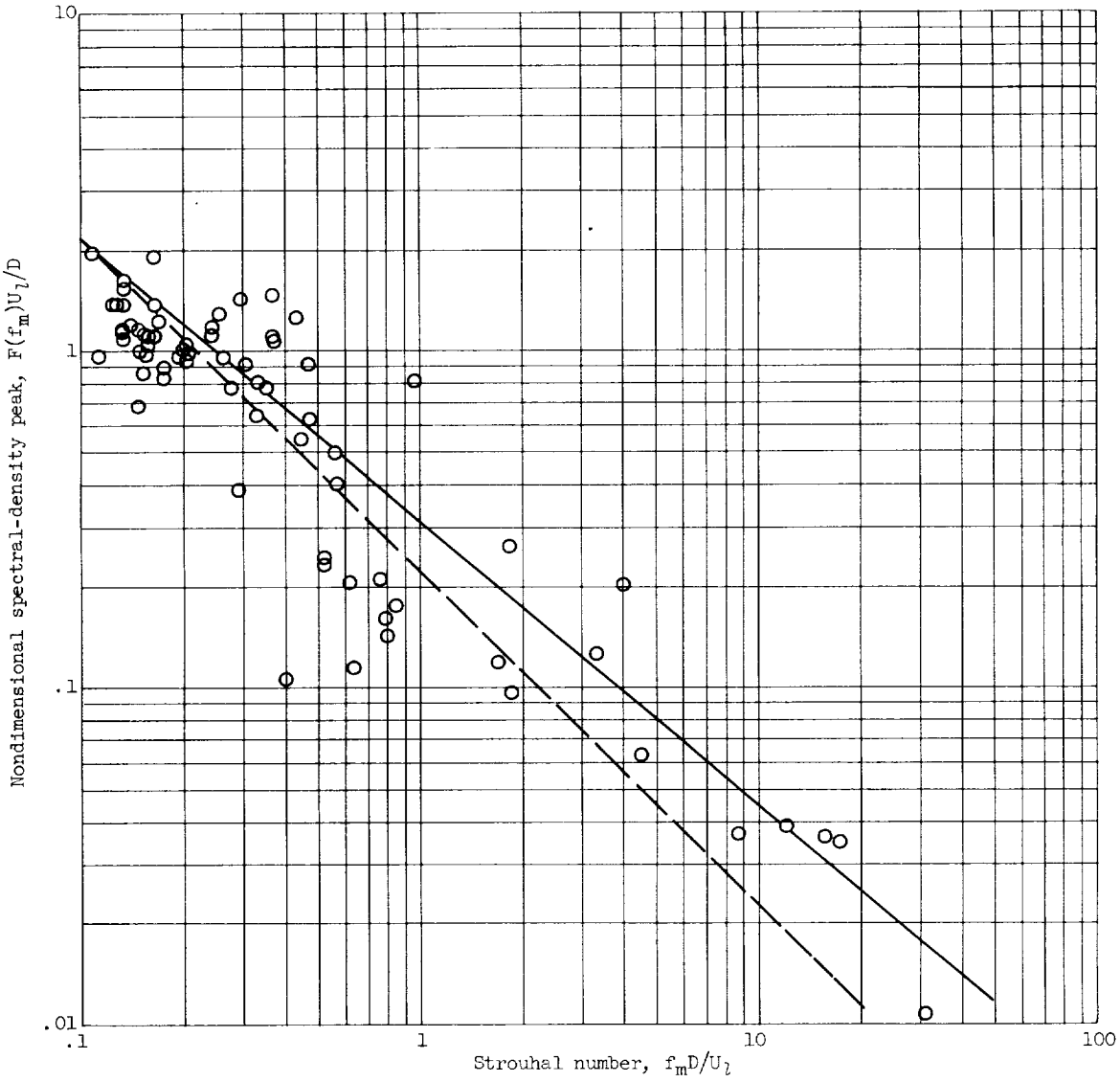

(b) s/w = 2.44.

Figure 11. - Continued. Relation of peak turbulent energy per cycle to frequency. All x/D, z/D, but y/D = 0.

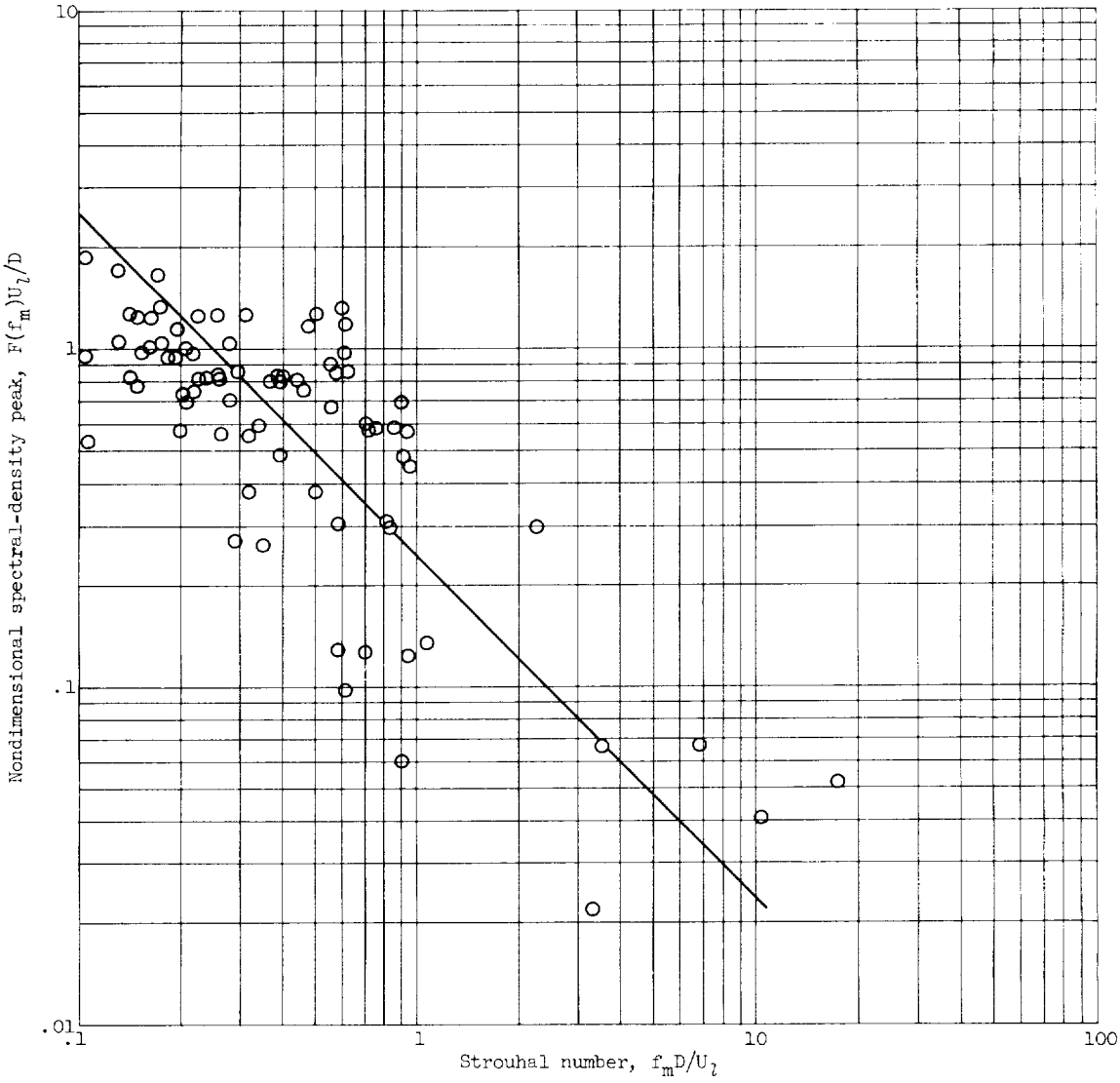

(c) s/w = 1.97.

Figure 11. - Continued. Relation of peak turbulent energy per cycle to frequency. All x/D, z/D, but y/D = 0.

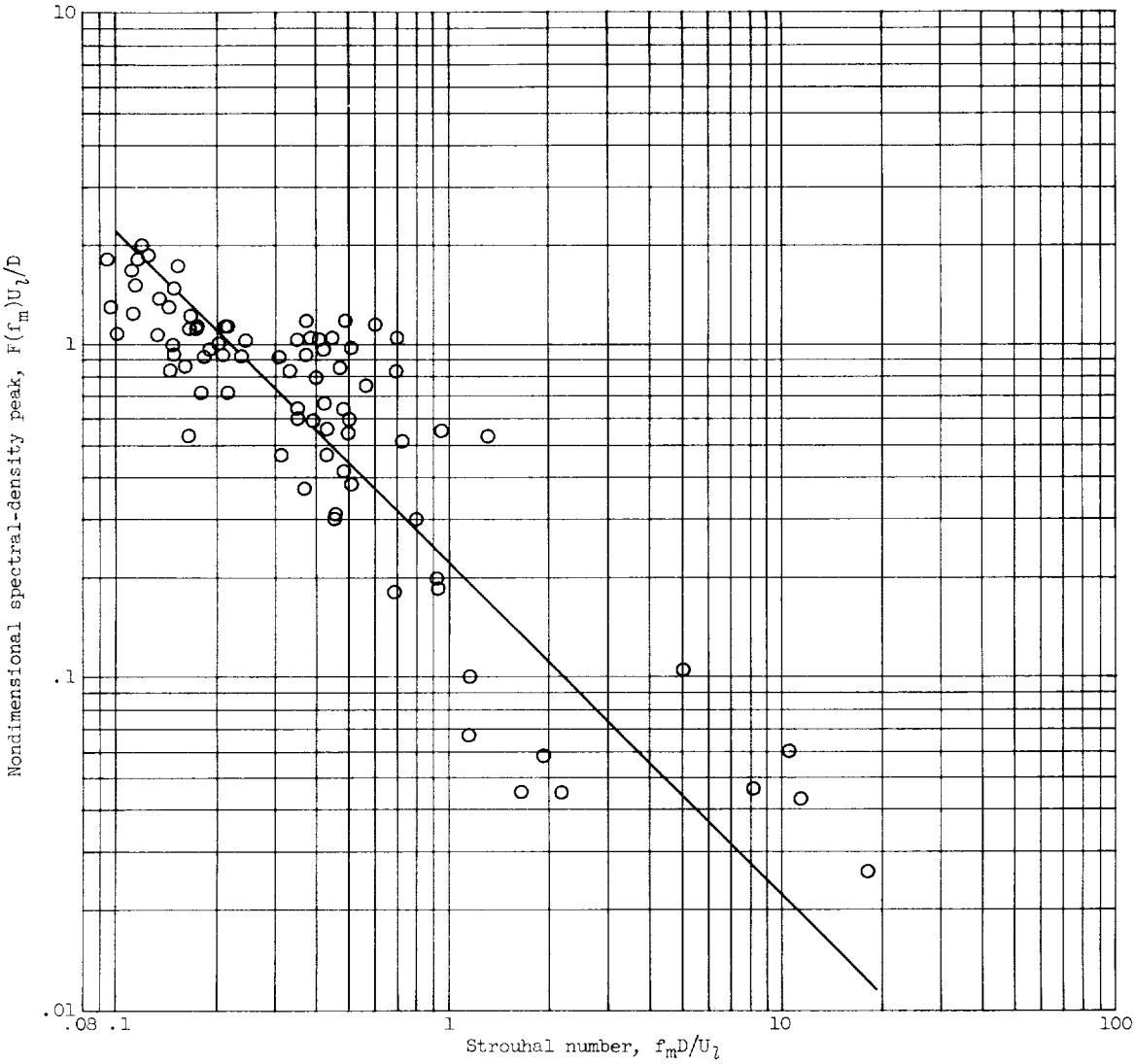

(d) s/w = 1.44.

Figure 11. - Continued. Relation of peak turbulent energy per cycle to frequency. All x/D, z/D, but y/D = 0.

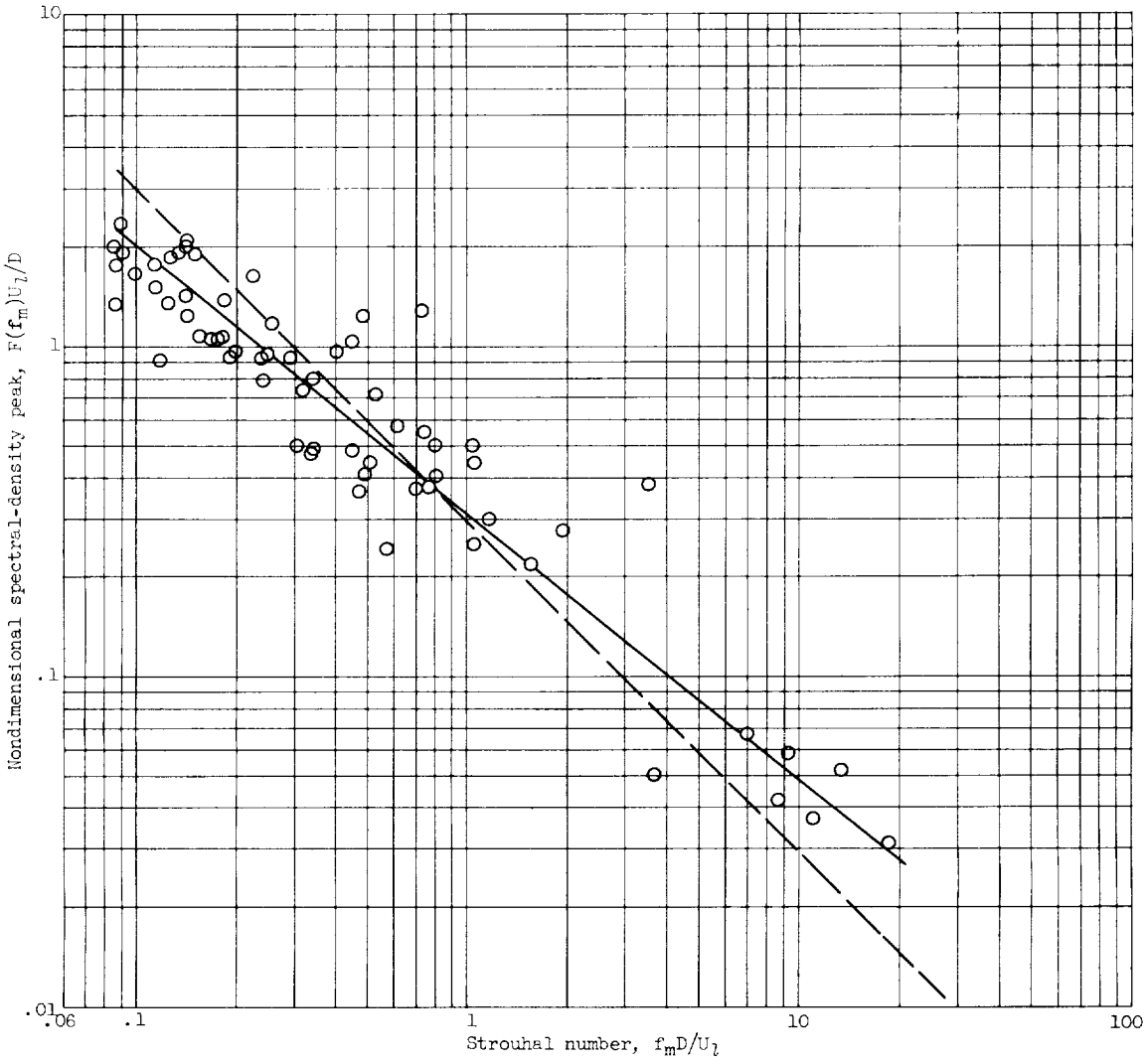

(e) s/w = 0.94.

Figure 11. - Concluded. Relation of peak turbulent energy per cycle to frequency. All x/D, z/D, but y/D = 0.

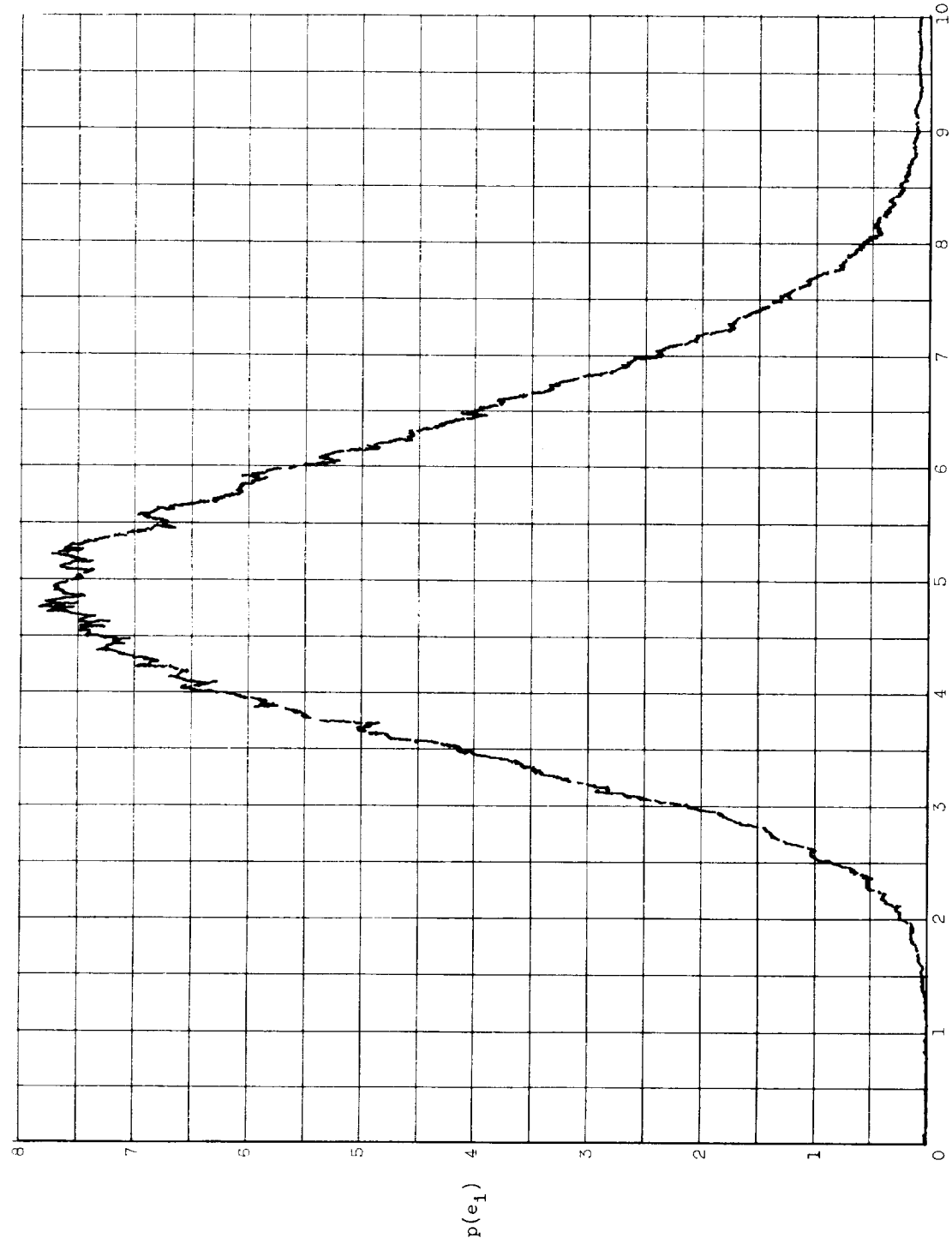

Figure 12. - Probability-density function (typical curve).

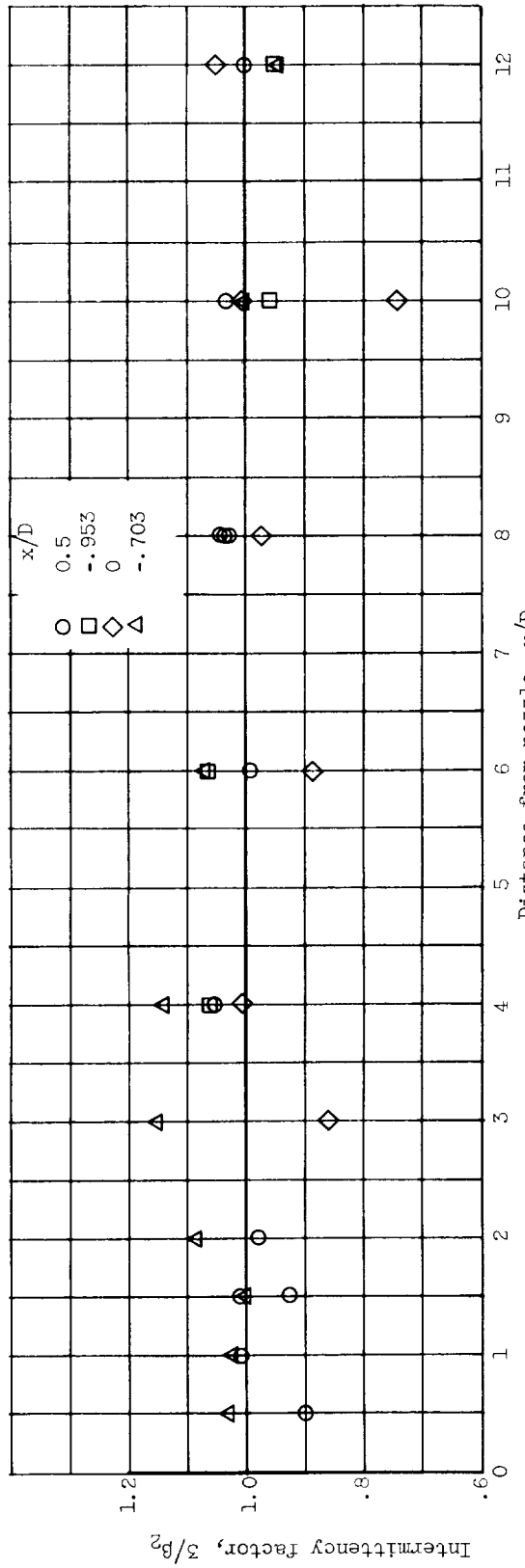

Figure 13. - Intermittency factor plotted against distance from nozzle. s/w = 0.94.

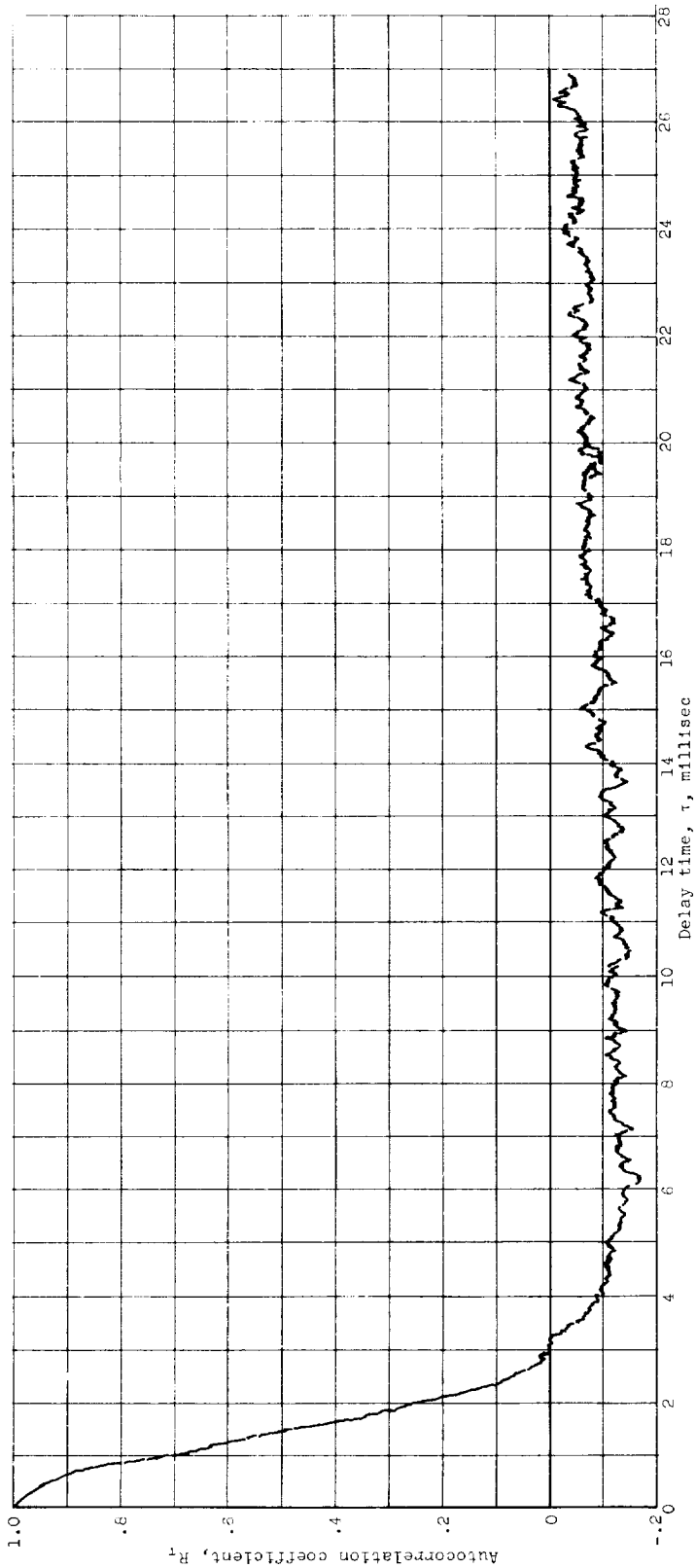

Figure 14. - Autocorrelogram (typical).

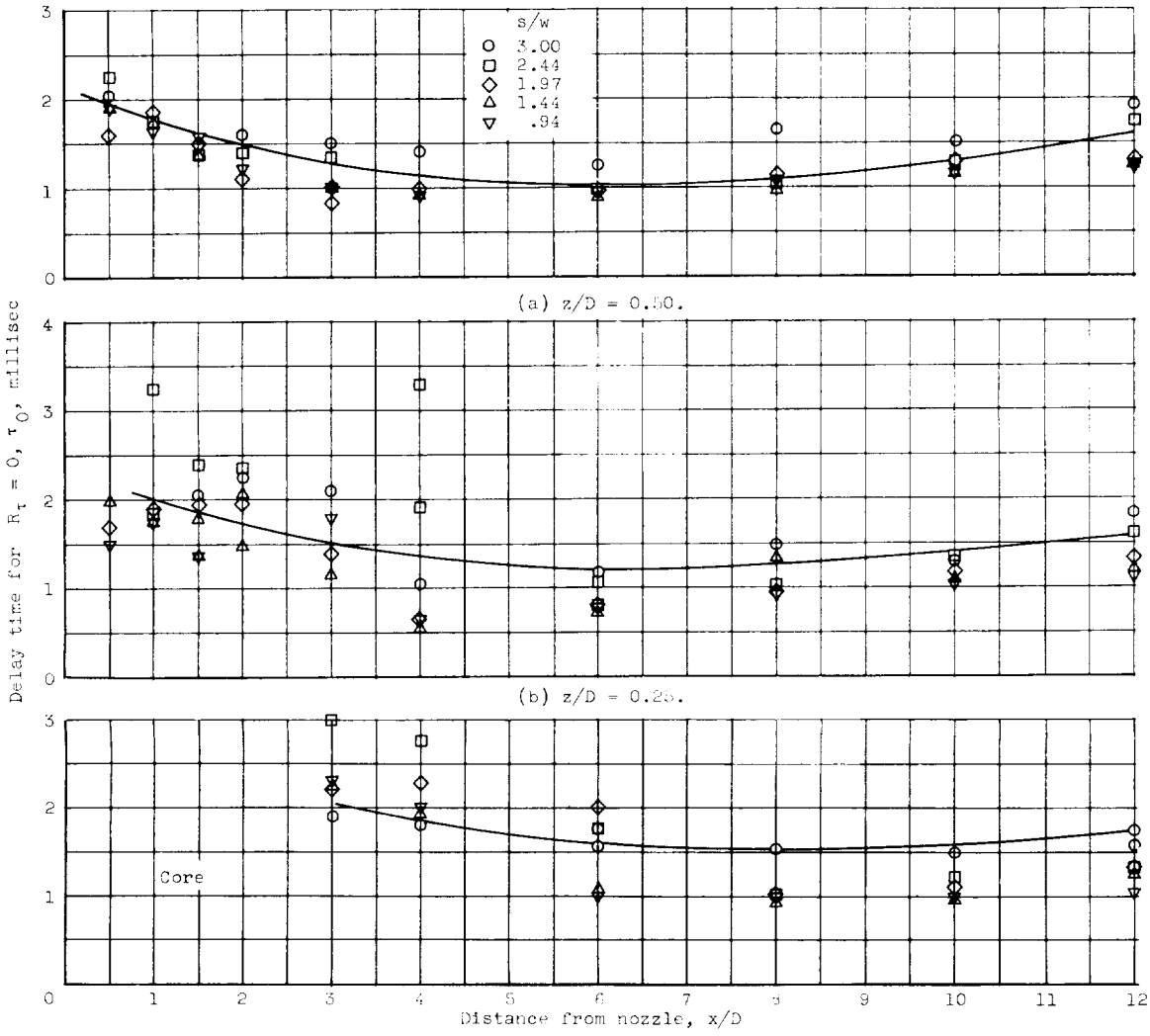

(a) z/D = 0.50.

(b) z/D = 0.25.

(c) z/D = 0.

Figure 15. - Variation of delay time τ_0 with distance from nozzle.

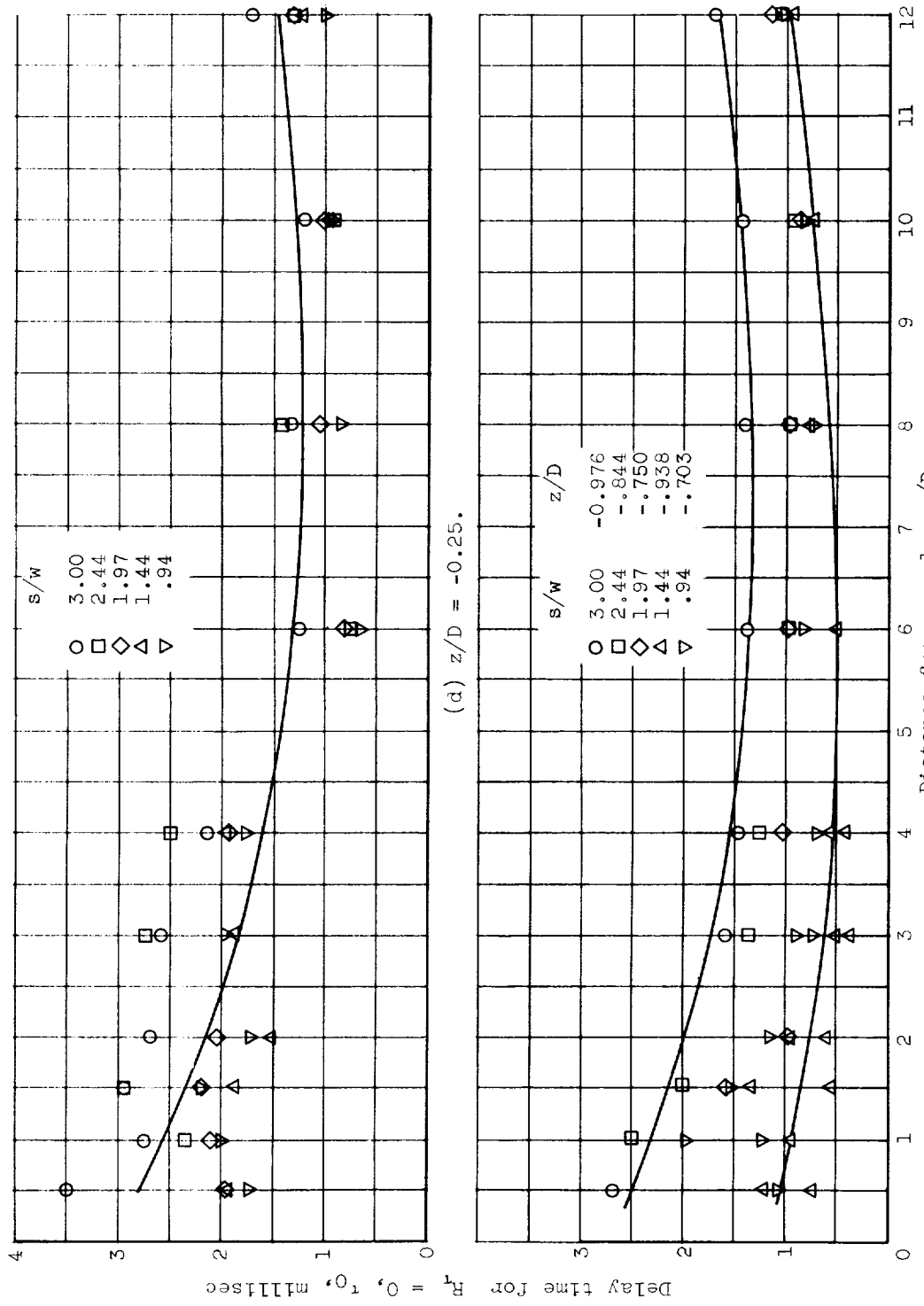

(e) Survey line halfway between outside nozzles.

Figure 15. - Concluded. Variation of delay time τ_0 with distance from nozzle.

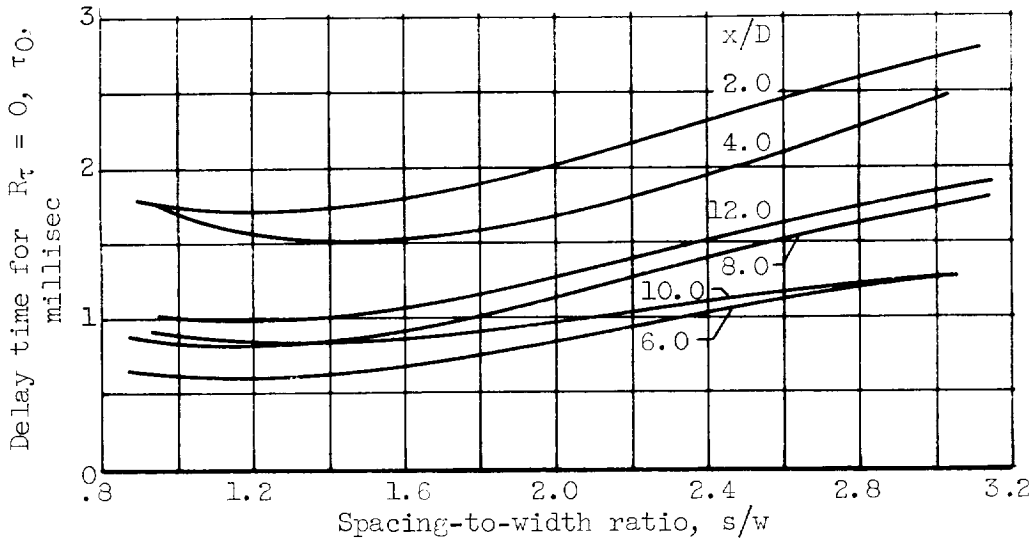

Figure 16. - Delay time for $R_\tau = 0$ as function of spacing-to-width ratio. $z/D = -0.25$; $y/D = 0$.

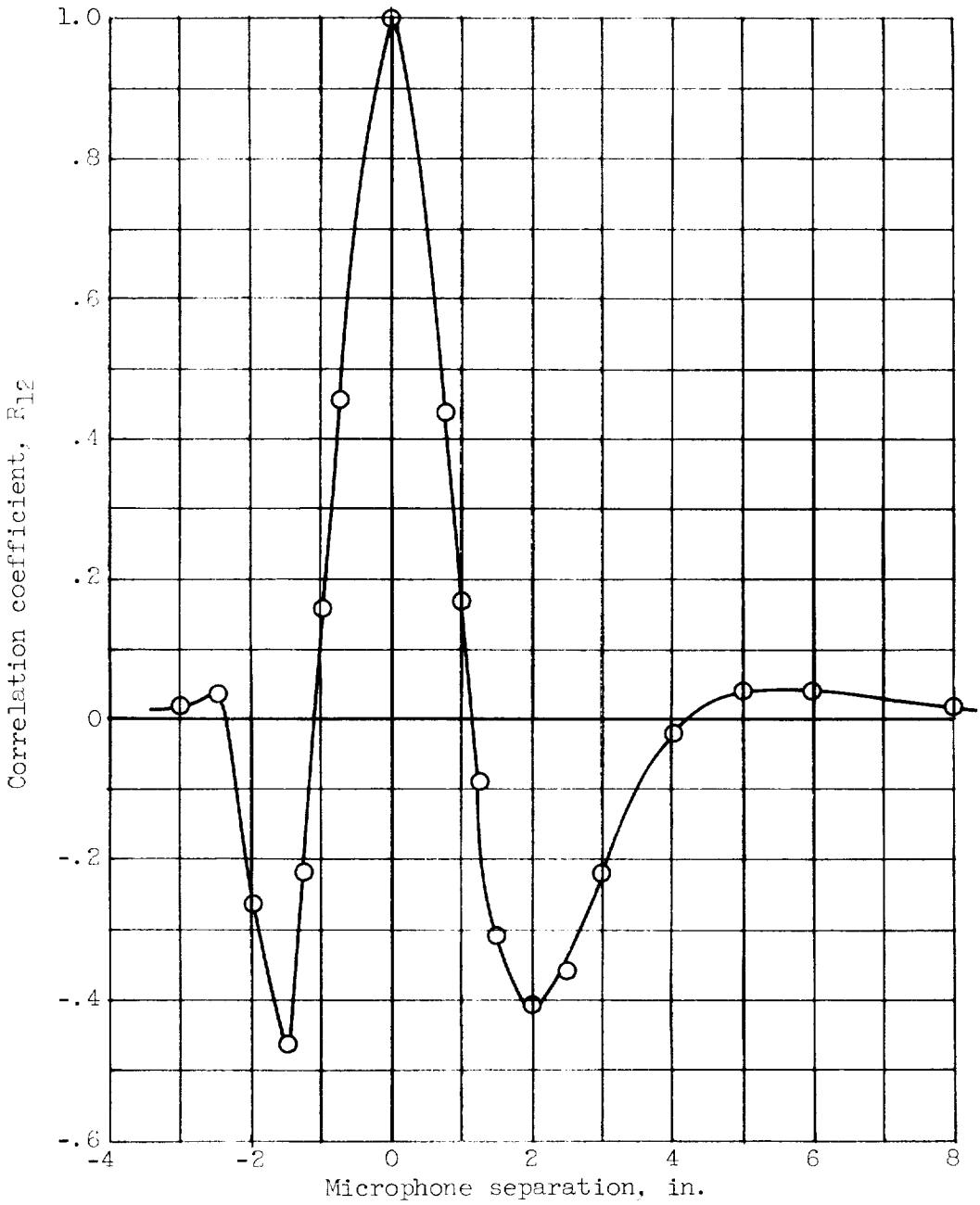

(a) s/w = 3.00.

Figure 17. - Pressure cross correlations. Fixed microphone located at x/D = 2.0; movable microphone located both upstream and downstream.

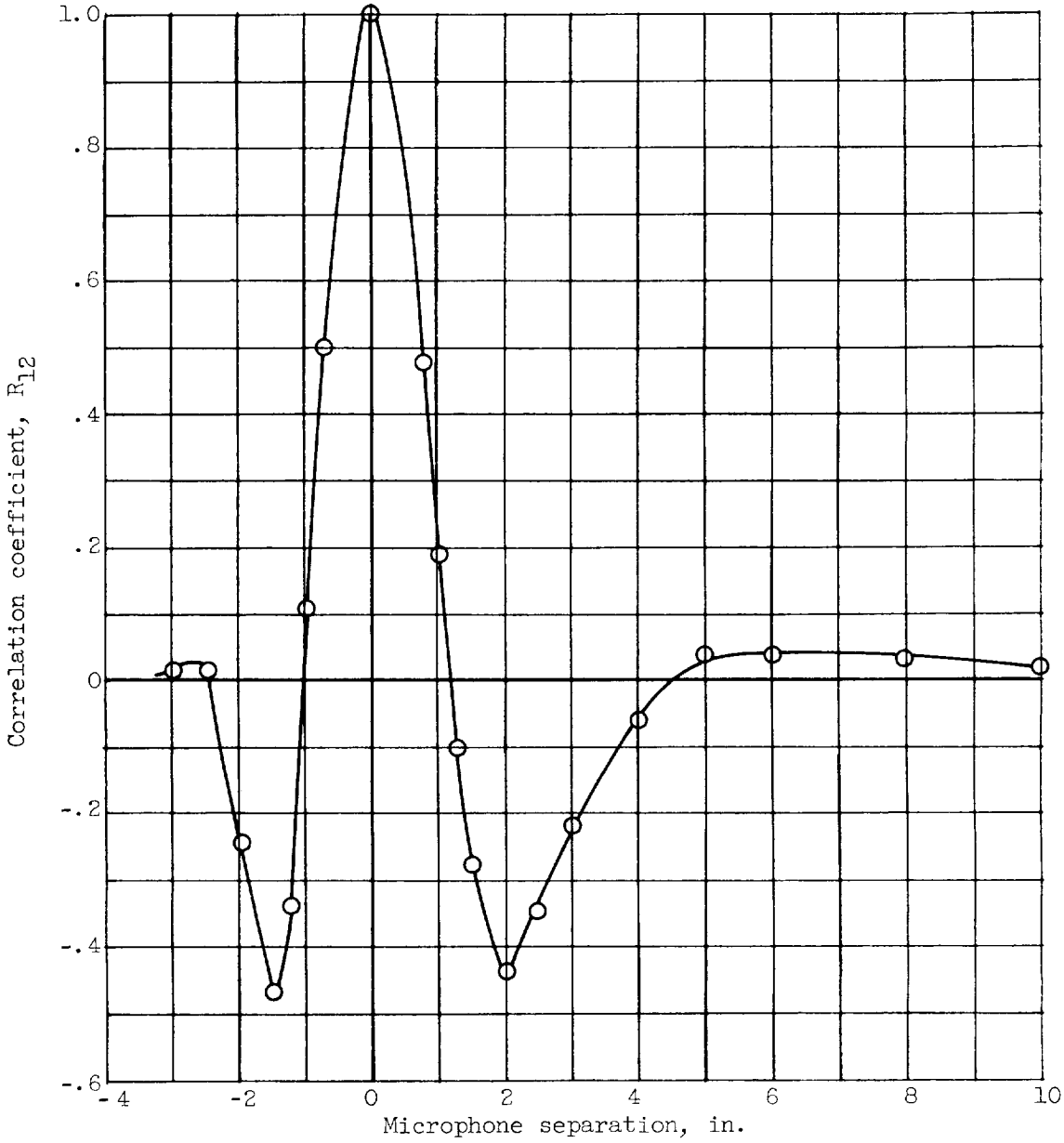

(b) s/w = 2.44.

Figure 17. - Continued. Pressure cross correlations. Fixed microphone located at x/D = 2.0; movable microphone located both upstream and downstream.

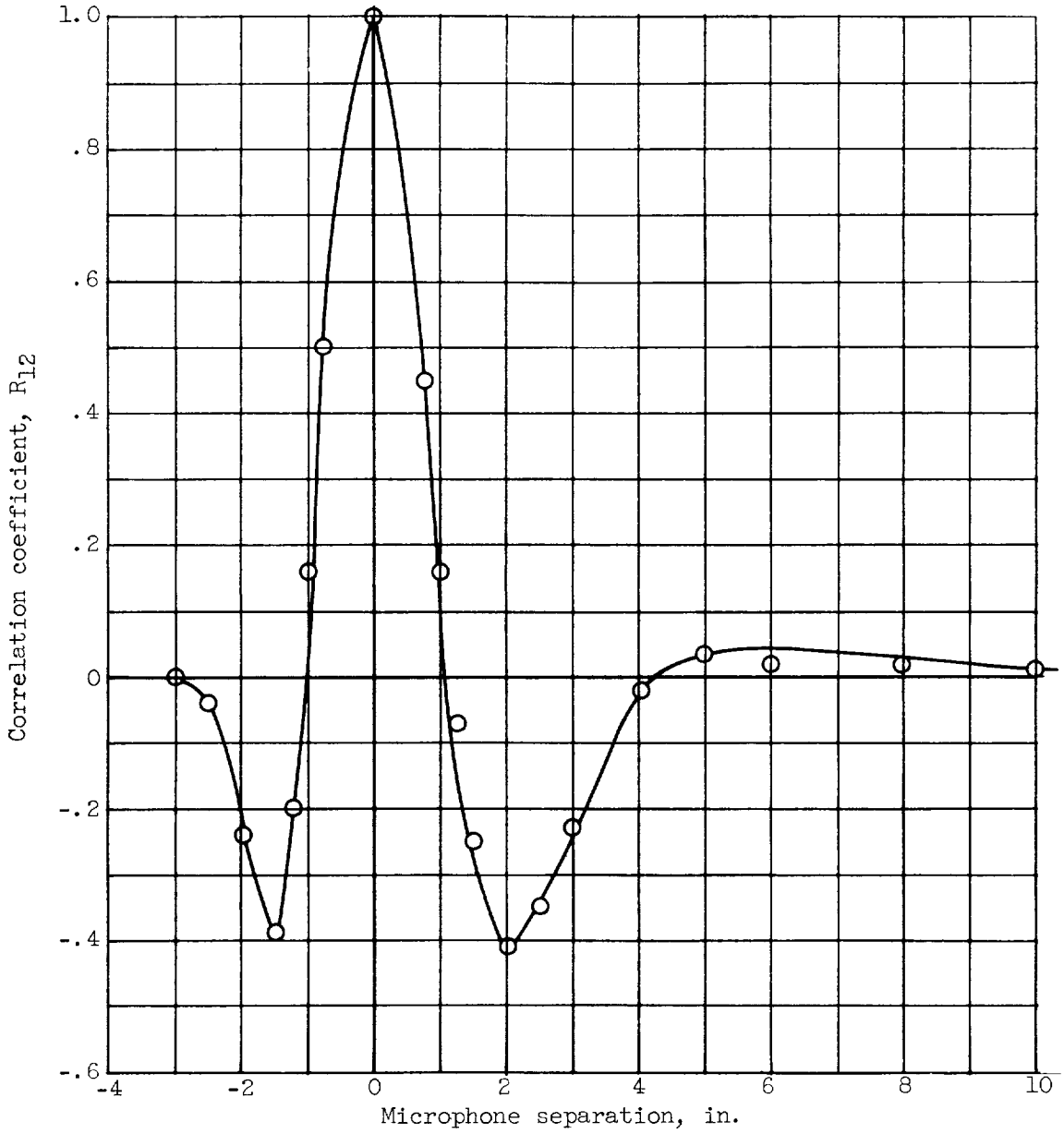

(c) s/w = 1.97.

Figure 17. - Continued. Pressure cross correlations. Fixed microphone located at x/D = 2.0; movable microphone located both upstream and downstream.

(d) s/w = 1.44.

Figure 17. - Continued. Pressure cross correlations. Fixed microphone located at x/D = 2.0; movable microphone located both upstream and downstream.

(e) s/w = 0.94.

Figure 17. - Concluded. Pressure cross correlations. Fixed microphone located at x/D = 2.0; movable microphone located both upstream and downstream.

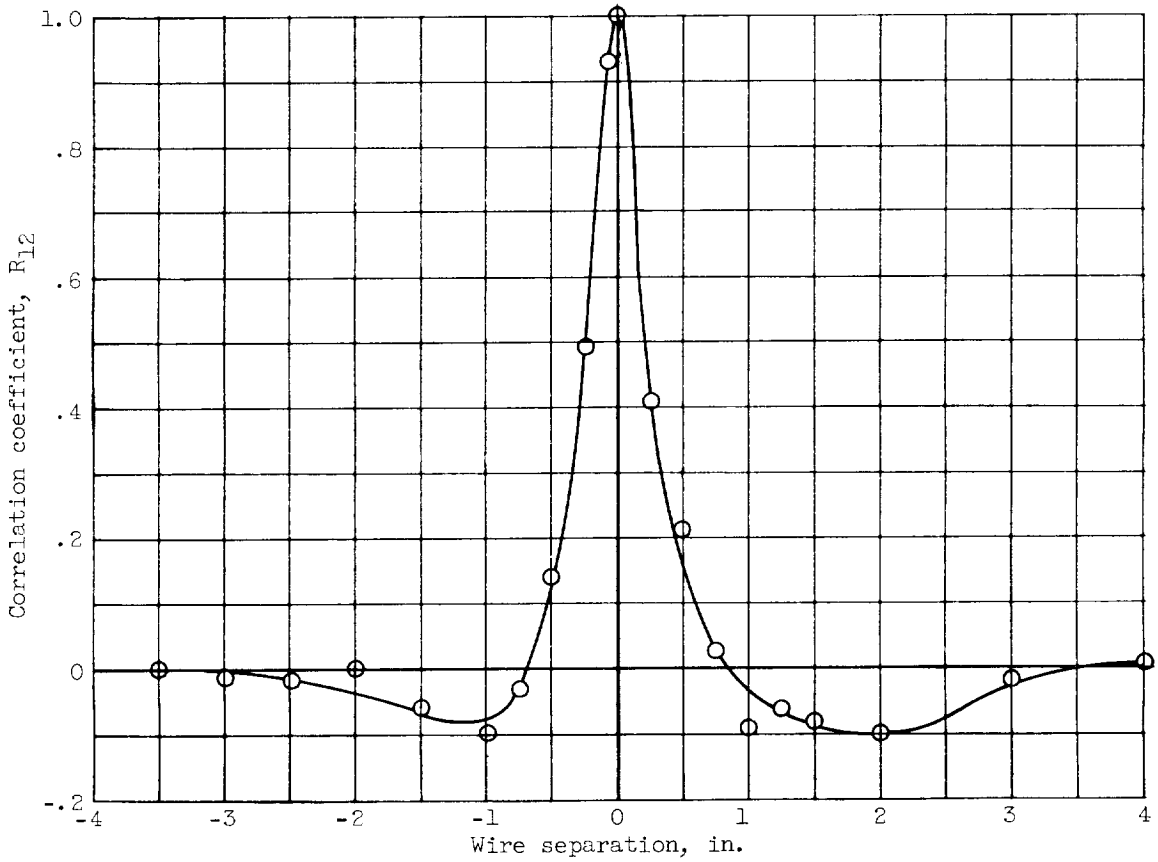

(a) Fixed wire located at x/D = 2.0.

Figure 18. - Longitudinal velocity cross correlations. s/w = 3.00; y/D = 0; z/D = 0.25; movable wire located both upstream and downstream.

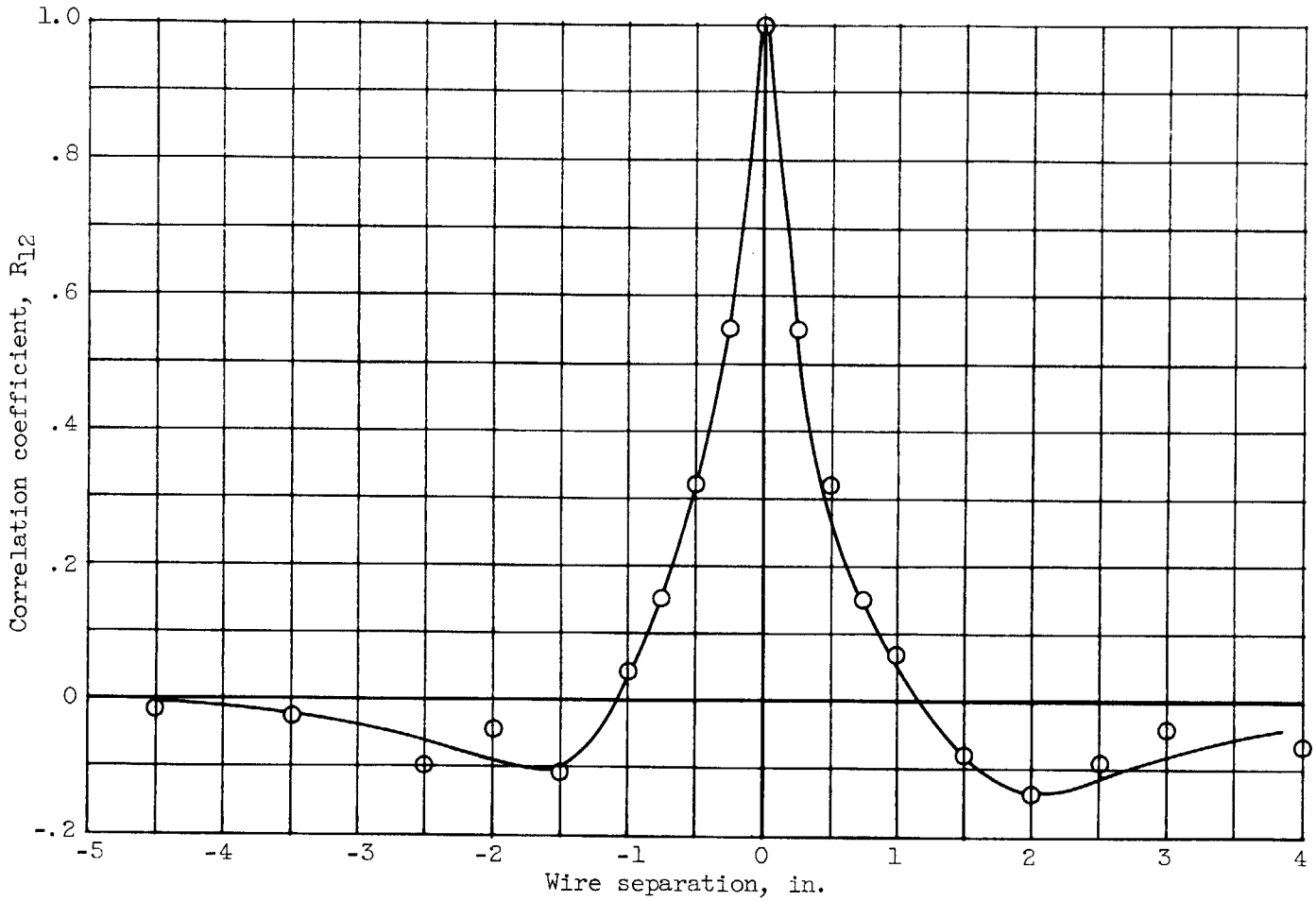

(b) Fixed wire located at x/D = 4.0.

Figure 18. - Concluded. Longitudinal velocity cross correlations. s/w = 3.00; y/D = 0; z/D = 0.25; movable wire located both upstream and downstream.

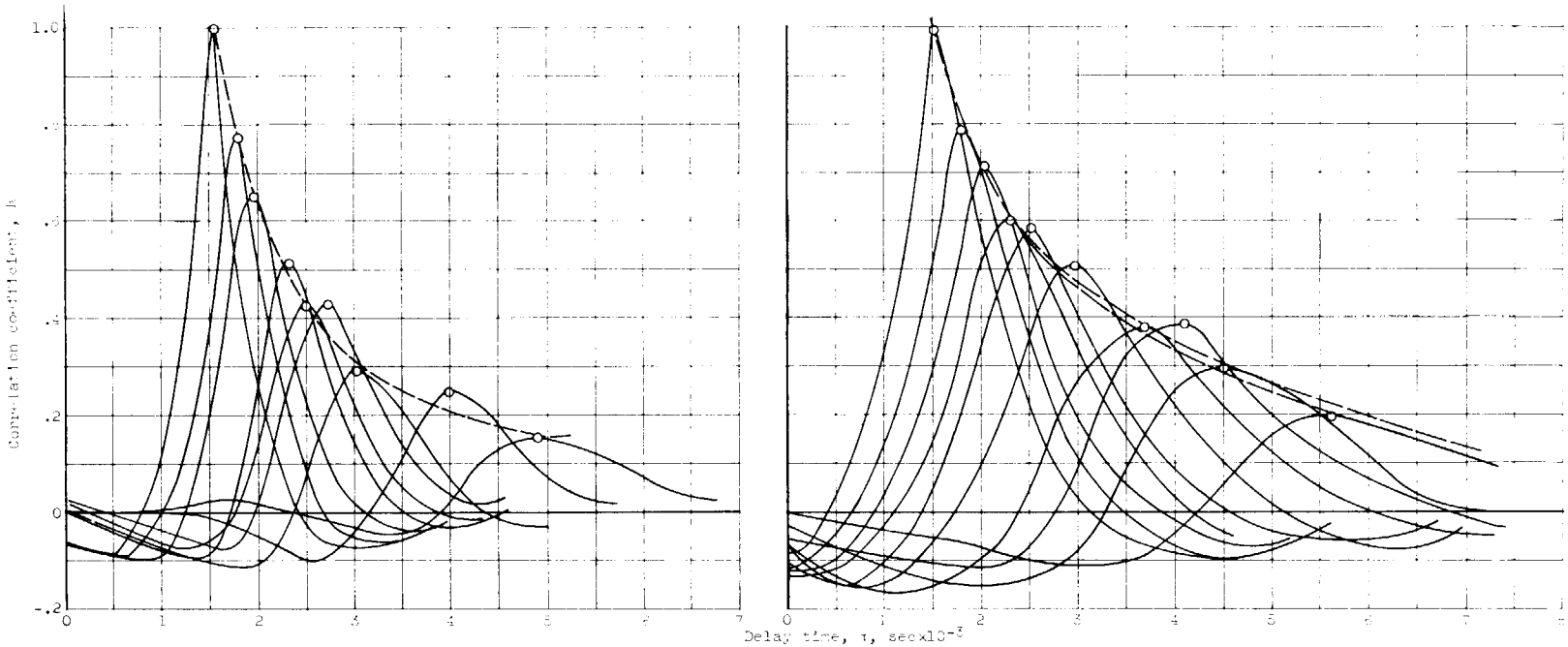

(a) x/D = 2.0; movable wire going downstream.

(b) x/D = 4.0; movable wire going downstream.

Figure 19. - Space-time correlations of longitudinal velocity components. y/D = 0; z/D = 0.25.

(c) x/D = 4.0; movable wire going upstream.

(d) x/D = 2.0; movable wire going upstream.

Figure 19. - Concluded. Space-time correlations of longitudinal velocity components. y/D = 0; z/D = 0.2.

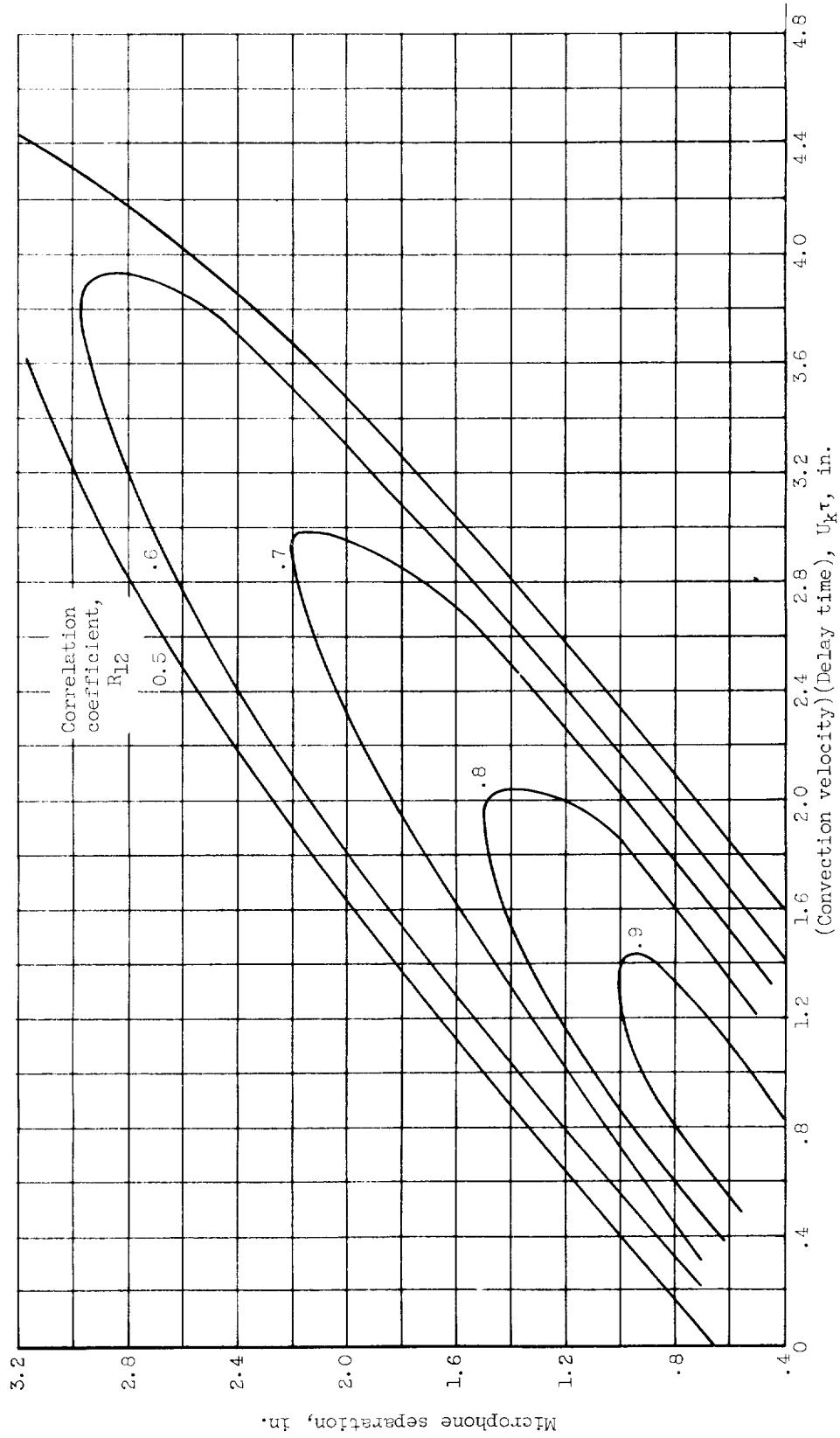

(a) Fixed microphone located at x/D = 4.0; z/D = 1.31; s/w = 3.00; movable microphone going downstream.

Figure 20. - Isocorrelation curves showing space-time correlation of fluctuating pressures. y/D = 0.

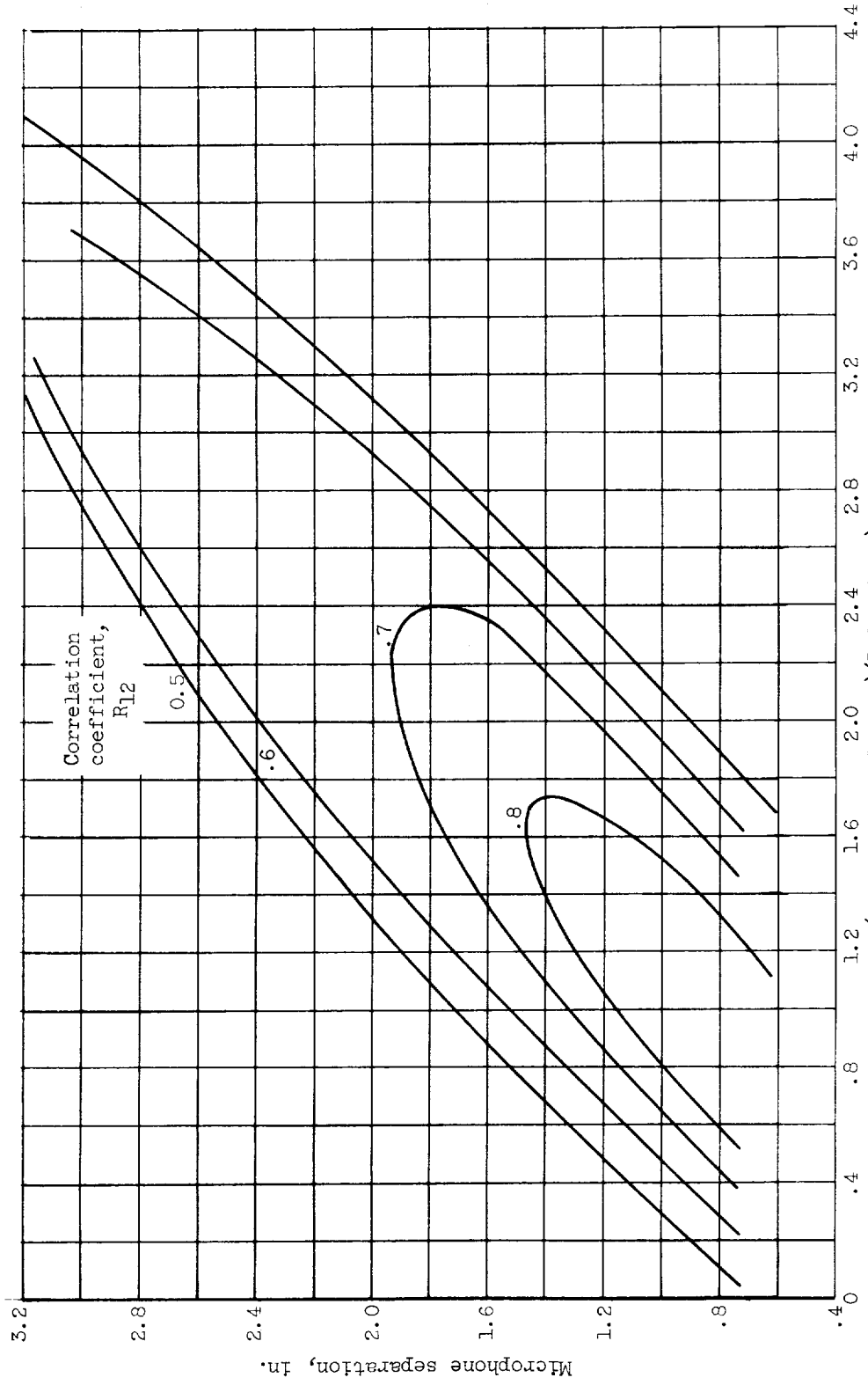

(b) Fixed microphone located at x/D = 4.0; z/D = 1.31; s/w = 2.44; movable microphone going downstream. y/D = 0.

Figure 20. - Continued. Isocorrelation curves showing space-time correlation of fluctuating pressures.

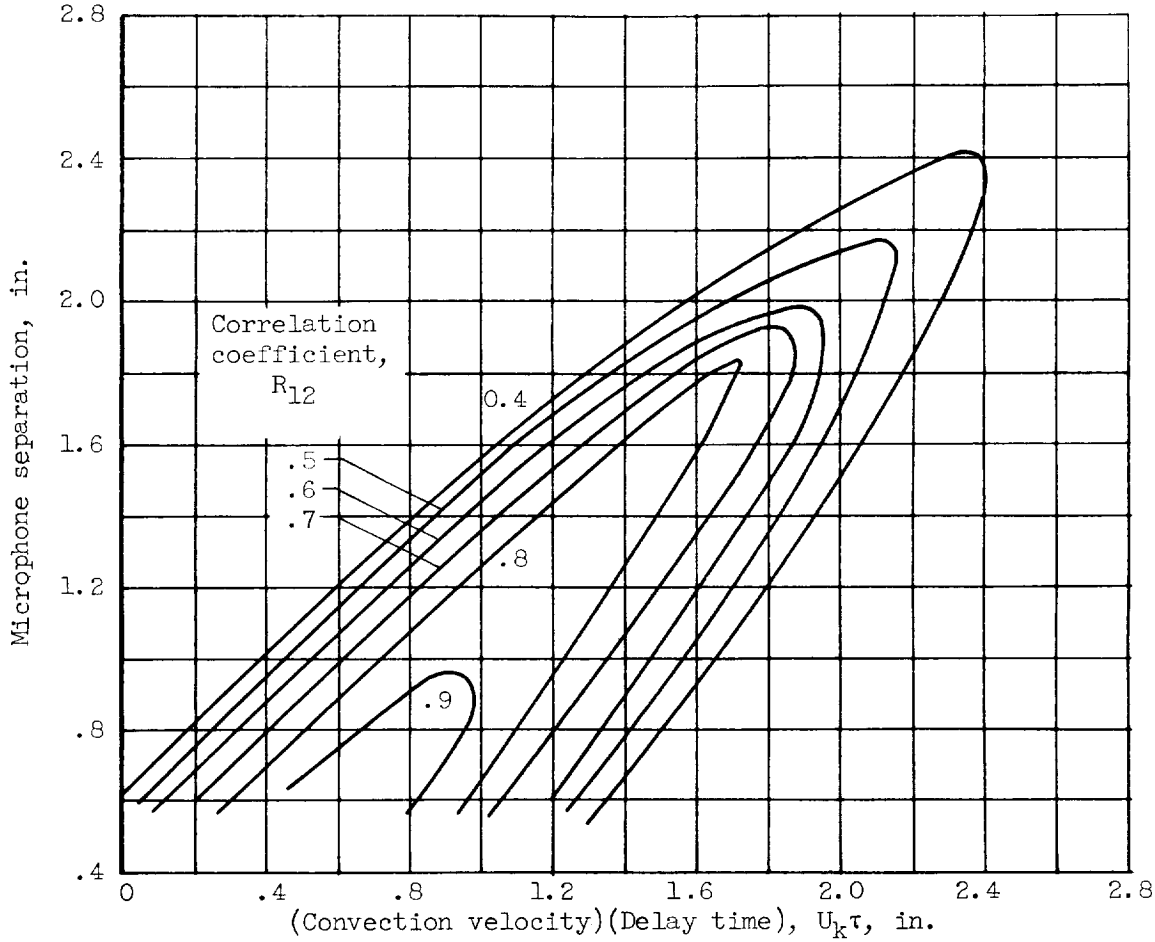

(c) Fixed microphone located at x/D = 2.0; z/D = 1.12; s/w = 1.97; movable microphone going upstream.

Figure 20. - Continued. Isocorrelation curves showing space-time correlation of fluctuating pressures. y/D = 0.

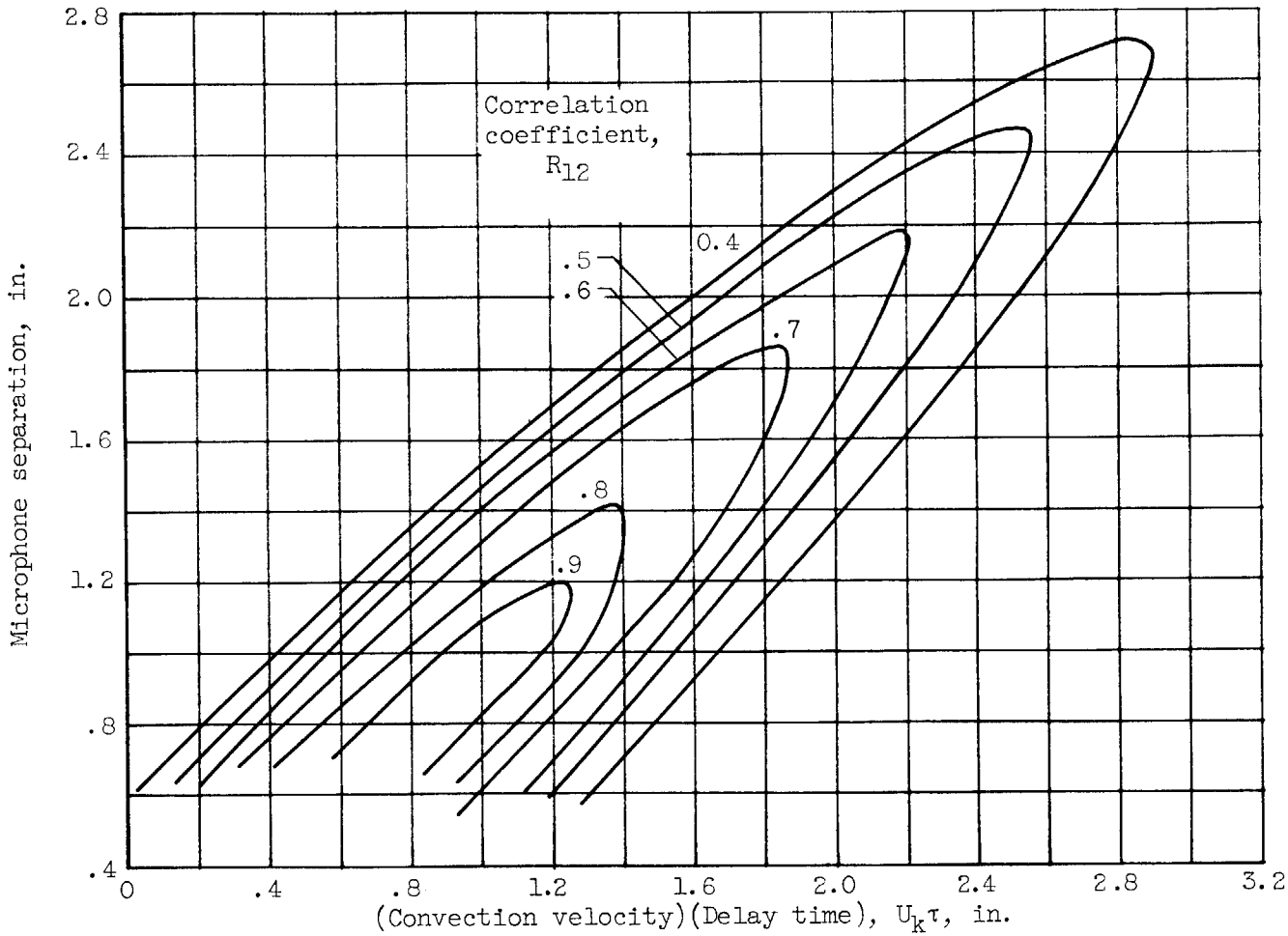

(d) Fixed microphone located at x/D = 2.0; z/D = 1.12; s/w = 1.44; movable microphone going upstream.

Figure 20. - Continued. Isocorrelation curves showing space-time correlation of fluctuating pressures. y/D = 0.

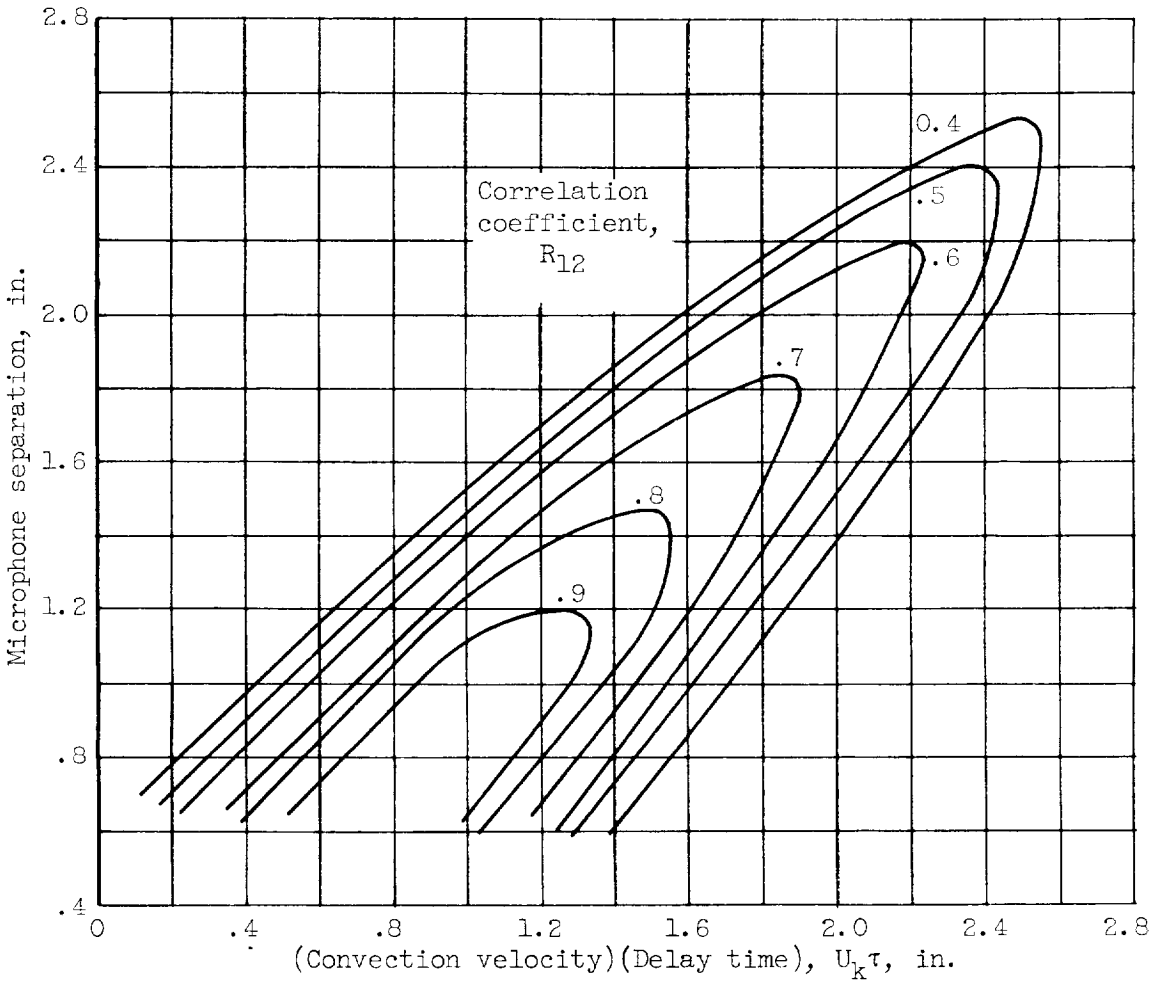

(e) Fixed microphone located at x/D = 2.0; z/D = 1.12; s/w = 0.94.

Figure 20. - Concluded. Isocorrelation curves showing space-time correlation of fluctuating pressures. y/D = 0.

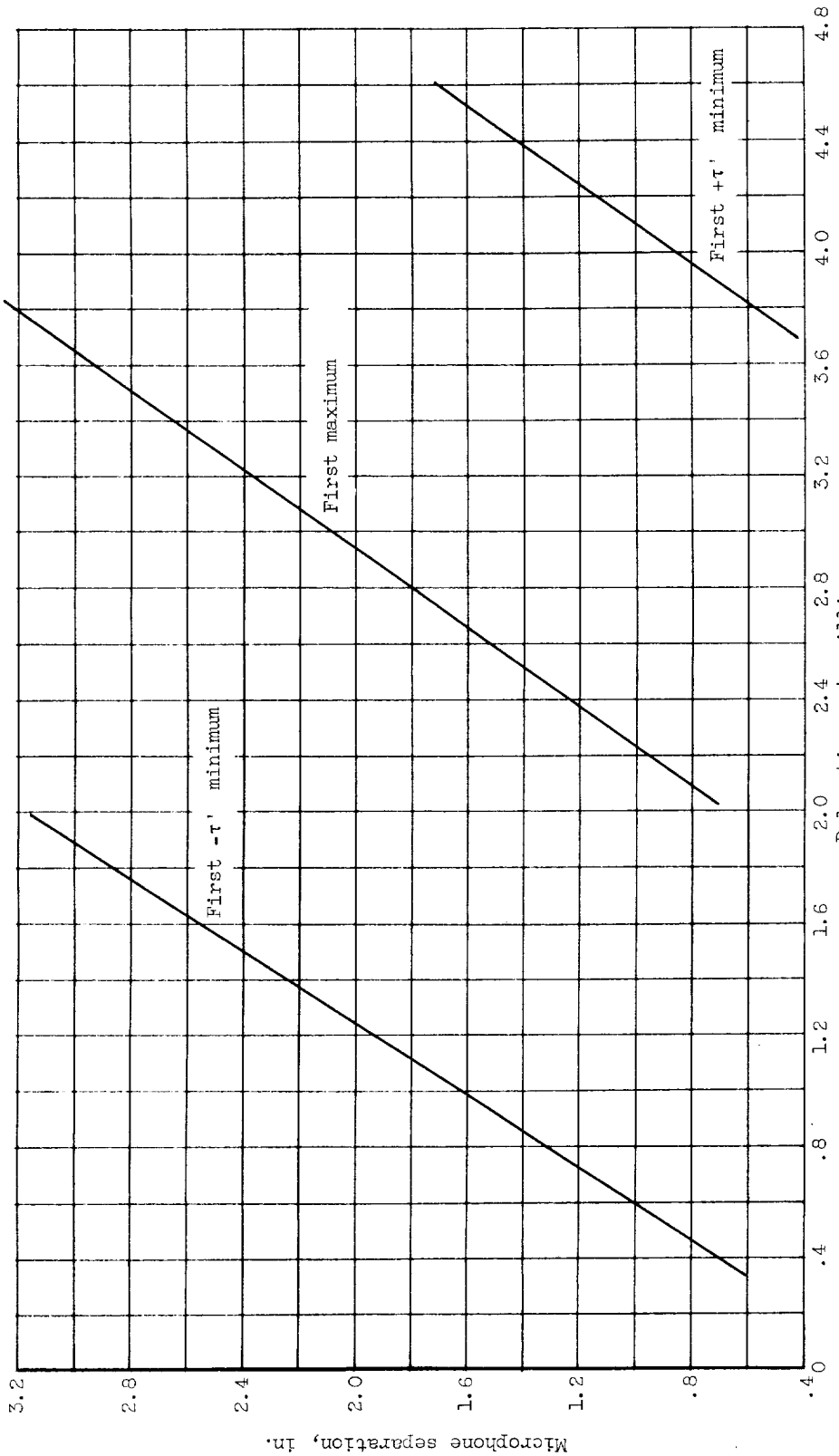

(a) Fixed microphone located at x/D = 4.0; z/D = 1.31; s/w = 3.00; movable microphone going downstream.

Figure 21. - Convection velocity diagrams. y/D = 0.

E-384

CC-10 back

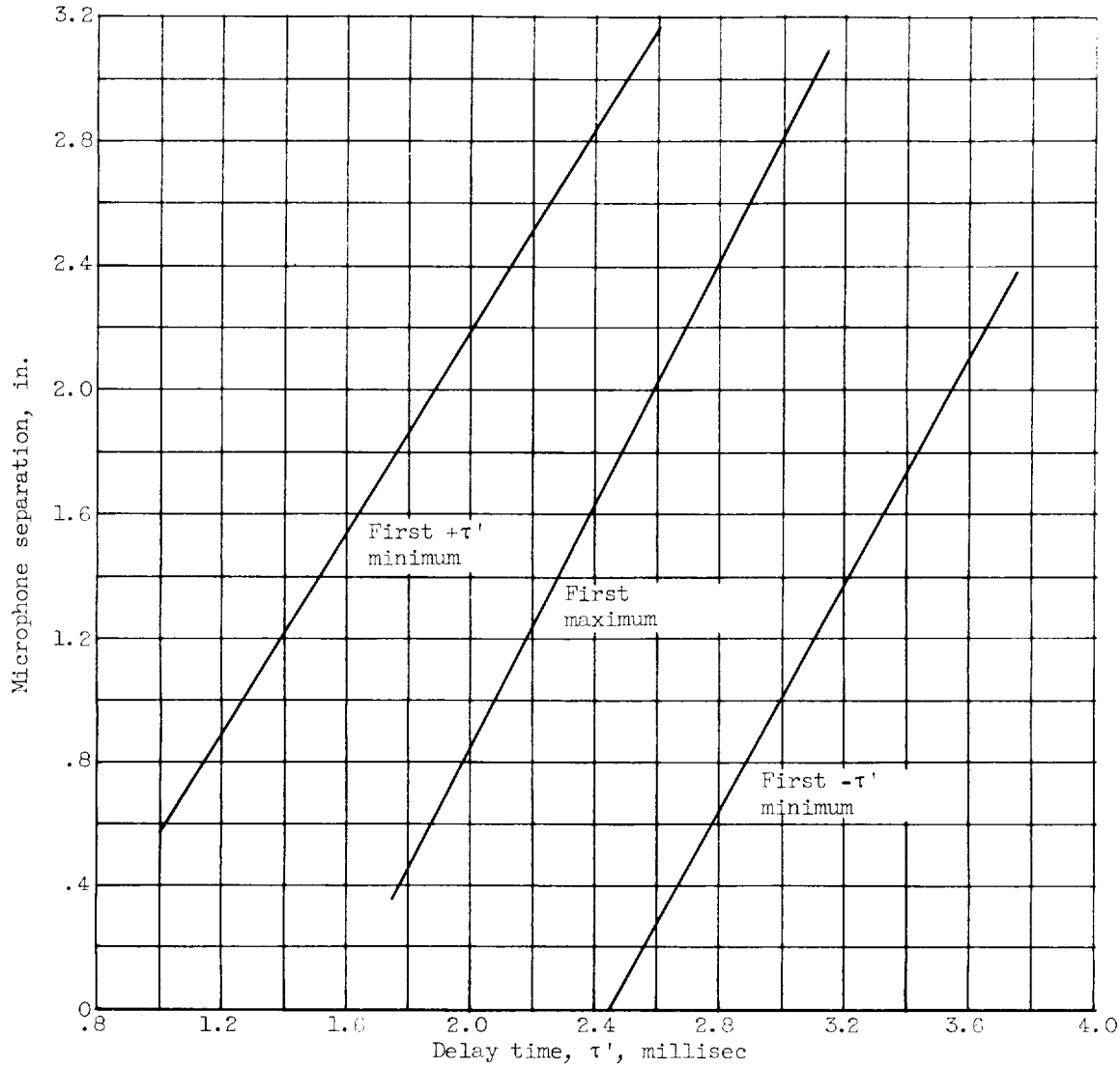

(b) Fixed microphone located at x/D = 2.0; z/D = 1.12; s/w = 2.44; movable microphone going upstream.

Figure 21. - Continued. Convection velocity diagrams. y/D = 0.

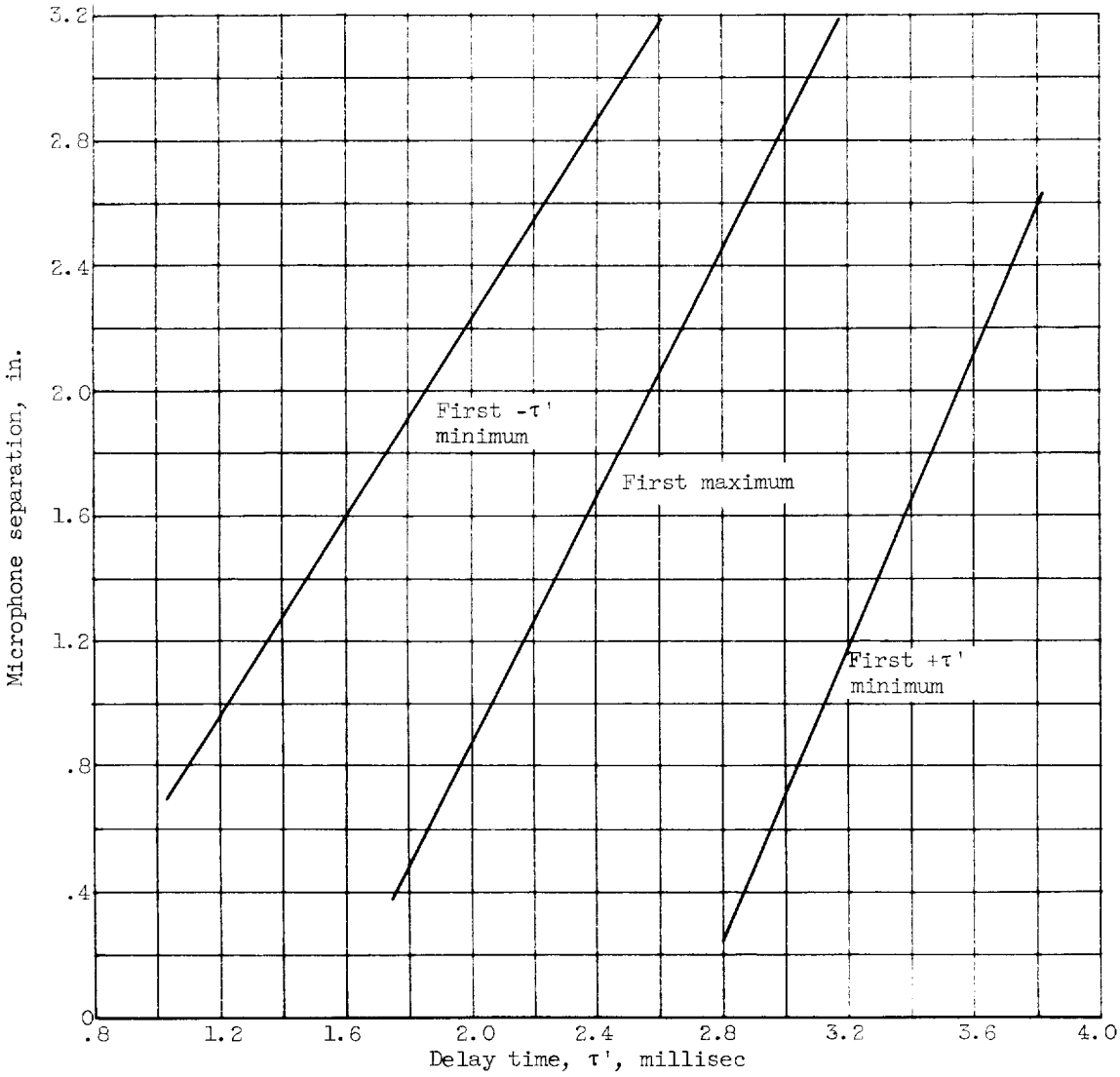

(c) Fixed microphone located at x/D = 2.0; z/D = 1.12; s/w = 1.97; movable microphone going upstream.

Figure 21. - Continued. Convection velocity diagrams. y/D = 0.

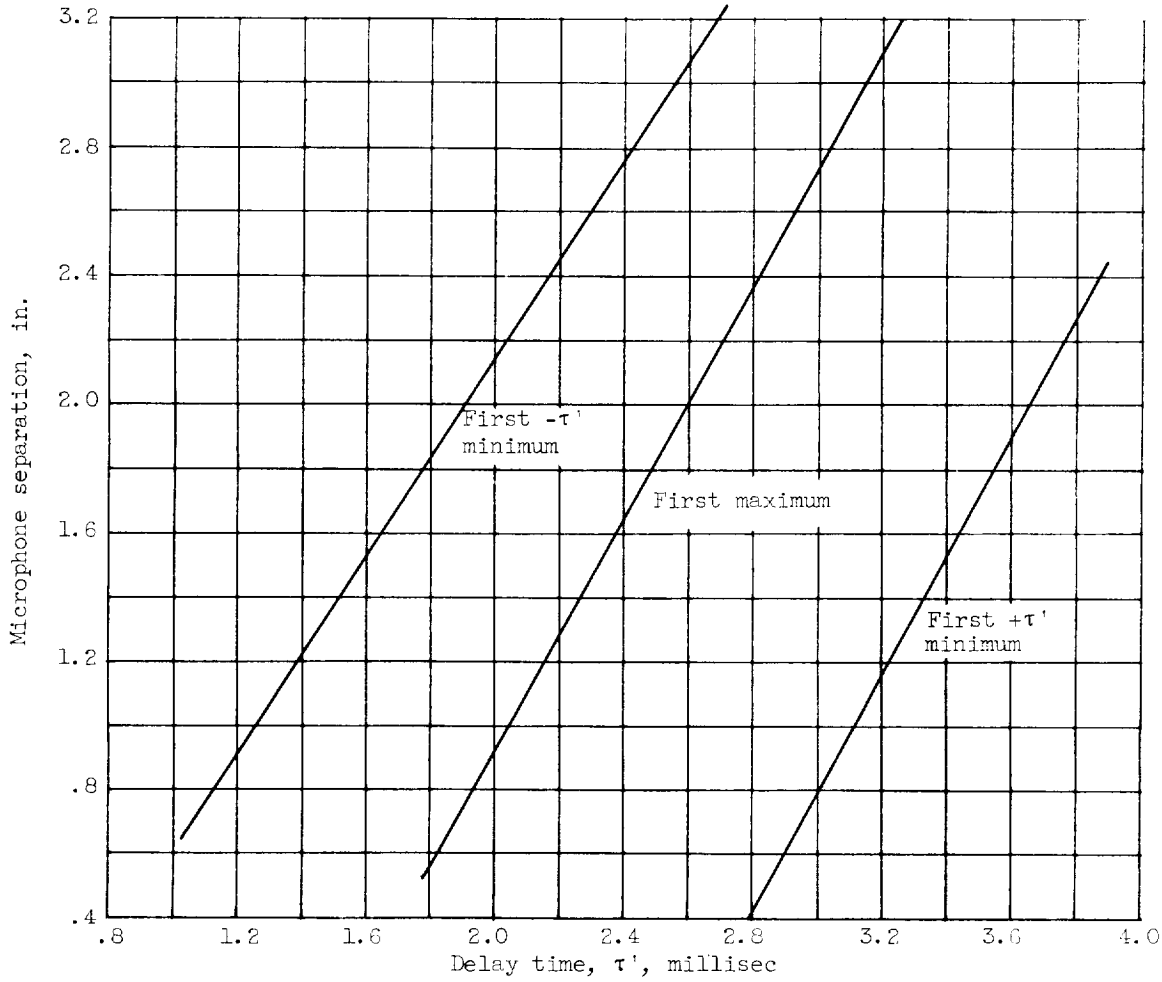

(d) Fixed microphone located at x/D = 2.0; z/D = 1.12; s/w = 1.44; movable microphone going upstream.

Figure 21. - Continued. Convection velocity diagrams. y/D = 0.

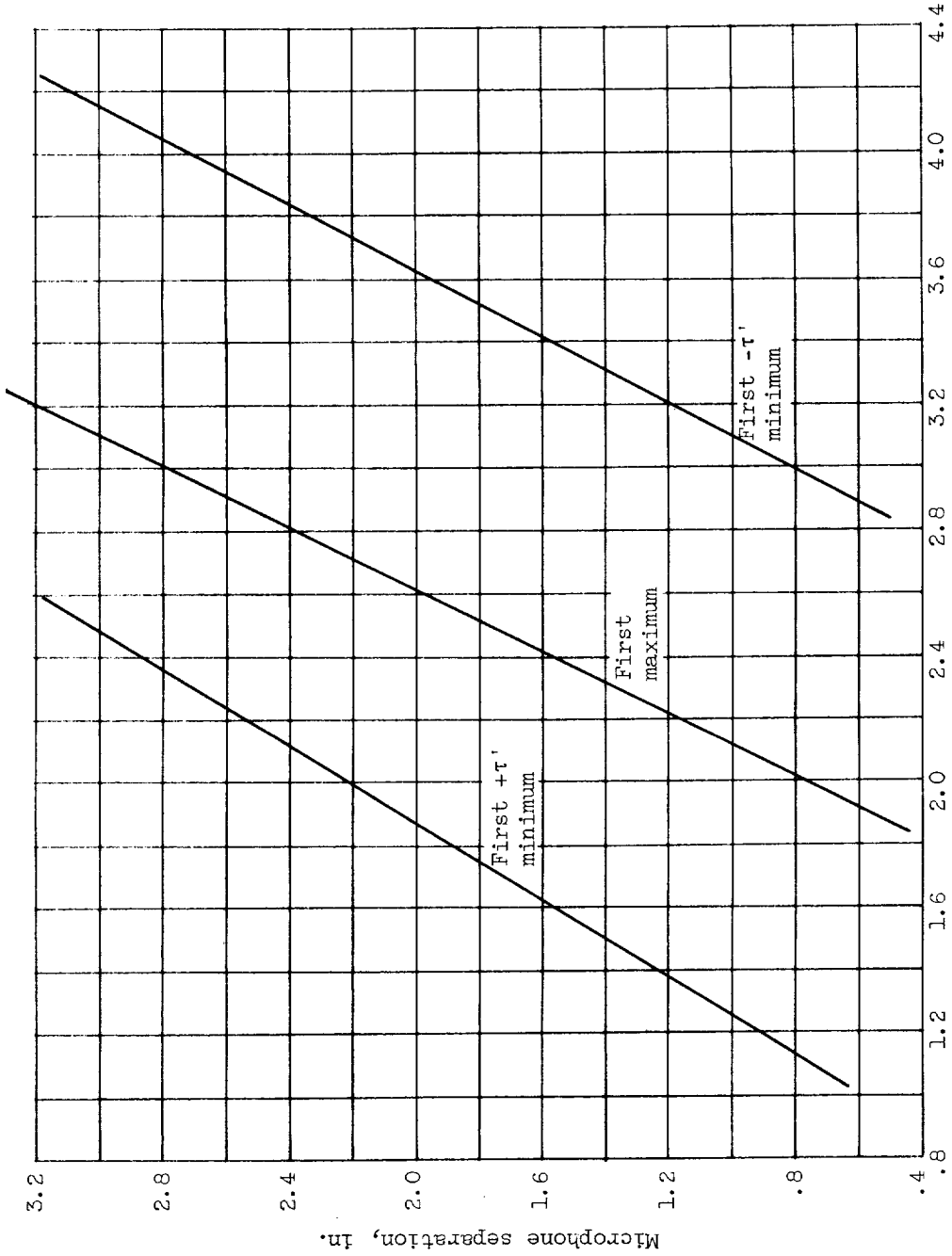

(e) Fixed microphone located at x/D = 2.0; z/D = 1.12; s/w = 0.94; movable microphone going upstream.

Figure 21. - Continued. Convection velocity diagrams. y/D = 0.

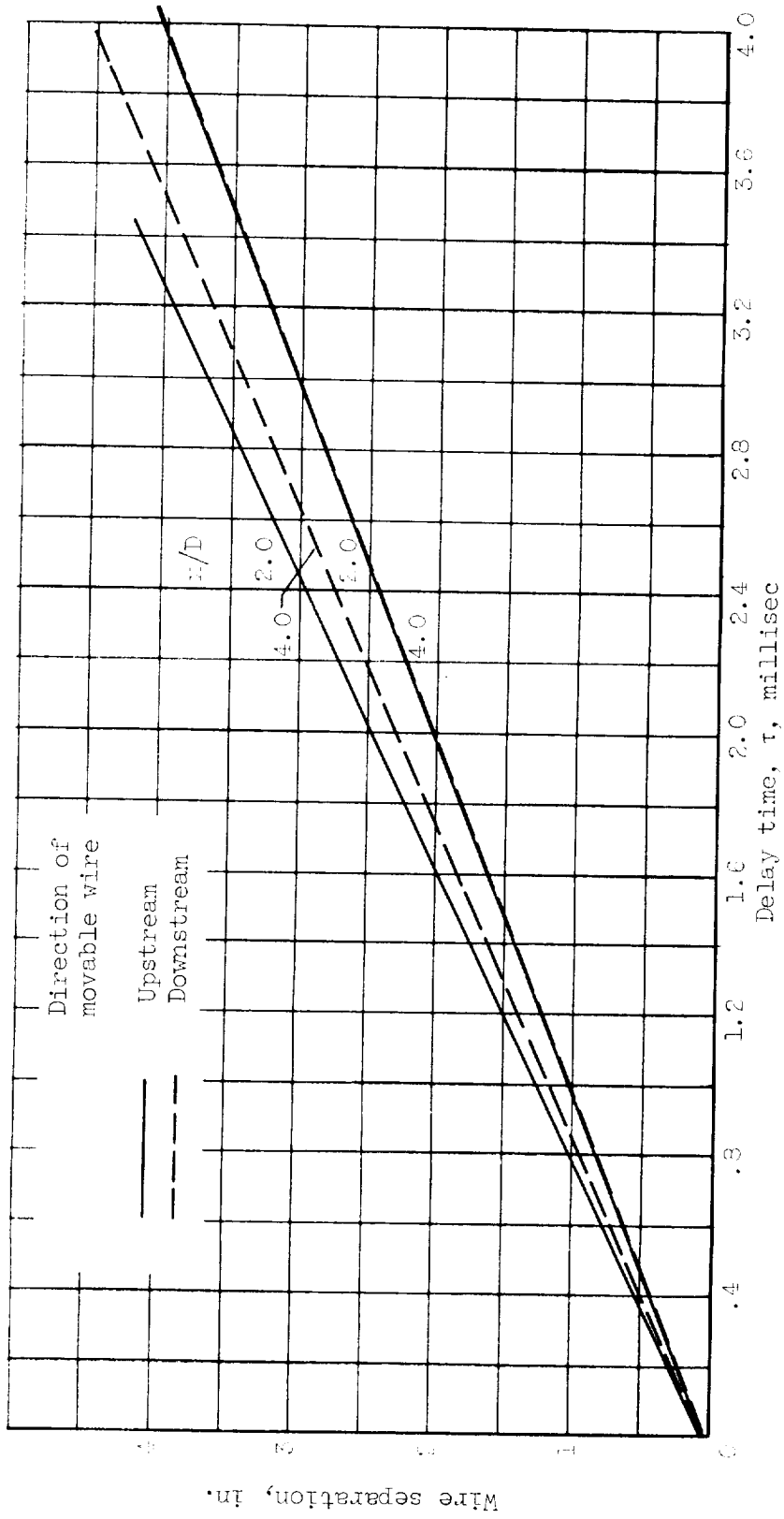

(f) $s/w = 3.00$; $z/D = 0.25$.

Figure 21. - Concluded. Convection velocity diagrams. $y/D = 0$.

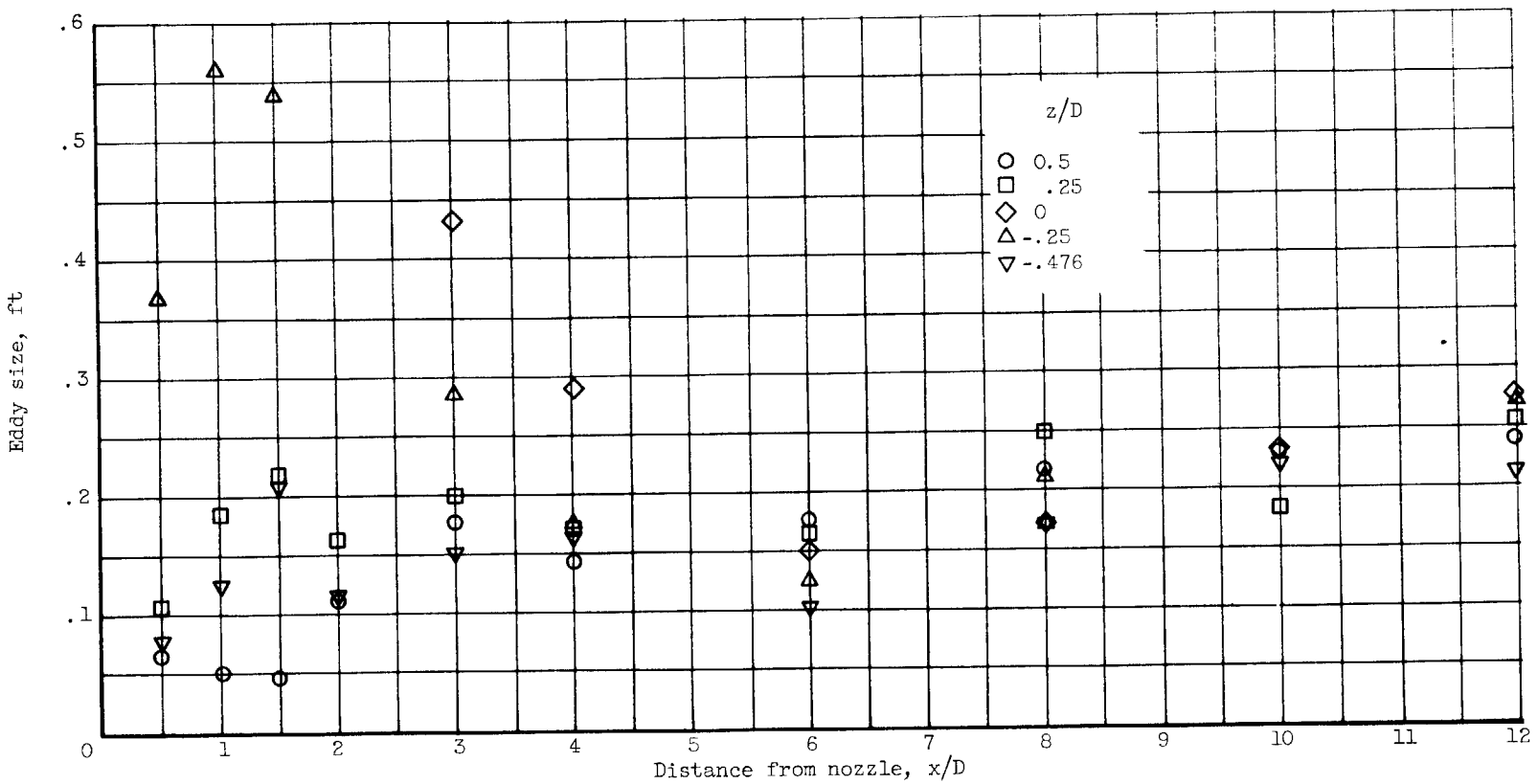

(a) s/w = 0.94; various distances from survey centerline.

Figure 22. - Eddy size as function of distance from nozzle.

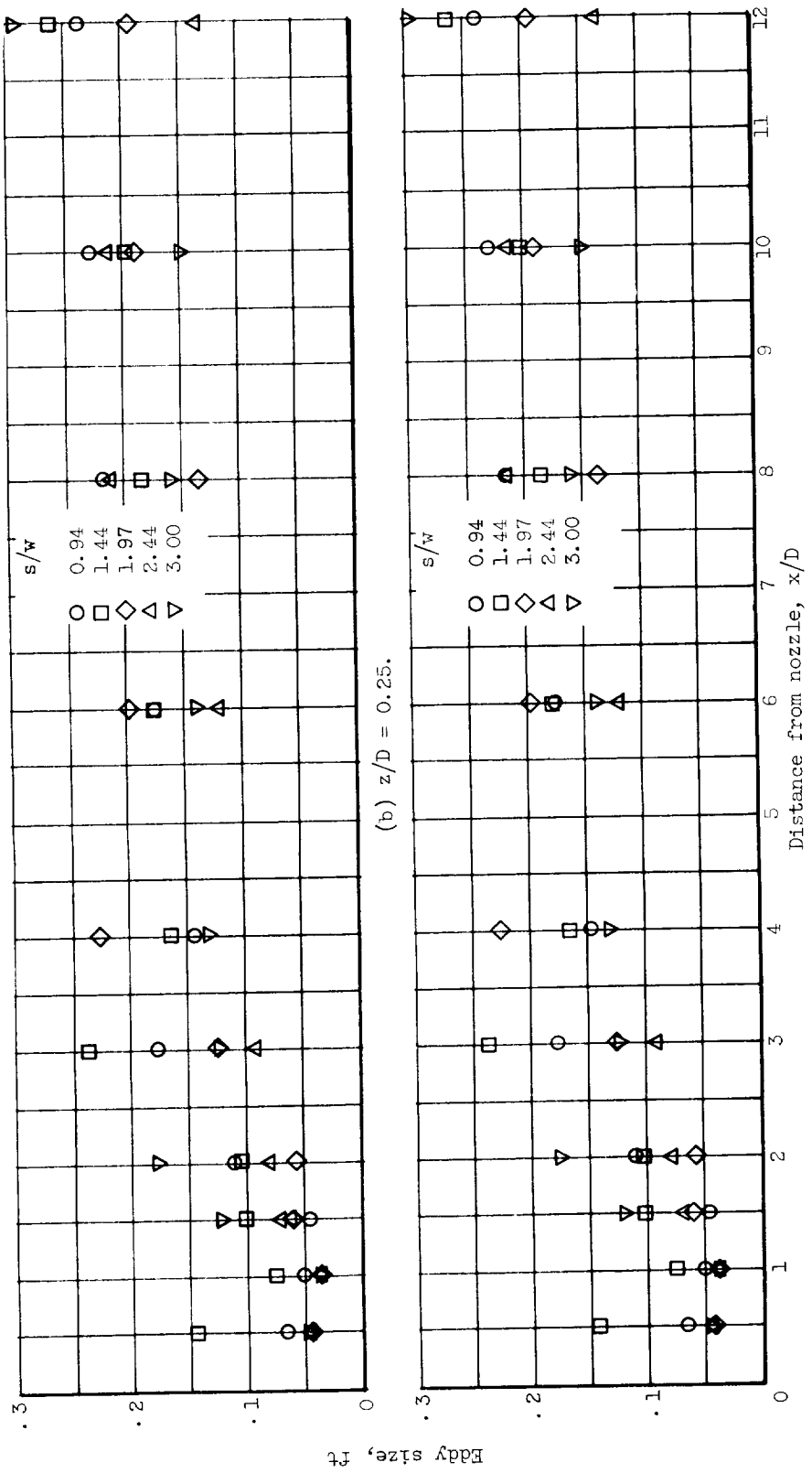

Figure 22. - Continued. Eddy size as function of distance from nozzle.

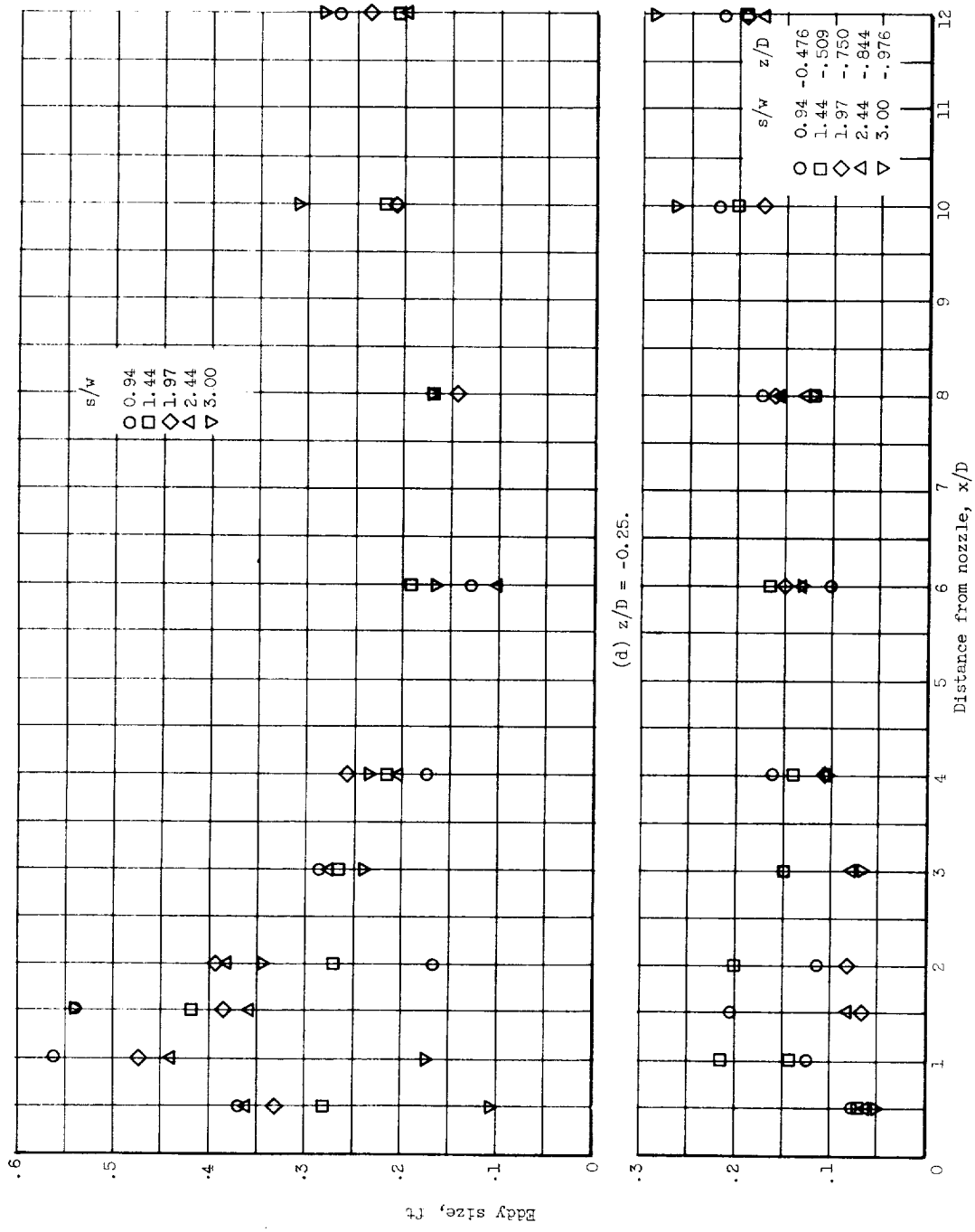

(e) Survey line halfway between outside nozzles.

Figure 22. - Concluded. Eddy size as function of distance from nozzle.

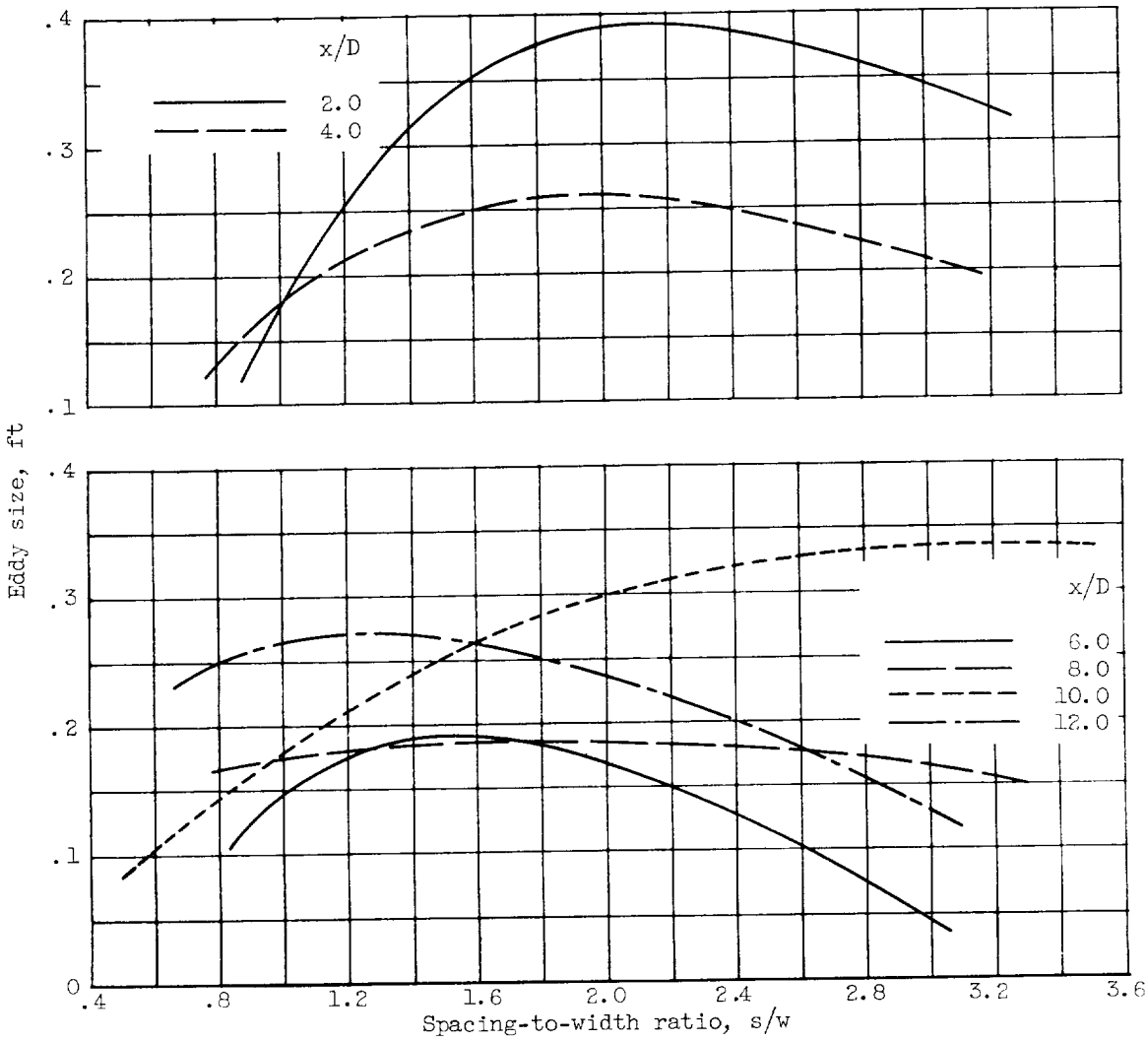

(a) z/D = -0.25.

Figure 23. - Variation of eddy size with spacing-to-width ratio.

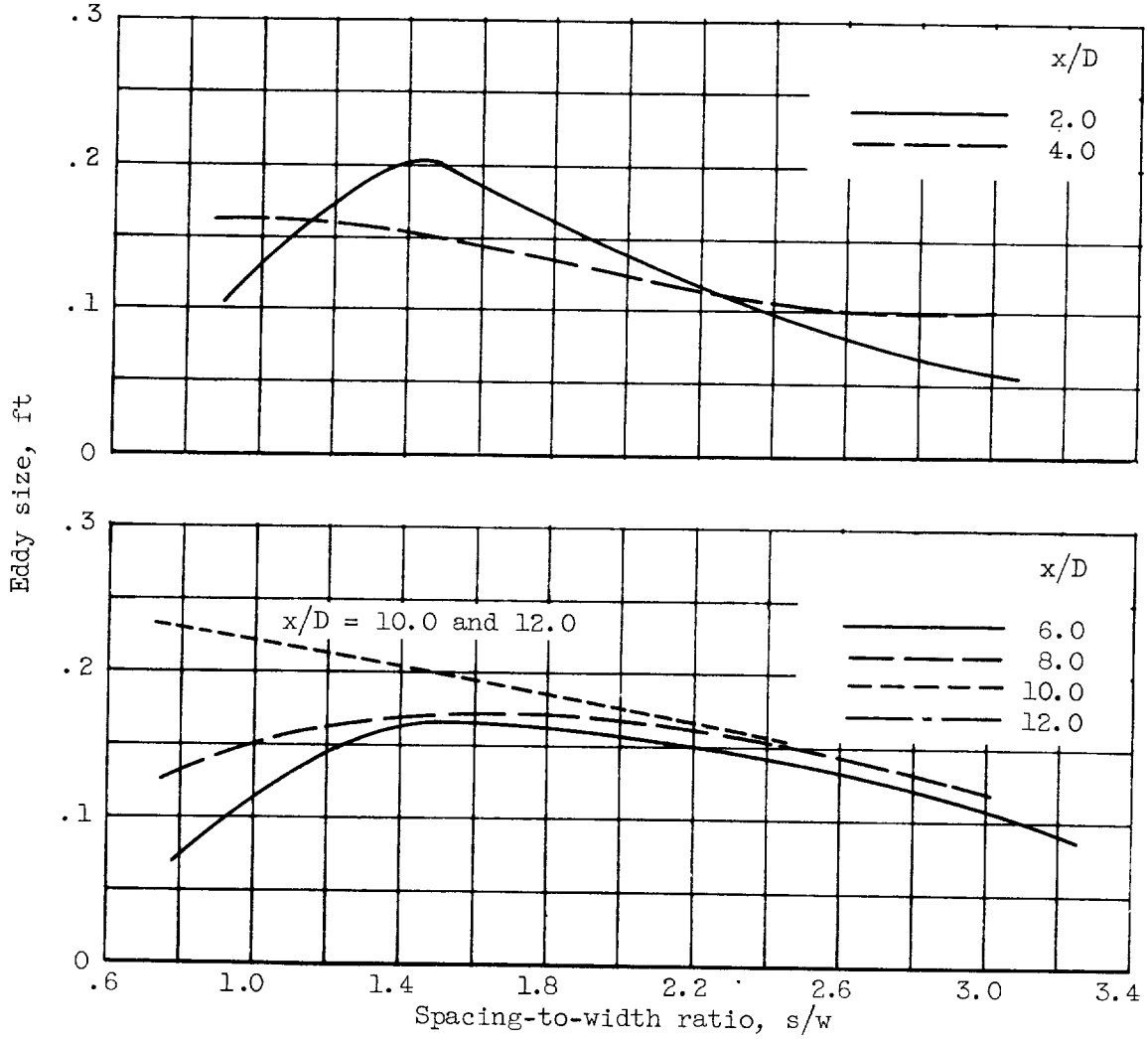

(b) Survey line halfway between outside nozzles.

Figure 23. - Concluded. Variation of eddy size with spacing-to-width ratio.

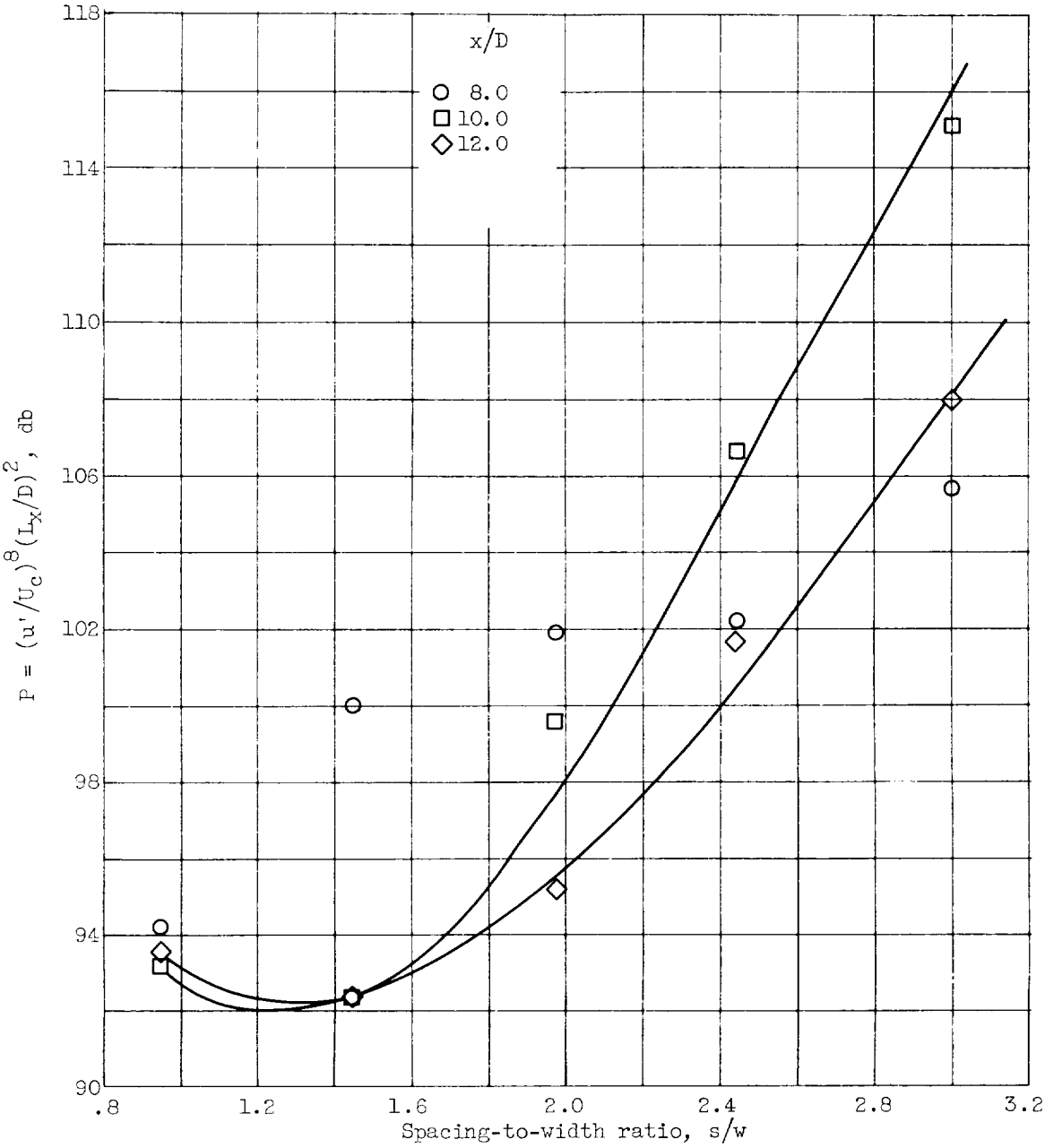

Figure 24. - Noise reduction parameter P as function of spacing-to-width ratio. z/D = -0.25.

NASA TN D-294
National Aeronautics and Space Administration.
TURBULENCE STUDIES OF A RECTANGULAR SLOTTED NOISE-SUPPRESSOR NOZZLE. James C. Laurence. September 1960. 85p. OTS price, $2.25. (NASA TECHNICAL NOTE D-294)

Turbulence studies, made in a model noise-suppressor-type nozzle, were aimed at the statistical properties of the fluctuating flow which may cause the attenuation of the sound power in some frequency bands and at the effect of the nozzle spacing on these properties. Mean and turbulent velocity profiles, intensity, scale, spectra, and probability densities of the fluctuating velocities and convection velocities of the pressure and velocity eddies are reported. The turbulence intensity, scale and spectral distribution, and the mean velocity profiles are changed by the spacing-to-width ratio of the rectangular slots.

(Initial NASA distribution: 4, Aircraft safety and noise; 20, Fluid mechanics.)
Copies obtainable from NASA, Washington

I. Laurence, James C.
II. NASA TN D-294

NASA

NASA TN D-294
National Aeronautics and Space Administration.
TURBULENCE STUDIES OF A RECTANGULAR SLOTTED NOISE-SUPPRESSOR NOZZLE. James C. Laurence. September 1960. 85p. OTS price, $2.25. (NASA TECHNICAL NOTE D-294)

Turbulence studies, made in a model noise-suppressor-type nozzle, were aimed at the statistical properties of the fluctuating flow which may cause the attenuation of the sound power in some frequency bands and at the effect of the nozzle spacing on these properties. Mean and turbulent velocity profiles, intensity, scale, spectra, and probability densities of the fluctuating velocities and convection velocities of the pressure and velocity eddies are reported. The turbulence intensity, scale and spectral distribution, and the mean velocity profiles are changed by the spacing-to-width ratio of the rectangular slots.

(Initial NASA distribution: 4, Aircraft safety and noise; 20, Fluid mechanics.)
Copies obtainable from NASA, Washington

I. Laurence, James C.
II. NASA TN D-294

NASA

NASA TN D-294
National Aeronautics and Space Administration.
TURBULENCE STUDIES OF A RECTANGULAR SLOTTED NOISE-SUPPRESSOR NOZZLE. James C. Laurence. September 1960. 85p. OTS price, $2.25. (NASA TECHNICAL NOTE D-294)

Turbulence studies, made in a model noise-suppressor-type nozzle, were aimed at the statistical properties of the fluctuating flow which may cause the attenuation of the sound power in some frequency bands and at the effect of the nozzle spacing on these properties. Mean and turbulent velocity profiles, intensity, scale, spectra, and probability densities of the fluctuating velocities and convection velocities of the pressure and velocity eddies are reported. The turbulence intensity, scale and spectral distribution, and the mean velocity profiles are changed by the spacing-to-width ratio of the rectangular slots.

(Initial NASA distribution: 4, Aircraft safety and noise; 20, Fluid mechanics.)
Copies obtainable from NASA, Washington

I. Laurence, James C.
II. NASA TN D-294

NASA

NASA TN D-294
National Aeronautics and Space Administration.
TURBULENCE STUDIES OF A RECTANGULAR SLOTTED NOISE-SUPPRESSOR NOZZLE. James C. Laurence. September 1960. 85p. OTS price, $2.25. (NASA TECHNICAL NOTE D-294)

Turbulence studies, made in a model noise-suppressor-type nozzle, were aimed at the statistical properties of the fluctuating flow which may cause the attenuation of the sound power in some frequency bands and at the effect of the nozzle spacing on these properties. Mean and turbulent velocity profiles, intensity, scale, spectra, and probability densities of the fluctuating velocities and convection velocities of the pressure and velocity eddies are reported. The turbulence intensity, scale and spectral distribution, and the mean velocity profiles are changed by the spacing-to-width ratio of the rectangular slots.

(Initial NASA distribution: 4, Aircraft safety and noise; 20, Fluid mechanics.)
Copies obtainable from NASA, Washington

I. Laurence, James C.
II. NASA TN D-294

NASA